Bulletin of the Seismological Society of America. Vol. 60, No. 4, pp. 1151–1197. August, 1970

AFTERSHOCKS OF THE 1966 PARKFIELD-CHOLAME, CALIFORNIA, EARTHQUAKE: A DETAILED STUDY*

By J. P. Eaton, M. E. O'Neill and J. N. Murdock

ABSTRACT

Hypocenters and magnitudes of more than 600 aftershocks of the 1966 Parkfield-Cholame earthquake were determined from recordings of a dense network of portable seismograph stations operated in the epicentral region from 3 to 82 days after the main shock. Hypocenters were virtually confined to a nearly vertical zone extending downward from the zone of visible ground fracturing at the Earth's surface to a depth of 12 to 14 km. Aftershocks were concentrated in patches on the slip surface, with large numbers of events in depth ranges of 2 to 4 km and 8 to 10 km and relatively few at depths of 5 to 7 km. First-motion patterns suggest that simple, nearly horizontal right-lateral strike-slip displacement was the source for an overwhelming majority of the aftershocks. The coefficient "*b*" in the frequency versus magnitude equation appears to be depth-dependent: it is about −0.6 for events between 8- and 10-km depth but averages about −0.95 for events at other depths. Individual stations with consistently late *P*-wave arrivals were also found to record abnormally large amplitudes, with both anomalies increasing, apparently, with increasing thickness of sediments beneath the site.

Introduction

A detailed study of the aftershocks of the June 27 1966 Parkfield-Cholame earthquake in central California was undertaken by the National Center for Earthquake Research, U. S. Geological Survey, in an attempt to establish the spatial relationship of the aftershocks to the zone of surface fracturing that accompanied the earthquake. Important features of the principal shock, which had a magnitude of 5.5, and of the aftershocks of magnitudes 2.0 and larger have been discussed by McEvilly *et al.* (1967); the surface fracturing along 40 km of the San Andreas fault that accompanied the earthquake has been mapped and described by Brown and Vedder (Brown *et al.* 1967). The initial objective of the work described in this report was to determine whether the aftershocks might reveal the slip surface over which movement occurred at the time of the principal shock, and if they do, to determine the underground location and extent, particularly the lower limit, of the slip surface. For this purpose it was clearly necessary to locate the aftershocks with higher precision than had been attainable by standard regional networks. Moreover, it was uncertain whether even a specially designed dense network would permit the determination of reliable focal depths in a region as complex geologically as that surrounding the epicentral tract of these earthquakes.

The basic field experiment to study the aftershocks was designed for maximum resolution in locating hypocenters beneath the southeastern half (especially the end) of the zone of surface fracturing. In that region, the eight U. S. Geological Survey portable stations initially available were deployed in a circular cluster, centered on the end of the fractured zone, with a diameter of about 20 km. Recording in this region

* Work done in cooperation with the Division of Reactor Development and Technology, U. S. Atomic Energy Commission. Approved for publication by the Director, U. S. Geological Survey.

was begun early on July 1 (GMT), about 70 hr after the main shock, and was continued until September 15 1966. During the first 3 weeks of July, the Earthquake Mechanism Laboratory (EML) of ESSA operated five portable stations (similar but not identical to the USGS stations) in a network surrounding the instrumental epicenter of the main shock, at the northwest end of the fractured zone. For this interval, data from the USGS net have been supplemented by arrival times from EML stations to permit the location of aftershocks along the northwestern half of the fractured zone. During September, this part of the aftershock region was again brought under reasonably adequate surveillance when five stations were added to the USGS network to extend it toward the northwest. For earthquakes of magnitudes 1.5 and larger, first P arrivals generally could be read at the University of California station at Priest, 44 km northwest of Gold Hill (GH). These data were also used in the hypocenter calculations.

To attain the required precision in hypocenter location, it also appeared necessary to develop an improved velocity model, especially for the highly variable uppermost part of the crust, in the region occupied by the network. Accordingly, two short refraction profiles, one on each side of the San Andreas rift zone, were run through the network during mid-September. A third profile was run across the rift zone and a calibration shot was detonated just northwest of the network in order to evaluate more fully the near-surface velocity variations near the fault. The refraction profiles were described in detail and analyzed by Stewart and O'Neill (S. W. Stewart and M. E. O'Neill, written communication, 1969), and crustal models based on their interpretations were adopted for use with the portable network in locating aftershocks.

This report deals primarily with the problem of locating the aftershocks and describing their spatial distribution. Within the limitations of the recorded data, it also discusses focal mechanisms (from first motions), distribution of aftershocks along the fault as a function of time, distribution of aftershocks as a function of magnitude and focal depth, relationship of aftershocks to creep along the fault and dependence of arrival time and amplitude anomalies on local geological conditions.

The portable seismograph stations, the equipment and methods employed in recovering data from the field tapes and analytical technics developed to aid in the interpretation of the data have not been adequately reported. These features of the work will be discussed prior to presentation of results on the aftershocks.

Characteristics of the Seismic Systems and of the Special Seismograph Network

The primary element of the portable seismograph station is a Precision Instrument 5100 tape recorder, which records for 10 days on a 14-in reel of $\frac{1}{2}$ in $\times$ 1 mil tape at a speed of 15/160 in/sec. Recording is in the FM mode with a center frequency of 84.4 cps, and the response is nearly flat from 0 to about 17 cps. With careful maintenance, a dynamic range slightly greater than 30 db can be attained. The seismometers are Electrotech EV17 (and EV17H) 5000-ohm coil electromagnet "moving magnet" instruments, and they are operated at approximately critical damping. Seismometer signals are amplified by UED 210A amplifiers, which have a maximum gain of 100 db within a passband of approximately 0.5 to 17 cps (between -3 db points) and provide two output levels, nominally 0 db and -30 db. The two levels are recorded on separate tape channels.

Primary timing is provided by recording the WWVB digitally coded radio time signal on a separate tape channel. Secondary timing is provided by a local crystal-

controlled clock, with distinctive second, minute, and hour marks, recorded on a separate tape channel.

One-component stations are usually equipped with a vertical seismometer and record on only four tracks—high- and low-gain seismic channels, WWVB channel and chronometer channel. Three-component stations record on seven tracks—high- and low-gain vertical seismic channels, high- and low-gain N-S horizontal seismic channels, high-gain E-W seismic channel, WWVB channel and chronometer channel.

Two systems are used for playback: one to provide a conventional 60 mm/min seismogram to permit easy identification of events for study, the other to provide high-speed strip chart records for detailed analysis. In the first system, the tape is played back at $7\frac{1}{2}$ in/sec (80 times recording speed) and the signal is recorded on a modified Sprengnether autocorder. An interlock between the autocorder and playback tape drive permits an entire tape (10 days of record) to be played back automatically in about $3\frac{1}{2}$ hr. At the beginning of each day's record, several minutes of WWVB radio time code mixed with chronometer minute and hour marks are played out. For the rest of the 24-hr day, a selected seismic channel mixed with chronometer minute and hour marks is played out. The tape recorder backs up between successive days' records to permit recording of a chronometer correction strip without loss of seismic record. The strip-chart playbacks used for event analysis are written by high-speed oscillographs: both photographic and direct-writing ink-jet systems are available. Normal tape playback speeds are $3\frac{1}{2}$ and $1\frac{7}{8}$ in/sec (40 and 20 times recording speed, respectively), and a variety of playback time-base speeds from 1 mm/sec to 50 mm/sec can be obtained. A WWVB time-code reader is normally used to locate and identify events (previously timed to the nearest minute on the autocorder playback) on the tape. All tape channels are played back simultaneously and displayed side by side on the strip chart (Figure 1).

Overall system magnification depends on playback gain level settings as well as on gain settings on the field equipment, but the shape of the response curve is determined by non-gain-dependent characteristics of the seismometer, amplifier, tape recorder, and playback system. In Figure 2, *curve A* is the empirically determined frequency response of the amplifier-recorder-playback system combination, and *curve C* is the calculated frequency response curve of the EV17 seismometer (1.0-sec free period, critical damping) for sinusoidal ground motion. The overall system magnification curve for a typical quiet site (12-db attenuation at the seismic amplifier) and for average playback sensitivity (5-mm playback peak-to-trough amplitude for a 10-μv calibration signal) is given by *curve B*. The magnification curve of the standard short-period Wood-Anderson seismograph (W-A) is also shown in Figure 2 for comparison with that of the portable system. Calibration of individual stations is accomplished by substituting a signal generator for the seismometer and introducing a 10-cps signal at rms levels of 10, 100, and 1000 μv into the amplifier and recorder, which are set up exactly the same as for recording the seismometer signal. On playback, the calibration signals are reproduced with exactly the same settings as are used for reproducing the seismic signals. Within the frequency range 0.2 to 20 cps, approximately, usable magnification is limited by background seismic noise. For quiet locations, the peak magnification of ground displacement typically is about 5×10^6 at 15 cps on the high-level seismic channels. The corresponding magnification at 1 cps is about 230,000.

Figure 3 shows a portable station operating in the field. The tape recorder with its electronics and chronometer is contained in one waterproof field case, the seismic amplifiers and WWVB receiver in a second. These two packages, with two 12-v auto-

mobile batteries (for 2 days' unattended operation), normally are placed on the ground under a tree or simple sunshade. The seismometer is buried directly in the ground at a convenient distance from the recorder. A 3-ft-long ferrite antenna for the WWVB

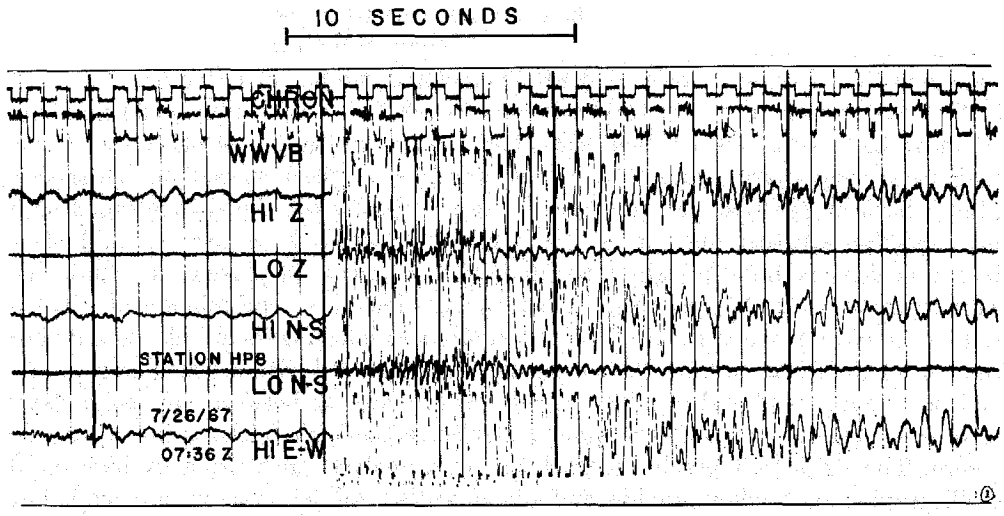

FIG. 1. High-speed playback from a three-component portable seismograph. This earthquake was of magnitude 0.5 and originated at a depth of about 2.5 km at an epicentral distance of 6 km from the recording station.

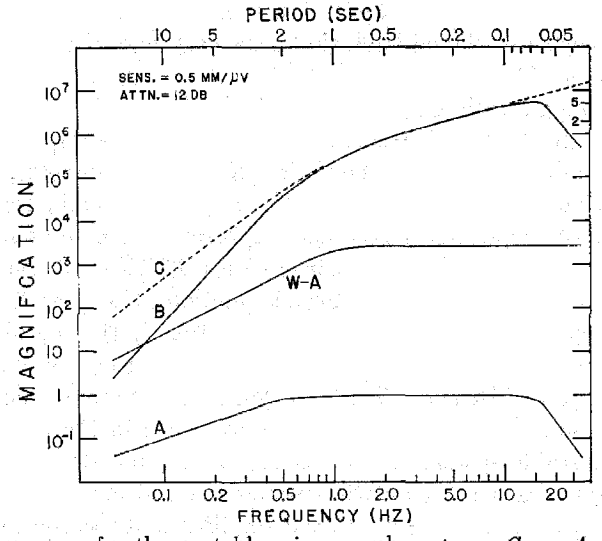

FIG. 2. Response curve for the portable seismograph systems. *Curve A* shows the combined response of the seismic amplifier, tape recorder, and playback system. *Curve B* shows the overall system response to ground motion for the operating conditions indicated on the graph (field attenuation = 12 db, playback amplitude/seismic amplifier input = 0.5 mm/μv (rms)). *Curve C* indicates the corresponding output from the seismometer. *Curve W-A* is that of the standard Wood-Anderson seismometer.

receiver, also laid on the ground after alignment to produce the maximum signal, completes the portable station. Use of a thermoelectric generator to float-charge the batteries permits longer term unattended operation of the system.

One 30-gal tank of propane powers the complete system for at least 30 days, but

the maximum period of unattended operation is limited to 10 days by the tape supply. However, during the Parkfield-Cholame field experiment, which was one of the first employing the portable stations in an intensive earthquake study, malfunctions of mechanical and electronic components were so frequent that the period of unattended operation was shortened to 2 or 3 days to bring the reliability of the network up to an acceptable level. The extreme fire hazard in the field area also argued against use of the thermoelectric generators, and only battery power was used in this experiment. Maintenance and servicing of the portable network, which gradually increased from

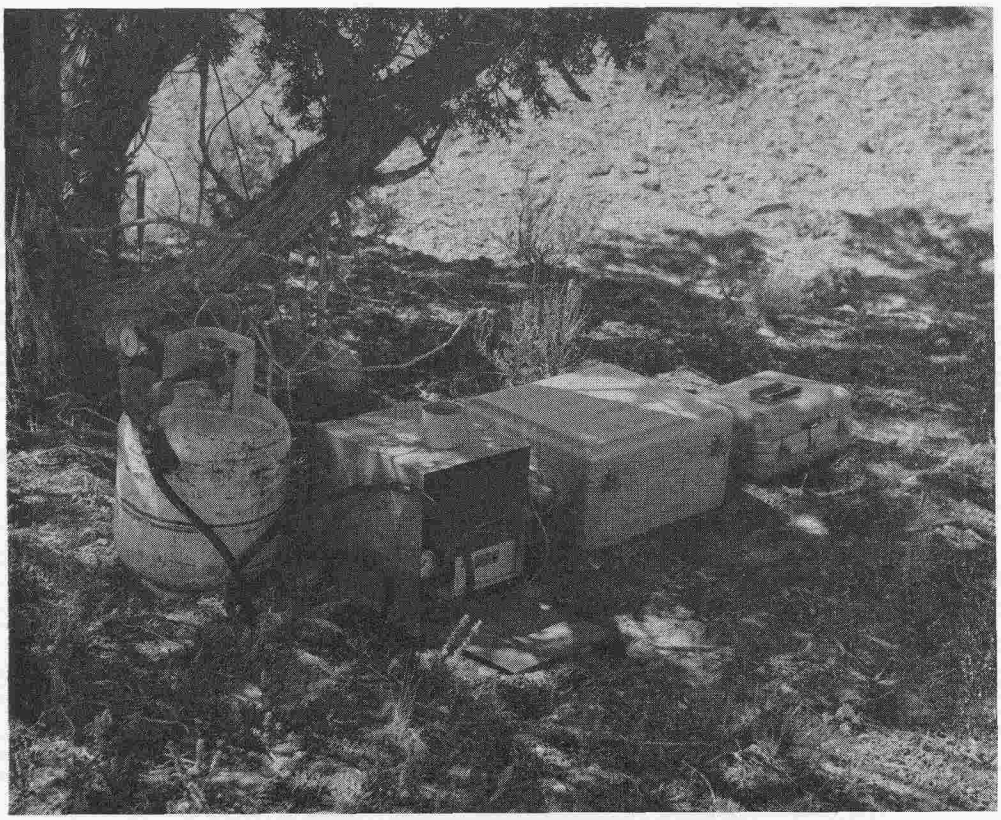

FIG. 3. Portable seismograph station. The units shown in the photograph are, *left* to *right:* propane tank, thermoelectric generator, 12-v battery, tape recorder, seismic amplifier. The antenna and seismometers are not in the picture.

six to 13 stations, required two field technicians. Later improvements in components and field procedures have reduced the maintenance and servicing load substantially.

The overall operation and performance of the portable network are summarized in Figure 4 which shows periods of satisfactory service and periods of unsatisfactory or interrupted operation for the USGS stations. This figure also shows intervals during which available P-arrivals of selected quakes were read from the EML stations and incorporated with the USGS data for hypocentral determinations. Station coordinates and elevations are listed in Table 1; locations of most stations are shown in Figure 7.

During October 1965, a Long-Range Seismic Measurements "van" was installed by the USGS at Gold Hill, a sliver of crystalline rock in the San Andreas rift zone on the northeast side of Cholame Valley, with support from the Advanced Research

Projects Agency of the Department of Defense. Gold Hill is located near the center of the zone of surface fracturing that accompanied the 1966 earthquake (Figure 7), and the seismometer pit was only ½ km from the foot of the hill. The Helicorder monitor record of the short-period vertical component Benioff seismograph in this station was used extensively in the analysis of the aftershocks of the 1966 quake. Its recording speed was 1 mm/sec, and it provided ground displacement magnifications for waves with frequencies of 1 cps and 3 cps of about 75,000 and 240,000 (peak magnification), respectively. Important features of the main earthquake and of the time history of the

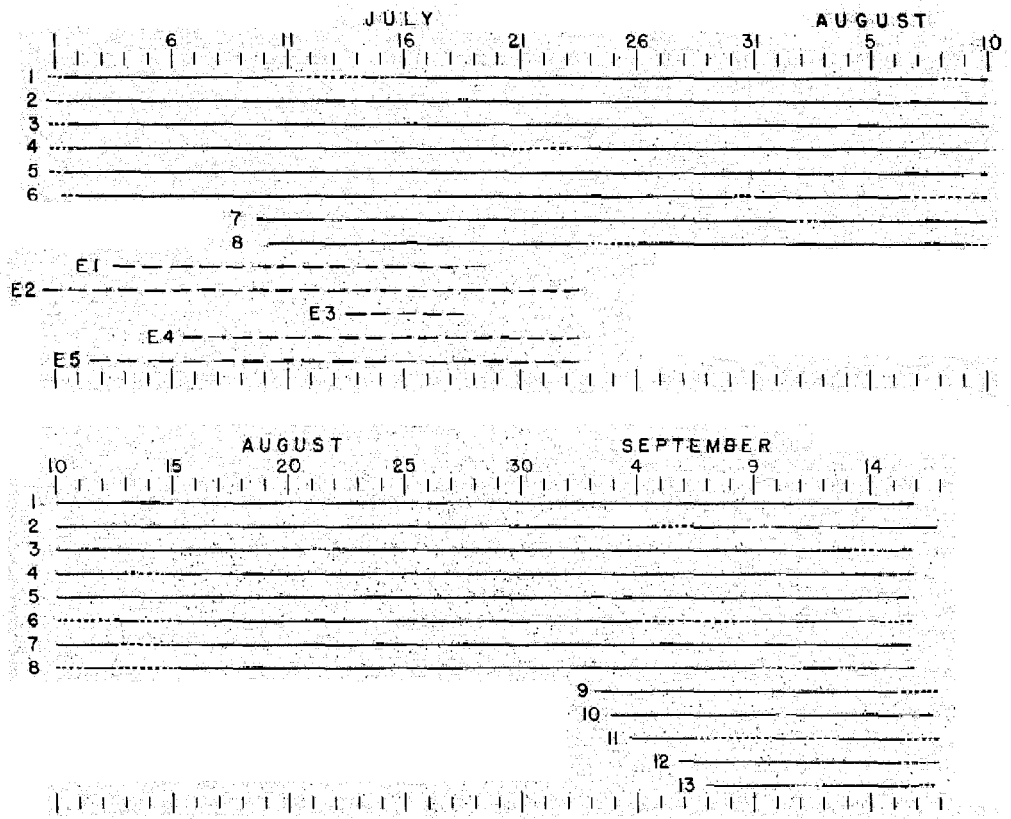

FIG. 4. Graphical summary of the period of operation of the portable network and its performance. *Solid lines* indicate satisfactory service, *dotted lines* unsatisfactory or interrupted service. The *heavy dashed lines* for stations *E1* through *E5* indicate intervals during which supplementary readings were available from the *EML* network.

aftershock sequence deduced from the Gold Hill station have been reported by Eaton (Brown *et al.*, 1967).

CRUSTAL STRUCTURE IN THE PARKFIELD-CHOLAME REGION

Geological characteristics of the contrasting crustal blocks that have been brought together by the San Andreas fault in the Parkfield-Cholame region have been summarized by Brown and Vedder (in Brown *et al.*, 1967). Southwest of the fault the basement of granitic Mesozoic rocks is buried to depths of 1,000 to 5,000 feet by marine and nonmarine sedimentary and volcanic rocks of Tertiary age and by chiefly nonmarine deposits of Quaternary age. Northeast of the fault the depth to crystalline basement rocks is unknown, but available evidence suggests it is much greater than

14,000 feet. The lowest known structural unit northeast of the fault is comprised of a complex group of cataclastic rocks, tabular serpentine masses and mafic volcanic rocks that has been assigned by many workers to a stratigraphic unit—the Franciscan Group or Formation—by lithogical correlation with its generally accepted type area in the San Francisco peninsula (Bailey and others, 1964, p. 11). This unit is separated from thick overlying(?) sequences of marine Cretaceous sedimentary rocks and chiefly marine Tertiary sedimentary rocks by major faults. Crystalline rocks of various compositions that crop out along the northeast side of the San Andreas fault, such as Gold Hill, are probably slivers enclosed by older branches of the fault that have been shifted laterally great distances from their original positions.

TABLE 1

STATION COORDINATES AND ELEVATIONS

Station	North Latitude		West Longitude		Elevation (km)	Delay (sec)	Model
	Degree	Min	Degree	Min			
1	35	45.35	120	18.73	0.372	−0.04	1
2	35	47.46	120	21.44	0.378	−0.07	1
3	35	43.20	120	16.85	0.418	0.01	1
4	35	48.84	120	16.07	0.485	−0.01	2
5	35	42.59	120	22.72	0.448	0.10	1
6	35	40.30	120	12.65	0.640	−0.07	1
7	35	39.06	120	19.22	0.466	0.10	1
8A	35	47.18	120	11.00	0.492	−0.08	2
8B	35	47.39	120	10.55	0.518	−0.08	2
9	35	52.79	120	24.72	0.469	0.09	2
10	35	49.47	120	26.31	0.646	−0.07	1
11(GH)	35	49.88	120	21.18	0.436	−0.07	2
12	35	53.33	120	20.55	0.549	0.11	2
13	35	55.09	120	28.69	0.603	−0.12	1
E1	35	56.97	120	28.28	0.538	0.25	2
E2	35	49.23	120	30.87	0.460	0.03	1
E3	35	51.10	120	36.50	0.460	0.10	1
E4	35	54.50	120	28.17	0.515	−0.18	1
E5	35	55.53	120	29.63	0.578	−0.26	1
PRI	36	8.50	120	39.90	1.187	0.33	2
PRS	36	19.90	121	22.20	0.363	−0.26	1
LLA	36	37.00	120	56.60	0.475	0.50	2

Gross features of crustal structure southwest of the fault have been outlined by seismic-refraction profiles, running parallel to the fault, that were recorded from a shotpoint at Camp Roberts about 30 km southwest of Parkfield (Healy, 1963). These profiles indicate that the crust near Camp Roberts is made up approximately as follows (Eaton, 1966): low velocity rocks, 2 to 4 km/sec, from near the surface to about 2 km; 6.0 km/sec rocks from 2 to about 15 km; 6.8 km/sec rocks from 15 km to about 25 km. The upper mantle rocks have a velocity near 8.0 km/sec. The near-surface structure was only poorly determined by these profiles because observations at short distances were extremely sparse.

Several much more detailed, but short (ca. 20 km) refraction profiles were run in the region of the special seismograph network to determine the structure of the upper crust in the Parkfield-Cholame aftershock region. Travel times from the principal Parkfield-Cholame shots are plotted on a graph (Figure 5) of $T - \Delta/6.0$ versus Δ,

where T is travel time in seconds and Δ is epicentral distance in km (S. W. Stewart and M. E. O'Neill, written communication, 1969). The profiles involve refraction paths that penetrate no deeper than a few kilometers, only to the top of the basement. The plotted curves fall into two distinct groups, one for profiles northeast of the fault and the other for profiles southwest of the fault. The two groups diverge widely, even at small epicentral distances: the southwest curves lag the northeast curves by about 0.3 sec at 2 km and by about 0.4 sec beyond 4 km. At 7 km, the latest southwest curve lags the earliest northeast curve by 0.8 sec. The sharpest changes in apparent velocity on both sides of the fault, occur at distances of 5 to 7 km. Deviation of individual

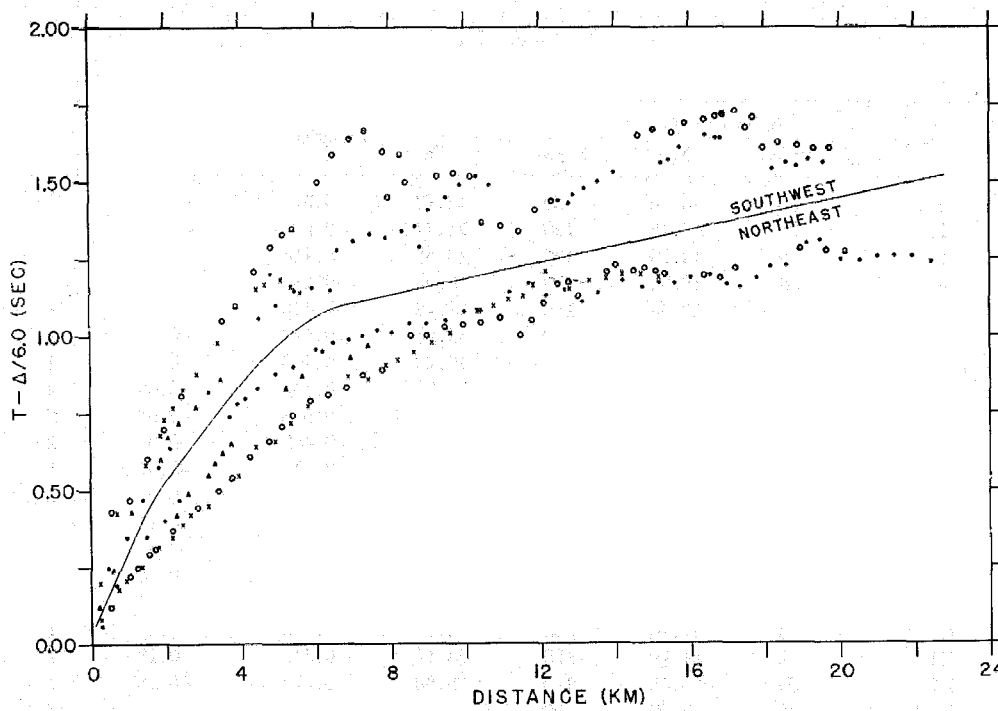

FIG. 5. Reduced traveltime-versus-distance plots for the longer Parkfield-Cholame refraction profiles. Distance, Δ, is in kilometers and first-arrival travel times T, are in seconds. Observations along different profiles are marked by different symbols; all points *above* the *solid line* (southwest of the fault zone) are on different profiles than those *below* the *solid line* (northeast of the fault zone).

observations from a smooth curve drawn to represent an average northeast profile is generally less than 0.1 sec, and the deviation of successive points on a single profile changes slowly with distance. The same can be said for the southwest profiles for distances less than 5 km, but, at greater distances, the individual southwest curves swing wildly about any smooth average curve, with individual observations deviating as much as 0.2 sec from it. Such behavior suggests high relief on the top of the basement southwest of the fault and introduces the necessity of deriving individual station corrections to supplement crustal models deduced from these data.

As expected from Figure 5, Stewart and O'Neill found different crustal structures on the two sides of the San Andreas fault. Although selection of velocities for the very thin uppermost layers and for the deepest horizons (about 5 km) penetrated by the short profiles was somewhat arbitrary, simple models composed of flat-lying constant

velocity layers were found to be consistent with the observed travel times. Separate models for the northeast and the southwest sides of the fault are shown in Figure 6. Below 5 km, both models are based primarily on the Camp Roberts profile data, with a slight increase in the upper-mantle velocity in accordance with other observations on P_n velocities in the Coast Ranges. The *upper portions* of the crustal models in Figure 6 are not identical to the final models reported by Stewart and O'Neill, but the differences are well within the uncertainties of the data. Previous results suggest that the velocity in the upper crust (at depths of 5 to 10 km, say) is lower northeast of the fault than southwest of it. The Parkfield-Cholame refraction profiles were too short and the basement refraction curves too rough to establish such a difference, however, and this suspected difference was not imposed on the model.

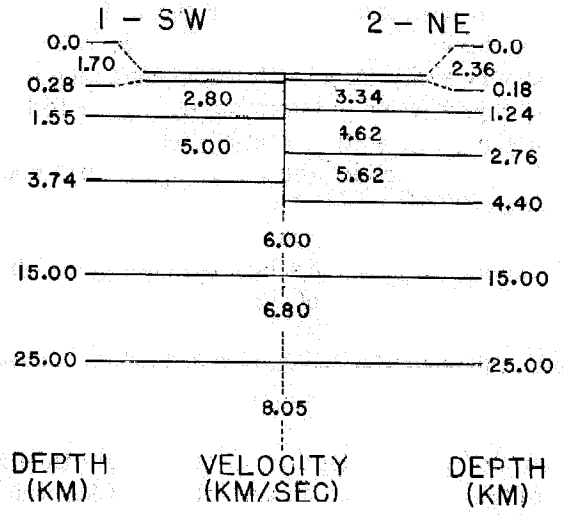

FIG. 6. Dual crustal model, split along the active trace of the San Andreas fault, used in calculating hypocenters of the aftershocks.

DETERMINATION OF HYPOCENTERS AND MAGNITUDES

Primary analysis of the Parkfield-Cholame aftershocks was carried out on the Geological Survey's IBM 360/65 computer using the program HYPOLAYR, which was designed to determine hypocenters and magnitudes of local earthquakes recorded at close range on a dense cluster of seismographs. This program is constructed along the same lines as that developed by Bolt and Turcotte (1964) for use at the University of California at Berkeley, and it incorporates features of an earlier USGS program (HYPOLO) written by Roger Greensfelder. It has been described in detail by Eaton (1969).

In the HYPOLAYR program, a first estimate of the hypocenter is adjusted by Geiger's method (Geiger, 1910) so as to minimize the sum of the squares of the residuals of observed arrival times with respect to those computed from an earth model consisting of flat-lying constant-velocity layers. Adjustment of the focal parameters (x_0, y_0, z_0, and t_0) is continued until the average residual, mean deviation of the residuals and change (from one adjustment to the next) in mean deviation of the residuals all become smaller than prescribed test values or until the number of iterations exceeds a prescribed limit. Adjustment is not terminated prior to the fifth iteration, and the test values for termination vary as the number of iterations increases. On the fourth

iteration, the depth is restored to the initial trial depth if effective depth control has been lost (i.e., if the calculated range in $\partial T/\partial z_0$ is less than 0.02 sec/km). On other iterations, it simply is not adjusted if this condition prevails. Negative focal depths are inadmissible physically and any calculated correction that would place the focus above ground is scaled down so that the hypocenter moves only 0.6 of the distance to the surface. Adjustments to the epicenter and origin time are also scaled down, but not to less than 0.4 of the values originally computed. In the calculation of adjustments, individual arrivals are weighted according to two factors: quality or clarity of the P-wave arrival and epicentral distance of the station (for later adjustments only). If amplitude, period and calibration data are available, the magnitude of the earthquake is also computed.

HYPOLAYR contains a number of features that should be noted:

(1) The travel time and derivatives of the direct wave are computed without recourse to interpolation between precalculated reference curves so that the earth model can be changed very easily. Any earth model consisting of fewer than 25 flat-lying constant-velocity layers, velocity increasing from layer to layer downward, can be used— it is read in along with station locations, etc., at the time of execution.

(2) For the special circumstance in which a group of earthquakes occurs along a known boundary between differing crustal-structure provinces (such as the Parkfield-Cholame aftershocks), two earth models can be read in and individual stations can be assigned to the model appropriate for the side of the fault on which they lie. As lateral refraction induced by the juxtaposition of the two structures is neglected, this option should be used with caution.

(3) Locations can be calculated for events recorded on any number of stations from three to 98. If only three stations record an event, the depth or origin time must be specified (depth assigned or origin time computed from S-P data).

(4) Several solution modes (free, depth restricted, origin time fixed by S-P) and combinations of modes can be called by an execution card for each event.

(5) If the epicenter lies far outside the network or if the adjustments are otherwise indeterminate, the azimuth to the source and the apparent velocity of the P-wave across the network are calculated instead of the hypocenter.

(6) Only limited use is made of S-phase data. Under the "origin time restrained" option, the origin time is set equal to that computed from available S-P data, but S-wave arrival times are not used in adjustments of the hypocenter.

(7) Station parameters include a station delay, which is added to computed travel times to allow for systematic arrival-time anomalies at individual stations.

The program is set up for batch processing of earthquakes. Station parameters (location, elevation, delay, model), crustal model parameters (depths to boundaries and layer velocities) and control parameters are first read in, and preliminary calculations are carried out. Data for the first earthquake (arrival times, amplitudes, periods and calibrations) are then read in, and the hypocenter and magnitude are computed and the results printed out. Additional earthquakes are located one at a time until the batch is finished. An optional batch statistical summary of arrival time and magnitude residuals at individual stations can be called by a control parameter.

Microearthquake Magnitude

Several extremely thorny problems arise when one attempts to compute magnitudes for microearthquakes recorded on high-gain, short-period instruments at short distances:

(1) Focal depth cannot properly be ignored at small epicentral distances; we there-

fore need a relationship between amplitude and hypocentral (not epicentral) distance for the zero-magnitude earthquake (Gutenberg and Richter, 1942).

(2) The response of the Wood-Anderson short-period torsion seismometer is implicitly included in Richter's definition of magnitude (Richter, 1935). These instruments are poorly suited to the study of microearthquakes. Moreover, their sensitivity is so much lower than that of most instruments used in microearthquake studies that it is difficult to calibrate new systems for magnitude calculations by simple overlap of observations.

(3) The Wood-Anderson records only horizontal ground motion, whereas the most widely deployed microearthquake seismographs are vertical-component instruments.

(4) Local earthquakes, unlike teleseisms, for which specific wave types (*P*, *PP*, *S*, etc.) can be identified and used for assignment of magnitudes, generally cannot be reliably resolved into their component waves. The waves that are largest in any given range of distance (indeed those which can be identified at all) vary from region to region, depending upon the details of crustal structure. In very general terms, the direct *S*-wave (through the upper crust) is largest on short-period instruments from near the epicenter to 100 to 200 km. Between 100 and 200 km (varying with crustal structure and focal depth), the *S*-wave reflected from the base of the crust emerges with much larger amplitudes than the direct *S*-wave. Beyond its point of emergence (critical distance), the *S*-wave reflected from the base of the crust diminishes rapidly; within the next 100 km it has dropped into the background, and waves with more complex paths become the largest on the seismogram.

(5) Attenuation of seismic waves within the crust and upper mantle varies widely from region to region, and assignment of magnitude to local earthquakes can be strongly affected by such variations.

Items (4) and (5) suggest the necessity of establishing the compatibility of any "standard" zero-magnitude earthquake amplitude-versus-distance curve with that actually prevailing in any region where the curve is used for computing magnitudes. If such compatibility does not exist, a local zero-magnitude earthquake amplitude-versus-distance relationship should be established. In this event, it is necessary to decide on the distance at which the new curve is to match the original one, and it is not clear that 100 km (the reference distance in the original definition of magnitude) is the best one.

Local earthquakes recorded on the combined USGS telemetry and portable seismograph network in the Central Coast Ranges during the late summer of 1967 were studied in an effort to establish the procedures and empirical relationships needed for the assignment of magnitudes to microearthquakes in this region. Locations were determined from arrival times at all available stations, including those of the Berkeley and EML nets, but amplitudes were studied only on records from the portable stations. A law of the form $AD^K = \text{const}$ (A = ground amplitude computed from the maximum vertical component trace amplitude, D = hypocentral distance) was fitted, earthquake by earthquake, to the observations for 107 earthquakes. Epicentral distances ranged from virtually 0 to about 150 km, and focal depths ranged from 0 to 14 km. A mean value of 1.7 was found for K. The standard deviation of a single determination of K was 0.5 and the standard error of the mean was 0.1. The value of K appears to be virtually independent of focal depth and magnitude.

The log B_0 versus Δ curve, where B_0 is the maximum trace amplitude recorded on a Wood-Anderson seismograph for a magnitude zero earthquake at an epicentral distance Δ (from Gutenberg and Richter, 1942), was replotted as log B_0 versus log D, where $D^2 = \Delta^2 + 18^2$ (Gutenberg and Richter assumed an average focal depth of 18

km for southern California earthquakes). Lines with slopes of -1.5, -1.7, and -2.0 were drawn through the plotted points to test the adequacy of a relationship of the form $B_0 D^K = \text{const}$. Between 50 and 150 km, the line for $K = 1.5$ fits the plotted points quite well, but, beyond 200 km, a k larger than 2.0 is required. A line with slope -1.7 (i.e., $K = 1.7$) fits the points reasonably well from $D = 30$ km to $D = 300$ km. No point lies further than 0.10 unit (of log B_0) from the line in this distance range. Thus, the zero-magnitude earthquake amplitude-versus-distance curve (based on southern California earthquakes) is compatible with that based on central California earthquakes. For D less than 30 km, the available B_0 values are too poorly established to be considered seriously. If the line with slope -1.7 is drawn to obtain the best fit of the zero-magnitude earthquake data over the range 30 to 100 km, and if we divide B_0 by 2800 (static magnification of the Wood-Anderson) to obtain A_0, the corresponding ground displacement amplitude, we find $A_{0(\text{microns})} \times D^{1.7} = 0.71$. This relationship is not independent of the Wood-Anderson response curve, which decreases from the static magnification at a rate of 12 db/octave for frequencies below about 1.25 cps.

If we ignore the analogous decrease in magnification of the portable seismograph system for frequencies below about 1.0 cps (the 12 db/octave decrease in the motion of the mass with respect to the ground), the equation for reducing the seismogram trace amplitude to ground displacement amplitude can be written

$$A'(\text{microns}) = 1.03 \times (T \times X/C_{10}) \times 10^{-2}$$

for frequencies between 0.5 and 15 cps, the passband of the system's electronic components. In this equation A' = ground amplitude in microns, X = maximum trace amplitude in millimeters (peak to trough), C_{10} = trace amplitude in millimeters (peak to trough) resulting from a 10-μv (rms) signal introduced into the seismic amplifier in place of the seismometer output and T = period in seconds of the wave with amplitude X.

From the definition of magnitude and the equations of A_0 and A',

$$M = \log A' - \log A_0 = \log\left(1.03 \frac{X \times T}{C_{10}} D^{1.7}\right) - 1.85.$$

This relationship should hold for a horizontal (EV17-H) channel, and allowance must still be made for the difference between peak horizontal and peak vertical seismogram amplitudes. During the central California study described above, both horizontal and vertical instruments were available in three-component portable stations in several locations. In the 90 cases in which it was measured, X_H/X_Z (maximum horizontal to maximum vertical trace amplitude) varied from about 0.2 to about 8, with a median value of 1.75 (mode = 1.25). A correction based on the median value of this ratio would require that the foregoing expression for magnitude be increased by 0.25 unit to permit the use of vertical component seismographs. Thus,

$$M = \log\left(1.03 \frac{X \times T}{C_{10}} D^{1.7}\right) - 1.60$$

where X is the maximum trace amplitude on the vertical component seismogram.

The magnitude assigned to an earthquake by HYPOLAYR is the arithmetic mean of values computed for individual stations by the foregoing equation.

SELECTION OF AFTERSHOCKS FOR STUDY AND CALCULATION OF THEIR HYPOCENTERS AND MAGNITUDES

Events for high-speed playback from tape and for subsequent study were selected primarily from the Helicorder record of the short-period vertical Benioff seismograph at Gold Hill, which is nearly at the middle of the zone of surface fracturing. Autocorder playback monitor records from selected portable stations were used to supplement and verify the list of events based on the Gold Hill record. To obtain a reasonably homogeneous sample of events from the entire aftershock zone and to minimize playback of events that would prove to be too poorly recorded for valid hypocenter determination, it was necessary to find some method of screening events on the Gold Hill seismogram. It was found that events at Gold Hill with maximum peak-to-trough amplitudes larger than L, where L (mm) $= 45/(S - P)^2$ and $S - P$ is in seconds, were generally recorded clearly enough on a sufficient number of stations to be located successfully. The threshold specified by this relationship corresponds approximately to magnitude 0.5. A simple curve embodying the threshold test was drafted on mylar so that individual events could be tested directly on the seismogram. For various reasons, some earthquakes smaller than the threshold were included in the list, and many of these were located successfully.

The percentage of earthquakes from sources northwest of Gold Hill (which was located at the northwest end of the basic USGS cluster on the southeast end of the fractured zone) that were located successfully depended most strongly on the availability of supplementary readings from stations farther toward the northwest. This percentage also decreased with decreasing magnitude, especially when supplementary readings from northwestern stations were sparse or lacking altogether.

Timing of wave arrivals on the high-speed playbacks was by direct comparison with the WWVB signal on the playback. Times were read to the nearest $\frac{1}{100}$ sec, but the actual precision was somewhat less, about $\frac{1}{50}$ sec. During periods without recorded WWVB code, arrivals were timed with respect to the internal chronometer and then corrected to WWVB. The maximum P-wave amplitude and the maximum recorded amplitude as well as the corresponding periods were scaled from the high-speed playbacks.

Hypocenters were computed on the basis of the dual crustal model presented in Figure 6. Stations northeast of the zone of surface fractures were ascribed to *model 2*, the others to *model 1*. To diminish the dependence of a computed hypocenter on the composition of the particular subset of stations used in its determination, a number of well-recorded, well-distributed aftershocks were located with station delays set equal to zero. The individual station average residuals for this group of aftershocks were then adopted as station delays to be used in the calculation of all hypocenters. For stations not represented in the original group of calibration earthquakes (the EML stations and Priest), station delays were determined from other select groups of earthquakes. These earthquakes were located by the calibrated network (with station delays previously determined) and the average residuals at the new stations (not utilized in the hypocenter adjustments) were calculated. These individual station average residuals were adopted as station delays for the new stations. Station locations, elevations, station delays and model assignments are given in Table 1.

Of the 641 earthquakes analyzed in detail, 630 were located along the Parkfield-Cholame section of the San Andreas fault; their hypocentral coordinates, origin times and magnitudes, as well as a number of other parameters related to the precision of

the hypocentral solutions and to the material available for computing them, are given in Table 2. These parameters are:

(1) The number of observations used in the hypocenter determination, *NO*.

(2) The mean deviation of observed arrival times from the computed arrival times

$$MD = \sum_{J=1}^{NO} | F(J) | /NO$$

where $F(J)$ is the arrival time residual at station J.

(3) The standard error in the calculated focal depth, *ERZ* (kilometers).

(4) The standard error in epicentral position *ERH* (kilometers), where

$$ERH = \sqrt{[(ERX)^2 + (ERY)^2]\ /2}$$

and *ERY* and *ERX* are the standard errors in the computed latitude and longitude, respectively.

(5) The standard error in the calculated origin time, *ERT* (seconds).

(6) The epicentral distance to the nearest station, *DMIN* (kilometers).

(7) The maximum gap in epicenter-to-station azimuths, *GAP* (degrees).

(8) The epicenter is flagged by a question mark if the solution fails to satisfy appropriate termination conditions by the 12th iteration.

(9) The focal depth is flagged by an asterisk if its adjustment is blocked on the final iteration because effective focal depth control was lost.

(10) Hypocenter quality estimate *Q* (A = excellent, B = good, C = fair, D = poor) based on the statistical parameters of the hypocentral determination and the number and distribution of observations available for the solution. Hypocenters based on fewer than six observations were not rated better than D, and those in which the focal depth was restrained on the last iteration were not rated better than C.

The number of observations available for locating individual earthquakes ranged from three to 15: 10 or more stations for 180 events, six to nine stations for 362 events, five stations for 65 events, four stations for 33 events and three stations for one event. For 68 events, adjustment of the focal depth was restrained because it could not be adequately determined from available arrivals. When all four parameters are adjusted, at least six stations are required for the estimation of the standard errors in the focal parameters. The location of the hypocenter is slightly overdetermined when five stations are available. With five or more stations, the mean deviation of the observed arrival times from the calculated ones, *MD*, is a measure of the consistency of the observations and aids in the detection of erroneous readings, which can go undetected when fewer stations are available. The average value of *MD* for events located with five or more stations was 0.04 sec. Only 20 events had $MD \geq 0.10$ sec.

For 93 events, *ERH* could not be estimated (too few stations). Of the remaining 537, *ERH* did not exceed 0.5 km for 59 per cent of the earthquakes, 1.0 km for 80 per cent of the earthquakes and 2.5 km for 91 per cent of the earthquakes. Most of the earthquakes with *ERH* greater than 2.5 km were northwest of the cluster, and their focal depths could not be reliably determined. In most cases, however, the standard error in focal depth, *ERZ*, is only slightly larger than *ERH*. In the calculation of the hypocenters, an initial focal depth of 5.0 km was assumed, and events without adequate network coverage generally remained at that depth throughout the adjustment of the hypocenter.

TABLE 2 SUMMARY OF PARKFIELD-CHOLAME AFTERSHOCKS

1966	HR	MN	SEC	LAT N	LONG W	DEPTH	MAG	NO	GAP	OMIN	ERT	ERH	ERZ	MD	Q
JUL 1	1	17	34.6	35-42.4	120-20.9	7.5*	1.1	4	324	6.5				0.05	D
1	1	55	9.6	35-47.5	120-19.8	3.9	0.3	4	108	2.5				0.00	D
1	2	30	9.5	35-47.8	120-20.2	4.6	0.7	4	96	2.0				0.00	D
1	3	1	40.3	35-55.5	120-28.3	2.9	2.1	7	160	12.2	0.0	0.4	0.8	0.03	B
1	3	51	34.7	35-46.2	120-18.6	3.8	0.9	6	102	1.6	0.0	0.8	0.8	0.06	B
1	5	46	23.5	35-46.9	120-20.0	8.7	1.1	6	89	2.4	0.3	1.0	2.4	0.05	B
1	6	2	35.2	35-50.6	120-23.6	2.9	1.3	6	291	3.9	0.7	3.1	1.0	0.04	D
1	7	31	14.4	35-44.6	120-17.5	10.1	0.4	4	187	2.3				0.00	D
1	9	8	11.4	35-48.6	120-20.9	11.0	0.6	4	302	2.3				0.00	D
1	9	24	9.2	35-47.0	120-20.8	2.8	0.5	4	181	1.3				0.00	D
1	9	41	22.0	35-56.9	120-28.0	5.0*	3.28	6	183	14.8	0.0	0.3		0.02	C
1	10	23	22.0	35-47.7	120-21.2	9.0	1.1	5	140	0.7				0.01	D
1	11	29	12.5	35-46.7	120-20.4	3.3	1.2	5	145	2.1				0.02	D
1	11	37	13.4	35-44.7	120-17.9	8.8	0.8	5	163	1.7				0.04	D
1	11	51	6.7	35-44.2	120-17.3	12.9	0.5	4	183	3.0				0.00	D
1	12	0	6.6	35-46.4	120-19.6	9.5	0.5	4	192	2.4				0.00	D
1	12	1	11.0	36- 1.1	120-33.4	13.6	2.1	6	173	16.7	0.3	4.7	3.4	0.11	C
1	12	28	5.9	35-49.3	120-22.4	5.2	1.7	5	235	2.1				0.00	D
1	12	31	8.6	35-46.3	120-19.0	7.4	2.68	6	166	1.8	0.1	0.6	0.9	0.03	B
1	12	52	0.8	35-46.8	120-19.4	4.0	0.6	5	165	2.9				0.06	D
1	13	9	19.4	35-46.7	120-20.1	2.9	0.8	5	151	2.5				0.04	D
1	13	18	11.1	35-49.0	120-21.3	14.4	1.0	4	311	2.9				0.00	D
1	13	29	44.2	35-45.2	120-19.2	6.0	0.8	5	94	0.8				0.10	D
1	13	33	7.9	35-46.7	120-19.8	3.8	0.7	4	196	2.9				0.00	D
1	13	39	56.9	35-46.5	120-21.1?	2.4	0.0	5	148	1.9				0.13	D
1	13	56	51.7	35-45.6	120-18.1	10.2	1.6	5	170	1.0				0.01	D
1	14	20	18.1	35-49.3	120-21.1	12.0	1.3	4	312	3.5				0.00	D
1	14	46	45.3	35-47.1	120-20.4	7.4	1.6	5	151	1.7				0.04	D
1	15	3	10.9	35-50.8	120-24.2	2.4	1.6	7	146	4.9	0.0	0.3	0.3	0.02	B
1	16	53	24.8	35-45.8	120-23.6	13.3	0.7	5	239	4.5				0.10	D
JUL 1	18	8	2.6	35-45.2	120-18.9	4.6	0.7	5	179	0.5				0.11	D
1	18	30	40.6	35-46.0	120-19.5	8.9	0.7	6	94	1.6	0.4	1.2	3.1	0.06	B
1	18	30	59.2	35-46.2	120-19.8	10.9	0.0	5	99	2.2				0.06	D
1	18	46	19.1	35-48.8	120-21.6	3.5	0.8	7	187	2.1	0.1	1.0	0.7	0.06	B
1	20	4	49.2	35-48.0	120-20.4	3.2	0.3	6	106	1.8	0.0	0.6	0.6	0.04	B
1	20	9	14.5	35-47.0	120-20.4	7.9	0.1	6	125	1.7	0.1	0.5	1.2	0.03	B
1	21	7	20.4	35-45.0	120-18.6?	4.5	0.0	6	106	0.7	0.1	0.8	1.6	0.07	B
1	22	6	47.6	35-46.4	120-18.6	3.7	2.08	7	102	1.9	0.0	0.5	0.5	0.06	A
1	22	14	58.3	35-47.7	120-20.6	11.4	0.7	5	250	1.3				0.01	D
1	23	9	36.8	35-49.7	120-22.4	3.4	0.3	6	260	1.9	0.0	0.5	0.2	0.02	C
1	23	10	40.7	35-48.5	120-21.2	4.7	0.6	6	170	1.9	0.0	0.2	0.4	0.01	B
1	23	57	32.6	35-49.5	120-22.1	4.1	0.4	5	241	1.6				0.03	D
2	1	8	40.5	35-52.7	120-25.9	3.2	2.7	8	152	8.8	0.0	0.3	0.5	0.02	B
2	1	42	55.8	35-47.6	120-20.6	8.9	1.7	7	92	1.3	0.2	0.8	1.9	0.05	A
2	2	17	31.8	35-49.7	120-22.8	5.2	0.8	6	264	2.5	0.2	1.0	1.0	0.02	C
2	2	50	31.1	35-45.4	120-18.9	8.3	0.8	5	88	0.3				0.06	D
2	2	51	22.6	35-47.8	120-21.1	5.0	0.6	7	138	0.9	0.2	1.1	2.2	0.09	B
2	3	38	26.6	35-46.6	120-19.9	7.0	1.0	5	110	2.7				0.01	D
2	3	58	28.1	35-46.7	120-20.1	6.0	0.0	4	112	2.5				0.00	D
2	4	6	3.3	35-58.6	120-30.9	5.0*	1.8	9	165	17.3	0.0	0.3		0.02	C
2	5	52	20.9	35-51.4	120-24.3?	1.9	0.2	5	299	8.4				0.05	D
2	6	22	59.7	35-48.1	120-20.7	4.2	0.6	7	122	1.7	0.1	0.5	1.1	0.04	B
2	6	39	52.3	35-46.0	120-19.3	9.5	0.3	6	94	1.5	0.2	0.6	1.6	0.03	B
2	7	3	31.3	35-51.2	120-24.3	2.5	2.0	9	146	5.3	0.0	0.3	0.3	0.03	B
2	7	11	19.6	35-47.9	120-20.5	3.1	0.3	6	106	1.6	0.0	0.5	0.5	0.04	B
2	7	21	13.0	35-47.8	120-20.9	8.6	1.0	7	118	1.0	0.1	0.5	1.1	0.03	A
2	7	37	19.9	35-45.9	120-19.3	7.3	1.1	7	94	1.4	0.1	0.4	0.9	0.03	A
2	7	51	21.9	35-48.4	120-20.9	3.2	0.5	7	143	2.0	0.0	0.6	0.6	0.06	B
2	7	58	26.6	35-46.8	120-20.6	3.1	-0.0	7	114	1.7	0.2	1.7	2.6	0.20	B
2	8	13	8.6	35-47.5	120-21.0	7.9	-0.0	6	170	0.7	0.2	0.7	1.4	0.03	B

TABLE 2 (CONTINUED)

1966		HR	MN	SEC	LAT N	LONG W	DEPTH	MAG	NO	GAP	DMIN	ERT	ERH	ERZ	MD	Q
JUL	2	8	28	16.9	35-46.3	120-19.6	4.1	-0.0	6	100	2.1	0.1	0.9	2.3	0.08	B
	2	9	30	12.4	35-47.1	120-19.5	3.4	0.8	7	85	3.1	0.0	0.3	0.4	0.04	A
	2	9	40	8.6	35-47.0	120-20.2	3.8	-0.0	4	126	2.0				0.03	D
	2	9	40	15.1	35-47.1	120-20.2	3.5	0.6	7	86	2.0	0.0	0.4	0.5	0.05	A
	2	10	44	38.0	35-55.8	120-28.2	5.0*	1.2	8	162	15.2	0.0	0.8		0.04	C
	2	11	31	53.2	35-45.6	120-19.6	7.1	0.5	5	184	1.5				0.01	D
	2	11	42	10.8	35-49.3	120-22.4	8.5	0.6	6	273	3.7	0.5	2.0	2.5	0.03	C
	2	12	8	34.3	35-46.9	120-19.9	8.0	3.7B	9	80	2.6	0.0	0.2	0.4	0.03	A
	2	12	16	14.9	35-47.3	120-20.6	9.1	3.4B	9	82	1.4	0.0	0.3	0.6	0.04	A
	2	12	25	6.1	35-47.5	120-20.0	8.2	3.1B	9	89	2.2	0.0	0.4	0.6	0.04	A
	2	12	37	14.6	35-46.9	120-20.0	7.0	1.0	7	89	2.4	0.0	0.2	0.6	0.02	A
	2	13	58	0.1	35-53.8	120-26.2?	0.9	1.6	9	158	10.5	0.1	0.7	1.1	0.06	C
	2	14	16	2.9	35-47.3	120-20.7	8.0	0.8	7	87	1.2	0.1	0.6	1.4	0.04	A
	2	14	33	26.2	35-47.4	120-20.0	1.2	0.4	7	88	2.2	0.1	0.5	0.6	0.06	A
	2	14	43	4.6	35-47.9	120-20.5	3.5	0.4	7	108	1.6	0.0	0.4	0.4	0.03	A
	2	20	49	22.3	35-47.6	120-20.6	8.2	1.1	5	170	1.3				0.01	D
	2	20	57	27.4	35-48.2	120-21.0	8.3	2.1B	8	118	1.5	0.1	0.7	1.0	0.06	A
	2	21	53	19.1	35-46.6	120-19.9	8.4	0.6	6	113	2.8	0.2	0.6	1.6	0.03	B
	2	22	9	37.1	35-47.2	120-20.0	8.9	2.0B	8	83	2.2	0.0	0.4	0.7	0.05	A
	2	23	11	58.7	35-47.4	120-19.5	4.4	1.8	6	91	2.9	0.0	0.4	1.1	0.03	B
	3	0	3	15.6	35-49.4	120-22.2	5.0	1.7	6	235	1.8	0.1	0.8	1.0	0.03	C
	3	0	14	58.9	35-47.5	120-20.8	8.3	0.8	5	145	1.0				0.06	D
	3	1	50	52.0	35-48.6	120-21.0	4.1	0.7	4	158	2.2				0.00	D
	3	2	3	43.6	35-48.4	120-20.8	11.1	1.6	5	152	2.1				0.01	D
	3	3	2	44.2	35-48.7	120-20.8	11.5	0.3	4	299	2.6				0.00	D
	3	4	49	3.5	35-48.2	120-20.3	3.6	1.4	5	165	2.2				0.00	D
	3	5	30	54.1	35-53.4	120-26.3	11.0	2.6	8	155	10.1	0.0	0.4	0.9	0.03	B
	3	5	59	23.5	35-50.2	120-23.3	3.3	0.1	4	286	5.7				0.00	D
	3	6	27	6.1	35-55.3	120-27.6	5.0*	1.1	6	162	17.2	0.1	1.4		0.07	C
	3	7	9	12.6	35-47.7	120-20.7	8.6	0.3	5	182	1.2				0.01	D
JUL	3	9	3	47.3	35-54.1	120-26.8	7.5	1.8	7	160	11.5	0.0	0.5	1.4	0.02	B
	3	9	24	23.1	35-45.4	120-19.1	5.9	0.0	5	92	0.6				0.03	D
	3	9	24	28.4	35-47.8	120-20.4?	4.1	0.4	4	183	1.6				0.05	D
	3	10	39	29.3	35-46.8	120-19.8	3.0	1.1	6	88	2.8	0.0	0.4	0.7	0.04	B
	3	10	53	21.1	35-52.6	120-25.7	2.0	1.3	8	151	8.0	0.0	0.4	0.4	0.03	B
	3	13	55	6.7	35-47.9	120-20.4	3.2	0.5	6	100	1.8	0.0	0.6	0.7	0.05	B
	3	15	51	23.6	35-46.4	120-19.7	8.7	0.8	5	102	2.4				0.02	D
	3	18	37	32.1	35-47.9	120-20.3	11.0	1.1	4	259	1.9				0.00	D
	3	20	22	25.9	35-55.4	120-28.3	2.9	2.9B	8	169	2.1	0.0	0.5	0.5	0.06	B
	3	20	27	20.1	35-55.5	120-28.0	5.0*	1.6	5	173	14.6	0.0	1.0		0.03	C
	3	21	11	7.6	35-47.8	120-22.6	2.7	0.1	4	289	1.9				0.00	D
	3	23	20	38.5	35-49.8	120-19.4	2.0*	0.7	4	293	5.3				0.07	D
	4	0	41	17.7	35-51.4	120-24.3	2.2	2.0	8	150	5.4	0.0	0.3	0.4	0.03	B
	4	0	42	54.8	35-51.4	120-24.4?	2.1	1.6	7	166	5.6	0.0	0.7	1.0	0.07	C
	4	2	29	55.9	35-48.3	120-20.8	9.5	1.3	6	185	1.8	0.0	0.4	0.6	0.02	B
	4	3	4	57.4	35-50.8	120-24.0	2.1	2.4	9	140	4.5	0.0	0.6	0.8	0.07	B
	4	3	34	11.9	35-47.4	120-20.3	9.0	0.7	5	225	1.7				0.00	D
	4	3	40	14.1	35-45.9	120-20.2	7.0	0.8	4	147	2.4				0.00	D
	4	5	28	48.7	35-51.1	120-23.9	2.5	2.9B	11	140	4.7	0.0	0.1	0.1	0.02	B
	4	6	9	27.9	35-45.7	120-20.8	7.9	0.7	7	135	3.2	0.2	0.8	2.2	0.07	B
	4	6	11	19.5	35-50.2	120-23.4	3.0	0.9	7	284	3.5	0.2	1.2	0.4	0.03	C
	4	6	56	36.9	35-47.2	120-19.9	6.3	0.8	6	82	2.3	0.1	0.6	1.8	0.04	B
	4	7	46	53.4	35-52.6	120-25.4	1.8	1.1	9	165	8.1	0.0	0.1	0.2	0.01	B
	4	7	52	20.5	35-52.6	120-25.6	2.1	1.3	9	164	8.1	0.0	0.1	0.2	0.01	B
	4	8	20	45.6	35-52.3	120-25.4	7.6	1.3	9	160	7.8	0.0	0.3	0.8	0.03	B
	4	8	30	36.8	35-48.3	120-20.8	3.4	0.7	6	226	1.8	0.0	0.6	0.4	0.03	C
	4	10	22	20.9	35-48.8	120-21.4	3.3	0.5	9	83	2.1	0.0	0.3	0.3	0.04	A
	4	13	59	52.3	35-45.2	120-18.5	8.5	0.2	5	107	0.4				0.03	D
	4	15	44	54.5	35-50.6	120-23.9	2.8*	0.7	4	293	4.3				0.00	D
	4	18	4	11.4	35-58.2	120-30.2	5.0*	1.9	7	166	23.8	0.0	1.4		0.06	C

TABLE 2 (CONTINUED)

1966	HR	MN	SEC	LAT N	LONG W	DEPTH	MAG	NO	GAP	DMIN	ERT	ERH	ERZ	MD	Q
JUL	4	19	32	48.0	35-47.4	120-20.7	9.0	1.2	6	159	1.1	0.3	1.0	2.1	0.04	C
	5	0	7	22.3	35-46.1	120-19.4	7.6	0.9	9	92	1.7	0.0	0.4	0.7	0.05	A
	5	1	27	42.4	35-54.7	120-27.9?	1.4	2.2	10	128	3.0	0.1	0.4	0.4	0.05	B
	5	1	37	28.9	35-46.0	120-19.8	8.1	0.9	4	101	1.9				0.00	D
	5	2	53	50.0	35-45.7	120-19.2	7.0	0.3	5	177	1.0				0.01	D
	5	3	15	58.8	35-47.5	120-20.6	8.3	1.6	9	81	1.3	0.0	0.2	0.4	0.03	A
	5	4	14	19.2	35-46.1	120-19.4	7.0	0.3	8	91	1.7	0.0	0.3	0.5	0.03	A
	5	4	34	27.3	35-47.2	120-20.7	7.2	0.6	5	133	1.2				0.02	D
	5	5	28	22.1	35-45.6	120-19.1	7.7	0.7	9	99	0.8	0.0	0.4	0.8	0.04	A
	5	8	6	4.4	35-44.1	120-17.0	5.0	0.0	6	128	1.7	0.0	0.5	1.0	0.04	B
	5	9	57	25.1	35-44.2	120-17.6	10.6	0.8	6	119	2.2	0.2	0.5	1.5	0.03	B
	5	13	1	12.1	35-47.8	120-21.3	8.3	0.8	6	240	0.7	0.2	0.8	1.5	0.03	C
	5	14	22	51.7	35-47.9	120-20.6	3.6	0.2	4	200	1.6				0.00	D
	5	16	13	9.9	35-47.0	120-20.3	7.5	1.0	5	126	1.9				0.01	D
	5	17	15	23.1	35-45.3	120-18.2	10.0	1.0	6	111	0.8	0.1	0.4	1.2	0.02	B
	5	18	3	45.0	35-49.2	120-22.1	4.9	1.5	6	223	2.0	0.1	0.6	0.7	0.02	B
	5	18	35	12.3	35-49.3	120-22.4	3.1	0.6	7	240	2.2	0.2	1.2	0.7	0.06	C
	5	18	50	32.4	36- 4.6	120-41.5	5.0*	1.6	6	233	7.7	0.3	3.0		0.05	D
	5	18	54	54.4	35-55.0	120-28.1	3.5	3.1	11	125	2.4	0.0	0.3	0.3	0.05	B
	5	19	44	23.1	35-44.6	120-17.5	10.3	1.2	7	122	2.3	0.1	0.4	1.1	0.03	B
	5	19	45	18.4	35-45.4	120-19.4	7.0	0.9	6	98	1.1	0.1	0.6	1.4	0.04	B
	5	19	45	53.8	35-44.6	120-17.7	10.3	1.2	9	120	2.1	0.0	0.2	0.4	0.02	A
	5	20	7	44.1	35-44.8	120-17.9	7.8	0.0	5	130	1.6				0.01	D
	5	22	18	50.0	35-47.5	120-20.4	3.4	1.0	8	112	1.6	0.0	0.3	0.2	0.04	A
	5	22	43	51.1	35-47.8	120-20.3	3.5	0.3	6	185	1.8	0.1	1.1	0.9	0.07	C
	5	22	52	11.5	35-51.4	120-24.1	0.4	1.1	9	158	5.2	0.2	0.4	1.0	0.05	B
	6	0	7	29.4	35-55.2	120-28.5	4.0	1.3	10	157	1.7	0.0	0.5	0.8	0.05	B
	6	1	18	16.4	35-55.5	120-28.4	5.0*	1.5	6	164	18.2	0.0	0.6		0.03	C
	6	1	43	30.7	35-45.6	120-19.2	10.1	0.6	5	92	0.8				0.03	D
	6	3	46	10.1	35-55.7	120-28.7	4.5	2.0	10	108	1.4	0.0	0.2	0.3	0.03	A
JUL	6	4	25	43.8	35-44.6	120-17.4	10.9	0.9	5	124	2.4				0.02	D
	6	6	54	5.4	35-46.4	120-20.1	11.8	0.5	5	105	2.7				0.05	D
	6	7	8	15.6	35-50.7	120-24.0	2.2	1.3	8	150	4.4	0.0	0.6	0.8	0.05	B
	6	7	12	46.4	35-46.7	120-19.6	1.3	1.5	8	84	2.8	0.1	0.5	0.5	0.06	A
	6	7	13	44.0	35-48.7	120-21.2	3.4	1.1	8	88	2.2	0.0	0.2	0.2	0.03	A
	6	9	33	54.1	35-49.4	120-21.9	3.9	0.4	4	271	3.7				0.00	D
	6	11	29	52.8	35-51.3	120-23.6?	2.0	0.6	5	296	4.5				0.03	D
	6	13	22	43.5	35-45.3	120-19.2	8.1	0.5	5	94	0.7				0.02	D
	6	14	28	29.1	35-48.6	120-21.7	7.1	1.0	5	259	2.1				0.02	D
	6	15	8	3.0	35-47.4	120-20.5	10.7	0.5	5	151	1.4				0.08	D
	6	15	57	36.6	35-52.7	120-25.7	9.9	1.8	9	152	7.9	0.0	0.3	0.6	0.03	B
	6	16	43	13.2	35-47.7	120-21.1	8.5	0.5	5	207	0.7				0.00	D
	6	17	19	22.0	35-47.9	120-20.4	3.3	1.2	6	102	1.7	0.0	0.5	0.6	0.04	B
	6	19	21	3.8	35-47.1	120-19.9	1.1	0.9	8	80	2.4	0.1	0.5	0.5	0.06	A
	6	20	14	7.9	35-48.3	120-20.7	3.3	1.1	6	127	1.9	0.0	0.7	0.8	0.06	B
	6	23	24	33.4	35-48.2	120-20.4	3.6	0.3	5	109	2.1				0.00	D
	6	23	41	19.5	35-44.6	120-18.6	9.3	0.0	4	213	1.4				0.00	D
	7	2	17	5.6	35-55.1	120-27.9	3.8	1.6	7	178	3.5	0.0	1.4	1.0	0.05	C
	7	4	27	18.6	35-47.0	120-19.4	2.0	0.7	8	86	3.2	0.0	0.4	0.6	0.06	A
	7	5	7	9.0	35-54.3	120-27.1	5.2	1.8	11	140	1.6	0.0	0.3	0.5	0.03	B
	7	5	7	54.0	35-58.5	120-36.0	5.0*	1.8	5	196	19.5	0.2	3.3		0.08	C
	7	14	37	7.4	35-46.3	120-20.7	5.0*	0.9	3	163	2.5				0.00	D
	7	15	46	50.2	35-56.2	120-29.3	4.9	1.4	11	210	1.3	0.1	0.9	1.1	0.04	B
	7	17	38	38.1	35-47.3	120-20.9	7.0	0.5	4	146	0.9				0.00	D
	7	19	18	15.1	35-46.9	120-19.8	3.0	0.5	4	123	2.7				0.03	D
	7	21	27	40.4	35-48.1	120-20.7	3.9	0.5	4	218	1.6				0.06	D
	7	22	27	22.7	35-56.5	120-28.9	5.1	2.3	6	163	1.3	0.0	1.1	0.7	0.02	C
	7	22	44	12.0	35-45.2	120-18.3	7.8	0.4	5	110	0.7				0.01	D
	7	23	4	33.0	35-50.7	120-24.0	5.7	1.0	5	293	7.1				0.07	D
	8	1	11	18.8	35-56.8	120-17.9	10.2*	1.0	5	329	14.9	0.7	3.7		0.03	D

TABLE 2 (CONTINUED)

1966	HR	MN	SEC	LAT N	LONG W	DEPTH	MAG	NO	GAP	DMIN	ERT	ERH	ERZ	MD	Q
JUL 8	1	33	27.1	35-46.4	120-19.7	2.1	-0.5	5	94	3.3				0.08	D
8	2	2	2.3	35-45.1	120-19.1	6.6	0.5	6	94	0.7	0.0	0.3	0.8	0.03	B
8	2	34	2.4	35-55.4	120-18.3	10.0	1.2	7	320	11.1	1.4	5.7	4.6	0.03	D
8	2	37	10.5	35-46.9	120-20.1	7.0	0.6	5	212	3.5				0.03	D
8	4	49	10.8	35-48.0	120-20.7	5.0	0.2	5	208	1.5				0.01	D
8	9	39	49.6	35-44.3	120-17.3	9.0	0.1	5	150	2.1				0.00	D
8	10	8	30.6	35-48.4	120-21.1	3.5	0.6	9	86	1.8	0.0	0.5	0.4	0.07	A
8	12	25	2.4	35-48.6	120-21.2	3.0	0.7	9	87	2.2	0.0	0.4	0.4	0.06	A
8	12	44	21.4	35-46.0	120-19.2	5.7	0.0	5	95	4.3				0.01	D
8	14	10	41.9	35-46.5	120-20.1	8.6	0.4	6	105	2.7	0.1	0.5	1.2	0.02	B
8	15	39	5.6	35-44.4	120-17.3	9.3	0.6	6	126	2.4	0.1	0.5	1.4	0.03	B
8	16	45	54.8	35-53.9	120-26.7	5.7	1.9	12	143	2.5	0.0	0.5	1.1	0.07	B
8	17	31	11.4	35-50.2	120-23.0	3.6	0.0	5	285	5.6				0.02	D
8	17	57	50.2	35-50.9	120-24.1	2.9	0.8	10	149	4.8	0.0	0.3	0.4	0.03	B
8	22	23	48.9	35-55.6	120-28.4	5.1	1.3	11	160	1.8	0.0	0.6	0.8	0.07	B
8	23	51	43.8	35-49.0	120-22.3	7.0	0.4	5	269	3.1				0.00	D
9	0	32	49.9	35-48.5	120-21.2	3.4	0.1	6	169	2.0	0.0	0.5	0.5	0.03	B
9	0	54	5.2	35-53.1	120-18.3	9.5	1.4	10	232	7.3	0.0	0.4	0.6	0.02	C
9	1	12	41.4	35-58.5	120-18.1	13.2*	1.2	5	336	18.1	0.3	1.9		0.01	D
9	1	28	3.4	35-48.9	120-22.0	6.6	0.6	5	266	2.8				0.00	D
9	1	53	13.8	35-47.7	120-20.8	9.6	0.3	4	236	5.3				0.00	D
9	3	33	39.9	35-52.9	120-24.9	3.7	1.6	11	157	5.8	0.0	0.6	1.5	0.08	B
9	4	14	28.1	35-46.9	120-19.8	2.3	0.5	9	82	2.7	0.0	0.2	0.4	0.05	A
9	5	26	42.6	35-54.5	120-18.7	9.7*	0.9	6	315	9.4	0.1	0.9		0.02	D
9	6	45	10.9	35-55.2	120-18.6	11.6*	0.9	5	321	10.6	0.0	0.4		0.01	D
9	7	0	59.9	35-47.3	120-20.7	7.3	0.3	5	140	1.2				0.03	D
9	10	4	47.7	36- 1.4	119-58.6	5.0*	2.9	7	286	35.2	0.4	2.3		0.04	D
9	13	1	28.1	35-46.1	120-19.2	6.7	0.8	9	94	1.6	0.0	0.2	0.5	0.03	A
9	14	7	47.8	35-49.4	120-22.3	7.0	1.5	10	106	1.9	0.0	0.3	0.7	0.04	A
9	14	56	44.8	35-51.0	120-23.8	4.9	0.5	7	216	4.4	0.1	0.8	1.7	0.05	B
JUL 9	17	21	4.6	35-48.2	120-20.0	3.0	0.6	5	110	2.6				0.05	D
9	21	37	59.0	35-48.1	120-20.6	3.4	0.6	9	92	1.7	0.0	0.4	0.4	0.05	A
10	0	6	22.3	35-47.2	120-20.4	7.7	0.1	4	135	1.7				0.00	D
10	0	42	6.8	35-47.0	120-20.2	8.0	2.4	11	79	2.0	0.0	0.3	0.5	0.04	A
10	3	11	31.4	35-45.6	120-18.7	2.8	0.0	7	104	0.5	0.0	0.3	0.3	0.04	A
10	6	46	29.1	35-57.2	120-28.7	10.2	1.5	12	164	5.0	0.0	0.6	1.0	0.06	B
10	7	39	6.2	35-46.3	120-19.7	8.0	0.4	8	100	2.2	0.1	0.4	0.9	0.03	A
10	8	39	42.2	35-47.0	120-19.6	3.9	0.2	6	132	2.9	0.0	0.4	0.7	0.03	B
10	8	43	51.7	35-49.6	120-22.3	4.4	1.4	10	143	4.2	0.0	0.2	0.7	0.03	B
10	9	22	30.2	35-47.4	120-20.4	9.9	2.4	12	83	1.6	0.0	0.3	0.7	0.06	A
10	13	6	52.0	35-47.0	120-20.1	6.3	0.4	6	129	2.2	0.2	0.9	2.3	0.04	B
10	21	31	31.1	35-49.4	120-22.4	5.2	0.7	9	187	3.9	0.0	0.1	0.3	0.01	B
10	23	9	33.3	35-48.8	120-21.2	3.5	0.6	9	88	2.0	0.0	0.3	0.3	0.04	A
11	0	13	59.5	35-54.4	120-27.0	5.0*	0.5	7	315	12.2	1.5	6.9		0.06	D
11	0	31	1.8	35-46.8	120-20.1	7.3	0.8	8	115	2.5	0.0	0.2	0.5	0.02	A
11	0	56	56.6	35-52.9	120-26.0?	4.3	1.1	11	163	4.4	0.0	0.5	1.1	0.05	C
11	1	35	56.4	35-49.0	120-21.9	6.0	0.4	8	265	2.9	0.0	0.4	0.4	0.01	C
11	2	17	35.5	35-55.6	120-28.6	3.5	1.2	12	156	2.2	0.0	0.4	0.3	0.05	B
11	3	44	7.2	35-51.4	120-24.6?	2.6	0.6	11	153	5.9	0.0	0.3	0.4	0.05	C
11	3	46	45.8	35-46.9	120-19.5	4.0	0.1	8	124	3.0	0.0	0.3	0.8	0.04	B
11	3	55	54.2	35-51.2	120-24.4	0.6	1.4	10	152	5.4	0.4	0.7	1.4	0.03	B
11	5	15	2.2	35-48.0	120-21.1	9.1	1.8	11	81	1.2	0.1	0.5	1.0	0.08	A
11	5	40	35.3	35-46.1	120-19.3	7.6	0.4	10	70	1.5	0.0	0.3	0.6	0.04	A
11	7	16	41.4	35-55.6	120-29.6	6.4	0.8	10	290	3.0	0.4	1.7	1.6	0.04	C
11	8	47	11.8	35-56.6	120-29.6	3.6	0.7	9	297	4.5	1.1	4.9	1.1	0.09	D
11	9	3	57.5	35-51.3	120-24.0	1.7	2.2	12	148	5.0	0.0	0.3	0.4	0.05	B
11	10	21	7.2	35-57.6	120-30.1	9.1	1.9	12	160	6.5	0.0	0.4	0.7	0.04	B
11	12	17	0.7	35-47.6	120-20.7	8.4	0.0	8	178	1.2	0.1	0.5	0.9	0.03	B
11	15	26	45.0	35-48.7	120-21.7	5.8	0.7	9	175	2.4	0.0	0.2	0.4	0.03	B
11	15	26	58.4	35-48.8	120-21.8	5.5	0.8	9	177	2.5	0.0	0.1	0.2	0.01	B

TABLE 2 (CONTINUED)

1966	HR	MN	SEC	LAT N	LONG W	DEPTH	MAG	NO	GAP	DMIN	ERT	ERH	ERZ	MD	Q
JUL 11	17	46	41.8	35-47.7	120-20.8	8.4	1.2	8	152	5.3	0.0	0.2	0.5	0.02	B
11	20	41	10.9	35-45.4	120-19.4	7.2	1.6	9	77	1.0	0.0	0.2	0.5	0.04	A
11	21	42	25.2	35-54.6	120-27.0	2.0	2.3	10	156	11.4	0.1	0.4	0.9	0.02	B
11	21	52	55.2	35-58.9	120-27.8	5.0*	1.9	10	177	18.5	0.0	0.9		0.09	C
11	23	45	43.3	35-45.6	120-18.5	4.8	0.6	6	85	5.5	0.2	0.9	5.9	0.03	C
12	1	19	5.6	35-47.3	120-19.8	3.6	0.8	9	86	2.5	0.0	0.2	0.3	0.03	A
12	1	38	25.9	35-47.9	120-21.2	8.5	1.3	9	160	1.0	0.1	0.4	0.8	0.03	B
12	4	25	12.8	35-47.8	120-20.6	2.2	0.2	10	86	1.4	0.0	0.3	0.5	0.08	A
12	6	14	16.7	35-47.9	120-19.9	1.6	0.4	8	100	2.4	0.0	0.3	0.8	0.05	A
12	6	27	50.5	35-50.6	120-23.7	2.0	0.5	8	210	4.1	0.0	0.2	0.2	0.01	B
12	8	24	45.3	35-51.2	120-24.5	7.8	1.2	8	220	8.3	0.0	0.3	0.7	0.02	B
12	11	37	27.8	35-45.6	120-19.8	6.5	0.4	7	105	1.6	0.0	0.2	0.5	0.02	A
12	19	53	6.4	35-44.9	120-17.9	10.9	1.2	8	103	1.5	0.2	0.9	2.4	0.09	B
12	21	17	32.2	35-44.5	120-18.0	9.7	0.3	5	173	1.9				0.01	D
12	22	32	43.5	35-47.2	120-20.9	9.5	1.0	7	144	0.9	0.0	0.3	0.4	0.02	B
13	0	1	53.2	35-47.0	120-18.7	0.8	0.2	4	127	3.0				0.00	D
13	4	20	2.7	35-51.3	120-24.3	2.3	2.2	11	146	5.4	0.0	0.2	0.2	0.02	B
13	4	21	30.3	35-52.5	120-25.7	0.6	0.5	9	308	8.4	0.8	1.9	1.9	0.06	C
13	4	37	46.3	35-49.2	120-22.1	6.3	0.8	10	136	1.9	0.0	0.3	0.5	0.03	B
13	5	30	12.8	35-52.1	120-24.9	9.1	1.3	8	304	6.9	0.3	1.4	1.1	0.02	C
13	6	44	3.8	35-53.0	120-26.0	10.5	1.9	10	151	9.2	0.0	0.3	0.7	0.03	B
13	9	30	15.3	35-46.0	120-19.2	7.7	0.9	9	72	1.4	0.0	0.2	0.6	0.04	A
13	9	52	13.4	35-48.6	120-21.1	4.0	0.7	10	89	2.1	0.0	0.2	0.4	0.04	A
13	12	7	36.0	35-48.1	120-20.6	4.1	0.2	8	116	1.8	0.0	0.5	0.9	0.05	A
13	12	36	25.3	35-45.6	120-18.6	5.0	0.2	6	83	5.1	0.1	0.4	1.9	0.03	B
13	16	44	28.9	35-56.2	120-27.9	5.0*	2.2	6	161	22.4	0.0	0.6		0.03	C
13	18	17	43.6	35-57.8	120-29.9	14.3	2.2	11	162	6.7	0.0	0.6	0.5	0.05	B
13	18	53	10.4	35-58.6	120-28.9	5.0*	1.4	7	170	19.8	0.0	1.1		0.05	C
14	6	29	58.2	35-51.3	120-24.0	1.9	1.6	14	143	5.0	0.0	0.2	0.3	0.05	B
14	8	31	31.6	35-45.2	120-18.2	8.9	0.6	8	75	0.8	0.0	0.2	0.7	0.03	A
JUL 14	9	7	17.1	35-45.5	120-19.5	7.5	0.4	8	99	1.2	0.1	0.7	1.5	0.06	A
14	9	28	7.4	35-48.2	120-20.6	3.2	0.2	8	121	1.8	0.0	0.4	0.4	0.05	B
14	14	2	0.2	35-48.1	120-20.6	3.2	0.3	8	117	1.7	0.0	0.4	0.4	0.05	A
14	17	0	32.8	35-48.5	120-21.1	4.3	0.6	9	119	2.0	0.0	0.2	0.4	0.03	A
14	18	9	18.3	35-49.3	120-22.3	5.8	1.2	14	88	2.0	0.0	0.2	0.4	0.04	A
14	23	4	37.4	35-52.9	120-25.6	3.6	2.88	12	144	4.9	0.0	0.2	0.2	0.03	B
15	0	20	21.1	35-48.9	120-23.2	3.7	1.4	6	275	3.8	0.8	4.2	1.2	0.07	D
15	0	24	29.5	35-52.8	120-25.7	3.0	1.4	11	142	4.9	0.0	0.4	0.5	0.04	B
15	0	30	40.6	35-47.6	120-20.4	1.8	2.0	11	87	1.6	0.0	0.2	0.4	0.06	A
15	1	43	9.3	35-50.6	120-23.9?	3.4	1.2	5	304	4.3				0.01	D
15	1	51	15.9	35-50.9	120-24.2	5.2	1.0	6	306	4.9	1.0	4.6	2.3	0.04	D
15	2	13	16.2	35-47.4	120-21.2	12.0	0.6	5	147	0.4				0.01	D
15	4	4	1.6	35-47.5	120-20.6	7.5	1.6	13	82	1.2	0.0	0.3	0.6	0.06	A
15	6	21	27.3	35-56.8	120-29.1	9.7	1.5	14	117	1.3	0.0	0.3	0.4	0.04	A
15	11	13	7.6	35-49.4	120-22.6	7.5	0.7	7	276	4.0	0.3	1.5	1.5	0.03	C
15	19	24	35.1	35-50.4	120-23.3	2.4	1.4	13	137	3.3	0.0	0.3	0.4	0.05	B
15	19	28	21.1	35-48.3	120-20.7	3.1	0.7	9	95	1.9	0.0	0.2	0.2	0.04	A
16	3	3	6.3	35-45.9	120-19.5	7.1	1.3	11	72	1.6	0.0	0.4	0.9	0.07	A
16	3	6	47.6	35-48.0	120-20.2	2.6	2.38	13	100	2.2	0.0	0.3	0.4	0.08	A
16	3	22	40.5	35-46.8	120-19.6	3.7	-0.1	7	123	3.0	0.0	0.3	0.9	0.03	B
16	4	8	42.3	35-44.6	120-17.8	10.5	0.7	8	70	2.0	0.0	0.2	0.7	0.02	A
16	4	39	55.9	35-48.6	120-20.6	4.4	0.3	8	129	2.5	0.2	1.0	2.0	0.06	B
16	4	47	26.3	35-48.0	120-20.2	2.6	0.4	10	99	2.1	0.0	0.2	0.2	0.04	A
16	5	42	9.9	35-50.5	120-23.2	2.4	2.2	14	139	3.3	0.0	0.2	0.2	0.04	B
16	7	5	23.9	35-55.7	120-28.8	3.6	1.9	15	100	1.2	0.0	0.3	0.2	0.04	A
16	7	45	57.0	35-47.9	120-20.4	3.1	0.5	11	93	1.8	0.0	0.2	0.2	0.03	A
16	17	13	16.4	35-47.5	120-20.6	8.2	0.8	9	81	1.2	0.1	0.3	0.7	0.03	A
16	17	51	39.9	35-51.6	120-24.3	2.4	0.7	10	143	5.7	0.0	0.1	0.1	0.02	B
16	19	7	39.5	35-52.8	120-25.9	3.4	1.2	13	140	4.7	0.0	0.3	0.4	0.03	B
16	19	31	1.1	35-50.0	120-22.6	3.5	0.5	7	282	5.1	0.4	2.2	0.6	0.05	C

TABLE 2 (CONTINUED)

1966	HR	MN	SEC	LAT N	LONG W	DEPTH	MAG	NO	GAP	DMIN	ERT	ERH	ERZ	MD	Q
JUL 16	20	24	32.1	35-53.2	120-26.4	8.9	1.2	11	140	3.5	0.0	0.2	0.6	0.02	B
16	23	26	22.4	35-47.5	120-20.8	9.3	1.6	11	104	1.0	0.0	0.3	0.7	0.05	A
17	7	25	20.4	35-51.9	120-24.8	2.5	1.8	14	143	6.6	0.0	0.1	0.2	0.02	B
17	8	43	46.4	35-45.1	120-19.2	5.7	0.9	12	65	0.8	0.0	0.3	0.7	0.06	A
17	9	5	50.1	35-49.7	120-22.8	6.6	0.6	7	294	4.7	0.5	2.2	1.7	0.03	C
17	9	51	30.8	35-48.3	120-20.8	4.1	0.5	9	136	1.9	0.0	0.4	0.6	0.03	B
17	10	47	1.9	35-47.0	120-19.3	2.3	0.8	11	84	3.2	0.0	0.3	0.5	0.08	A
17	10	50	32.4	35-48.0	120-21.2	9.6	1.8	15	82	1.1	0.0	0.3	0.5	0.05	A
17	15	4	5.3	35-48.3	120-20.8	3.1	0.5	7	153	3.1	0.0	0.5	0.6	0.04	B
17	20	45	24.3	35-52.9	120-26.0	9.9	1.0	14	140	4.4	0.0	0.3	0.6	0.03	B
17	21	16	3.0	35-55.7	120-28.7	3.9	1.2	15	105	1.4	0.0	0.2	0.3	0.04	A
17	22	39	49.8	35-48.8	120-21.9	7.3	0.8	11	123	2.6	0.0	0.2	0.6	0.04	B
18	0	31	2.7	35-54.6	120-27.5	4.2	1.8	12	134	1.0	0.0	0.2	0.3	0.03	B
18	1	5	28.8	35-47.4	120-20.7	8.9	0.4	7	159	1.1	0.0	0.2	0.5	0.01	B
18	1	55	20.2	35-57.7	120-30.8	14.5	1.6	13	145	4.0	0.0	0.5	0.4	0.06	B
18	4	50	16.0	35-47.2	120-20.1	6.9	0.3	6	138	2.0	0.0	0.3	0.7	0.01	B
18	5	2	2.8	35-48.9	120-21.7	6.2	0.4	7	262	2.7	0.1	0.6	0.7	0.02	C
18	5	13	10.5	35-45.4	120-18.9	5.1	0.2	6	86	5.1	0.1	0.5	2.2	0.04	B
18	6	1	33.7	35-55.8	120-28.2	10.0	1.7	14	126	2.1	0.0	0.2	0.3	0.03	B
18	12	45	41.3	35-48.0	120-21.0	9.3	0.8	11	111	1.2	0.0	0.3	0.6	0.04	A
18	14	13	59.3	36- 1.9	120- 8.6	5.0*	1.4	9	263	26.6	0.1	0.8		0.04	D
18	23	48	49.2	35-47.3	120-20.5	7.8	1.2	12	79	1.4	0.0	0.3	0.7	0.06	A
19	0	22	16.6	35-48.1	120-20.5	3.5	0.6	11	95	1.8	0.0	0.1	0.2	0.03	A
19	4	21	50.4	35-47.2	120-19.6	3.8	0.5	10	86	2.8	0.0	0.4	1.4	0.07	A
19	5	51	20.0	35-47.9	120-21.1	9.4	0.7	11	110	1.0	0.0	0.3	0.7	0.04	A
19	6	16	27.3	35-47.4	120-20.5	7.9	0.5	7	157	1.4	0.1	0.4	0.8	0.02	B
19	6	45	11.2	35-47.9	120-21.0	7.7	0.6	7	216	1.1	0.0	0.2	0.4	0.01	B
19	14	50	4.0	35-53.5	120-26.8	10.9	1.2	10	148	2.8	0.1	0.7	1.4	0.04	B
19	16	21	24.9	35-51.5	120-24.4	2.7	0.8	10	157	5.8	0.0	0.3	0.3	0.04	B
19	23	2	6.6	35-44.7	120-17.9	12.0	0.7	8	91	1.8	0.1	0.4	1.4	0.04	A
JUL 20	0	23	21.1	35-48.7	120-21.7	7.1	0.6	7	261	2.4	0.0	0.3	0.3	0.01	C
20	7	3	28.1	35-47.1	120-20.1	7.3	0.8	10	80	2.2	0.0	0.2	0.5	0.03	A
20	10	48	27.4	35-52.7	120-25.4	1.6	0.8	11	166	5.2	0.0	0.2	0.3	0.03	B
20	23	37	37.6	35-46.2	120-19.5	8.5	0.4	8	97	1.9	0.1	0.3	0.7	0.02	A
21	5	43	59.0	35-56.1	120-19.7	5.0*	0.7	9	311	11.7	1.0	4.4		0.06	D
21	9	12	38.4	35-49.9	120-23.0	4.8	0.4	10	135	2.8	0.0	0.4	0.7	0.05	B
21	11	29	50.3	35-44.1	120-17.0	10.9	0.9	10	81	1.7	0.0	0.3	0.7	0.04	A
21	13	50	0.1	35-46.9	120-20.2	7.7	1.6	12	80	2.1	0.0	0.3	0.6	0.05	A
21	13	56	43.8	35-50.4	120-23.6	9.1	0.9	10	148	6.3	0.0	0.3	0.8	0.03	B
21	16	19	48.3	35-51.2	120-24.0	2.5	2.38	13	147	4.9	0.0	0.2	0.3	0.05	B
21	20	10	49.8	35-59.5	120-32.2	5.0*	1.9	7	334	27.5	2.1	9.3		0.04	D
21	21	23	49.5	35-57.0	120-29.0	9.0	2.78	13	161	2.8	0.0	0.3	0.4	0.03	B
22	0	35	47.0	35-50.9	120-24.0	2.7	0.7	9	153	4.6	0.0	0.2	0.3	0.02	B
22	2	35	54.2	35-47.1	120-20.8	11.4	0.7	7	132	1.2	0.3	1.2	2.7	0.06	B
22	2	42	29.0	35-58.3	120-31.6	6.7	1.6	11	160	5.9	0.0	0.4	0.5	0.03	B
22	6	47	20.5	35-49.4	120-22.1	8.0	1.1	10	147	3.6	0.0	0.2	0.4	0.02	B
22	11	27	29.1	35-56.8	120-29.1	9.4	1.4	12	160	2.5	0.0	0.7	0.8	0.06	B
22	13	40	6.6	35-54.9	120-27.5	9.5	1.0	11	191	1.3	0.1	0.6	1.2	0.04	B
22	16	42	52.0	35-44.9	120-18.4	2.3	0.7	8	105	1.0	0.0	0.3	0.4	0.04	A
23	2	43	56.4	35-51.2	120-23.9	1.8	2.68	12	148	4.7	0.0	0.2	0.3	0.04	B
23	2	48	46.5	35-49.8	120-22.4	2.0*	0.4	6	279	1.9	0.8	3.7		0.09	D
23	3	2	39.5	35-52.6	120-25.4	1.0	1.3	10	165	5.4	0.2	0.3	0.8	0.05	B
23	8	57	60.0	35-49.9	120-23.0?	4.6	0.3	10	135	2.7	0.0	0.4	0.7	0.05	B
23	15	5	42.7	35-58.4	120-31.4	11.5	1.5	11	158	5.9	0.0	0.5	0.5	0.03	B
23	16	21	30.0	35-51.1	120-24.4	4.4	0.9	11	153	5.4	0.0	0.4	1.0	0.06	B
23	20	47	3.6	35-46.8	120-19.6	3.0	0.1	7	151	2.9	0.0	0.4	0.4	0.04	B
23	22	18	3.1	35-49.1	120-21.3	4.0	0.3	5	263	3.0				0.05	D
23	23	15	16.4	35-55.4	120-28.3	3.1	1.9	12	156	2.0	0.0	0.5	0.4	0.06	B
23	23	40	17.7	35-44.2	120-17.7	13.4	1.2	9	71	2.3	0.1	0.3	0.9	0.04	A
24	0	4	2.3	35-44.2	120-17.6	11.1	0.9	8	73	2.2	0.1	0.4	1.3	0.03	A

TABLE 2 (CONTINUED)

1966	HR	MN	SEC	LAT N	LONG W	DEPTH	MAG	NO	GAP	DMIN	ERT	ERH	ERZ	MD	Q
JUL 24	1	25	11.9	35-48.9	120-21.3	4.5	0.3	6	259	2.6	0.4	2.3	2.7	0.06	C
24	3	30	38.6	35-55.7	120-28.1	5.0*	1.0	10	162	15.0	0.0	0.7		0.05	C
24	5	49	1.1	35-53.1	120-26.7	0.1	1.0	10	162	10.2	0.1	0.6	0.4	0.03	B
24	6	42	43.1	35-52.7	120-25.3	1.7	1.0	8	307	8.1	0.2	0.9	0.3	0.03	C
24	6	56	52.8	35-47.4	120-20.1	6.0	0.6	7	85	2.1	0.2	0.8	2.3	0.06	B
24	8	22	5.7	35-48.0	120-21.0	8.7	0.7	8	225	1.1	0.0	0.3	0.5	0.01	B
24	10	32	2.3	35-42.0	120-15.6	8.9	1.4	9	101	3.0	0.1	0.5	1.4	0.05	A
24	21	27	1.9	35-50.2	120-23.4	6.5	0.6	9	284	3.4	0.1	0.7	0.7	0.02	C
24	22	34	2.7	35-44.3	120-17.6	11.0	0.3	8	74	2.3	0.1	0.4	1.4	0.04	A
25	0	17	25.1	36- 1.9	120-35.2	5.0*	2.1	10	178	14.1	0.0	0.9		0.05	C
25	4	2	0.1	35-52.1	120-24.9	1.7	1.2	6	305	6.9	1.0	3.7	1.9	0.02	D
25	4	45	12.4	35-50.8	120-24.0	7.2	0.9	6	294	4.6	0.1	0.8	0.7	0.01	C
25	11	8	48.4	35-51.6	120-25.0	5.5	0.7	8	302	6.5	0.4	1.7	1.2	0.03	C
25	22	49	46.5	35-59.5	120-18.2	5.0*	0.9	9	230	18.3	0.2	1.8		0.10	D
26	0	41	59.5	35-56.8	120-28.8	5.0*	2.0	9	166	17.2	0.0	0.6		0.03	C
26	1	31	32.3	35-49.5	120-22.1	5.3	1.4	9	240	1.6	0.1	0.5	0.6	0.03	C
26	1	45	1.3	35-58.0	120-29.5	5.0*	2.0	10	165	19.6	0.0	0.7		0.05	C
26	5	26	11.0	35-49.1	120-21.7	4.0	1.2	8	200	1.6	0.1	0.7	0.8	0.04	B
26	11	40	38.5	35-56.6	120-28.0	5.0*	2.0	10	163	16.2	0.0	0.4		0.03	C
26	22	13	24.5	35-53.7	120-26.4	10.5	1.7	10	158	10.5	0.0	0.4	0.8	0.03	B
27	8	5	33.9	35-54.3	120-27.1	5.0*	2.4	10	161	12.0	0.0	0.3		0.03	C
27	8	12	0.4	35-54.2	120-27.0	5.0*	3.08	10	161	11.8	0.0	0.2		0.02	C
27	10	8	25.7	35-48.3	120-20.9	3.7	0.7	9	144	1.8	0.0	0.4	0.3	0.04	B
27	11	47	21.1	35-51.1	120-23.6?	5.0*	0.7	9	296	4.4	0.9	4.4		0.07	D
27	12	21	54.9	35-52.9	120-26.1	7.7	2.3	10	159	9.3	0.0	0.5	1.3	0.04	B
27	15	29	17.9	35-51.2	120-24.0	5.0*	0.7	9	297	4.9	1.0	4.8		0.09	D
27	17	27	50.1	35-55.8	120-28.3	5.0*	1.6	10	162	15.2	0.0	0.8		0.06	C
28	0	23	57.6	35-59.9	120-32.8	5.0*	2.1	10	171	19.1	0.0	0.7		0.04	C
28	5	51	18.4	35-49.0	120-21.7	4.6	1.2	9	199	1.9	0.1	0.6	0.7	0.03	B
28	10	15	48.4	35-51.4	120-23.8?	5.0*	1.2	9	298	4.9	1.6	7.1		0.09	D
JUL 28	16	20	55.9	35-47.7	120-20.2	3.5	1.0	9	90	1.8	0.0	0.2	0.2	0.03	A
28	21	7	32.2	35-46.0	120-19.2	8.0	1.6	9	88	1.4	0.0	0.2	0.6	0.03	A
29	13	20	11.3	35-57.8	120-30.6	5.0*	2.0	9	168	20.3	0.0	0.4		0.03	C
29	14	5	21.6	35-54.6	120-27.1	5.0*	2.0	9	160	12.5	0.0	0.4		0.04	C
29	15	25	44.1	35-47.6	120-20.9	8.0	2.0	9	78	0.8	0.0	0.4	0.8	0.05	A
29	15	55	42.6	35-47.7	120-20.9	7.8	1.1	8	109	0.9	0.1	0.4	0.9	0.02	A
29	16	1	26.6	35-47.7	120-21.1	8.4	2.1	9	95	0.6	0.0	0.3	0.5	0.03	A
30	8	58	26.4	35-55.7	120-28.8	5.0*	2.1	9	166	15.7	0.0	0.7		0.05	C
30	9	11	5.5	35-56.1	120-28.5	5.0*	1.3	9	162	15.8	0.0	0.4		0.03	C
30	12	41	37.7	35-51.2	120-24.4	2.6	1.7	9	153	5.4	0.0	0.2	0.3	0.02	B
30	17	1	36.9	35-47.9	120-21.2	8.8	1.4	8	161	1.0	0.4	1.4	2.8	0.09	C
30	17	3	5.3	35-49.9	120-22.5?	2.7	1.4	8	272	2.1	0.1	0.6	0.2	0.03	C
30	21	44	15.3	35-48.4	120-20.6	3.3	0.8	7	129	2.1	0.0	0.3	0.3	0.03	B
30	22	38	16.4	35-48.3	120-20.3	3.4	0.2	6	106	2.3	0.0	0.6	0.8	0.06	B
31	0	38	41.3	35-47.7	120-20.9	9.1	1.8	9	109	1.0	0.1	0.4	0.8	0.03	A
31	1	58	49.1	35-49.6	120-24.0	2.2	0.1	6	271	4.2	0.4	1.9	1.0	0.04	C
31	3	13	38.9	35-48.8	120-21.2	3.3	1.0	8	171	2.0	0.0	0.4	0.3	0.04	B
31	3	59	10.5	35-47.5	120-20.7	7.4	0.6	8	83	1.1	0.0	0.3	0.7	0.02	A
31	5	5	31.2	35-45.6	120-19.6	8.2	0.3	8	101	1.4	0.1	0.4	1.0	0.04	A
31	6	43	55.5	35-47.3	120-20.4	8.8	0.0	9	80	1.6	0.1	0.4	0.9	0.03	A
31	7	57	38.4	35-54.7	120-26.7	5.0*	0.5	9	316	12.2	1.8	8.1		0.09	D
31	10	38	56.8	35-53.1	120-26.3	9.0	0.9	9	311	9.8	0.7	3.2	2.1	0.05	D
31	12	59	6.4	35-45.5	120-19.6	6.8	0.3	9	101	1.4	0.1	0.4	1.0	0.05	A
31	16	47	23.7	35-56.7	120-28.0	5.0*	2.0	10	164	16.3	0.0	0.8		0.06	C
31	17	55	44.5	35-44.6	120-17.7	12.4	0.4	9	72	2.1	0.2	0.5	1.9	0.06	A
AUG 1	3	13	38.7	35-48.3	120-20.8	3.0	-0.1	7	133	1.8	0.1	0.8	0.9	0.10	B
1	4	42	35.1	35-47.0	120-20.4	8.9	1.7	9	95	1.7	0.1	0.6	1.4	0.05	A
1	7	15	43.0	35-48.2	120-21.0	3.0	-0.1	9	147	1.5	0.0	0.7	0.7	0.11	B
1	7	53	28.1	35-57.0	120-28.5	5.0*	1.7	10	164	17.2	0.0	0.5		0.04	C
1	11	39	2.7	35-48.0	120-21.3	10.6	1.5	9	171	1.0	0.2	0.8	1.6	0.05	B

TABLE 2 (CONTINUED)

1966	HR	MN	SEC	LAT N	LONG W	DEPTH	MAG	NO	GAP	DMIN	ERT	ERH	ERZ	MD	Q
AUG 1	11	39	53.5	35-46.6	120-20.4	11.9	1.0	9	111	2.2	0.3	0.8	2.2	0.06	B
1	12	5	33.9	35-47.8	120-21.0	10.1	2.7B	10	93	0.9	0.0	0.5	0.8	0.06	A
1	12	8	33.9	35-47.9	120-21.1	9.9	0.3	9	148	1.0	0.1	0.4	0.9	0.03	B
1	12	53	36.8	35-49.1	120-22.6	11.0	0.2	8	236	2.6	0.7	2.6	4.3	0.10	D
1	14	1	49.6	35-54.0	120-26.7?	3.2	1.9	9	160	11.3	0.0	0.5	0.6	0.03	C
1	18	44	14.3	35-48.3	120-20.6	3.5	0.1	6	124	2.0	0.0	0.3	0.3	0.02	B
2	6	31	28.6	35-50.9	120-23.9	3.0	0.8	8	295	4.5	0.1	0.8	0.3	0.02	C
2	6	32	7.3	35-47.2	120-20.4	8.0	0.0	7	138	1.6	0.1	0.5	1.1	0.03	B
2	11	11	27.8	35-47.8	120-21.2	10.1	0.8	8	147	0.8	0.2	0.7	1.6	0.04	B
2	20	9	36.6	35-47.3	120-20.7	9.0	1.6	9	91	1.1	0.1	0.4	1.0	0.03	A
3	0	27	10.2	35-59.0	120- 2.9	5.0*	2.6	10	275	25.0	0.2	1.2		0.04	D
3	1	43	2.1	36- 0.9	120- 1.2	5.0*	2.6	9	280	29.4	0.5	2.6		0.06	D
3	5	36	11.1	35-51.6	120-24.1?	5.0*	0.8	9	299	5.3	1.5	6.7		0.08	D
3	8	9	43.4	36- 0.2	120-32.7	5.0*	2.0	10	170	18.8	0.0	0.6		0.04	C
3	9	41	37.5	35-56.1	120-27.9	5.0*	2.9B	9	161	18.7	0.0	0.5		0.04	C
3	12	39	5.8	35-48.4	120-21.4	5.1	3.4B	10	132	1.7	0.0	0.2	0.3	0.02	B
4	8	5	32.6	35-46.8	120-20.3	8.8	0.0	8	113	2.2	0.1	0.4	0.9	0.03	A
4	11	20	5.8	35-49.2	120-21.6	4.7	0.3	7	267	3.3	0.1	0.5	0.5	0.02	C
4	19	56	55.4	35-48.9	120-22.2	6.9	0.6	8	267	3.0	0.1	0.7	0.7	0.02	C
4	23	10	6.8	35-47.4	120-20.4	2.7	0.1	7	227	4.6	0.1	0.5	0.4	0.02	C
5	8	24	10.8	35-48.5	120-21.5	7.9	0.5	7	257	7.2	0.0	0.1	0.2	0.00	C
5	8	43	28.1	35-46.3	120-19.6	7.5	0.0	7	193	2.1	0.0	0.3	0.6	0.02	B
5	9	12	6.9	35-48.1	120-20.6	2.2	0.6	8	148	3.3	0.0	0.3	0.4	0.04	B
5	11	50	44.9	35-50.7	120-22.6	2.2	0.6	8	288	2.5	0.2	1.2	0.4	0.03	C
5	13	26	15.1	35-45.1	120-18.3	10.3	1.2	8	76	0.8	0.1	0.5	1.3	0.05	A
5	15	5	39.3	35-49.3	120-22.5	8.4	0.9	6	273	9.2	0.2	0.9	1.4	0.02	C
5	19	37	28.3	35-47.7	120-20.8	8.0	1.0	7	156	4.1	0.0	0.3	0.7	0.02	B
5	21	41	7.4	35-47.5	120-20.5	8.6	1.0	8	146	4.5	0.0	0.2	0.4	0.01	B
6	4	45	8.9	35-52.8	120-26.9	10.0	1.3	7	311	10.2	3.1	12.4	9.8	0.10	D
6	7	7	45.4	35-49.3	120-24.0?	0.3	0.4	8	265	4.4	0.8	3.7	2.3	0.18	D
AUG 6	8	31	11.3	35-48.4	120-21.1	2.1	0.2	7	251	6.7	0.1	0.6	0.5	0.03	C
6	9	42	40.0	35-51.8	120-24.3?	5.0*	0.5	8	301	5.9	1.5	6.9		0.07	D
6	9	47	17.2	35-52.5	120-25.4	9.6	1.1	8	306	8.0	0.3	1.4	1.2	0.02	C
6	10	32	3.7	35-48.2	120-20.8	2.6	0.8	8	153	3.2	0.0	0.3	0.4	0.03	B
6	10	35	9.6	35-51.3	120-23.8	2.1	1.9	9	149	4.8	0.0	0.2	0.3	0.02	B
6	12	26	0.4	35-48.0	120-21.1	3.4	0.4	6	245	6.1	0.0	0.3	0.2	0.01	C
6	17	9	11.6	35-45.6	120-19.1	6.6	0.4	6	174	0.8	0.2	1.1	2.1	0.06	C
6	18	41	57.1	35-53.7	120-26.0	5.0*	0.8	7	315	10.1	1.3	5.9		0.06	D
6	19	28	44.5	35-53.9	120-26.7	5.0*	0.9	8	314	11.1	0.5	2.4		0.03	D
6	21	4	55.9	35-55.3	120-27.3	8.6	2.9B	9	317	13.6	0.5	2.5		0.04	D
7	2	1	43.6	35-47.1	120-20.4	10.6	0.8	9	87	1.7	0.1	0.5	1.3	0.04	A
7	2	4	4.1	35-47.5	120-20.9	7.8	0.4	7	165	0.8	0.1	0.6	1.0	0.02	B
7	7	26	58.9	36- 3.6	120-30.6	11.5*	1.5	8	338	29.1	1.9	8.8		0.04	D
7	11	59	34.6	35-51.8	120-24.3?	5.0*	0.8	9	301	5.8	1.3	5.8		0.07	D
7	16	33	30.8	35-46.1	120-19.3	7.0	-0.1	8	95	1.6	0.0	0.2	0.6	0.02	A
7	16	33	32.4	35-47.3	120-20.7	11.2	0.8	9	88	1.1	0.5	1.5	3.9	0.11	B
7	17	3	24.3	35-55.8	120-28.0	5.0*	3.0B	10	161	15.1	0.0	0.6		0.05	C
8	0	52	37.6	35-47.9	120-21.1	8.5	0.9	7	231	1.0	0.1	0.5	0.8	0.02	C
8	6	0	48.4	35-49.3	120-21.8	4.6	0.7	6	269	3.4	0.1	1.0	0.8	0.02	C
8	9	32	32.9	35-48.7	120-22.0	7.4	0.4	6	262	2.4	0.2	0.9	1.1	0.02	C
8	11	52	34.5	35-51.9	120-24.1?	5.0*	0.6	7	301	5.7	1.6	7.2		0.07	D
8	12	7	11.1	35-46.1	120-19.5	7.9	0.0	6	94	3.9	0.1	0.4	1.3	0.02	B
8	17	24	26.9	35-52.9	120-25.2?	1.5	0.6	8	307	8.2	0.2	1.0	0.4	0.03	C
8	19	15	43.0	35-52.5	120-25.2	9.6	0.9	7	306	10.9	0.8	3.7	2.5	0.04	D
9	3	13	45.7	35-47.0	120-19.6	3.0	0.3	6	131	3.0	0.1	0.8	1.2	0.07	B
9	6	2	42.7	35-47.4	120-19.6	3.7	1.8	8	90	2.7	0.0	0.5	0.9	0.06	A
10	8	57	1.8	35-48.4	120-20.8	4.4	0.8	8	135	2.0	0.0	0.4	0.9	0.03	B
10	15	52	28.4	35-46.1	120-19.4	8.6	0.4	7	94	1.7	0.2	0.7	1.6	0.05	A
11	10	25	38.6	35-51.9	120-24.9	7.4	0.8	7	304	6.8	0.2	1.1	0.8	0.01	C
11	18	26	55.5	35-52.6	120-26.0	0.7	0.7	7	310	8.8	0.4	1.1	1.1	0.03	C

TABLE 2 (CONTINUED)

1966	HR	MN	SEC	LAT N	LONG W	DEPTH	MAG	NO	GAP	DMIN	ERT	ERH	ERZ	MD	Q
AUG 11	20	38	8.2	35-51.5	120-24.2	2.5	2.1B	8	151	5.4	0.0	0.2	0.2	0.02	B
12	3	42	0.4	35-51.9	120-25.1	5.8	1.1	7	304	7.0	0.7	3.1	2.0	0.04	D
12	11	56	17.1	35-45.1	120-18.1	8.6	0.1	6	128	1.0	0.1	0.4	1.0	0.02	B
12	20	27	45.7	35-46.1	120-19.6	9.2	0.2	6	97	1.9	0.3	1.0	2.6	0.05	B
12	20	28	31.9	35-46.2	120-20.0	10.9	0.4	5	106	2.5				0.03	D
12	21	14	10.7	35-48.5	120-21.2	3.6	0.8	8	170	1.9	0.0	0.5	0.4	0.05	B
13	3	47	6.2	35-50.7	120-23.6	2.2	0.5	7	292	6.8	0.5	2.1	1.1	0.03	C
13	8	20	23.7	35-51.5	120-24.9	9.1	1.4	8	302	6.4	0.4	1.7	1.7	0.03	C
13	8	24	58.9	35-52.4	120-25.9	6.1	1.2	8	309	8.5	0.5	2.2	1.4	0.03	C
13	9	11	23.9	35-44.0	120-16.8	5.4	0.6	7	131	1.5	0.0	0.3	0.5	0.03	B
13	9	15	4.8	35-44.1	120-16.6	4.6	0.0	7	135	1.8	0.0	0.4	0.7	0.04	B
13	11	21	31.8	35-44.7	120-17.7	12.0	0.2	7	120	2.0	0.2	0.4	1.4	0.03	A
13	12	18	32.7	35-52.1	120-25.1	7.2	1.8	8	306	7.2	0.5	2.3	1.6	0.03	C
13	15	44	12.1	35-53.5	120-27.5	0.5*	1.0	8	317	11.7	0.3	1.4		0.05	D
13	22	13	11.6	35-57.8	120-32.4	5.0*	2.2	6	192	22.4	0.0	1.2		0.03	C
13	22	35	14.1	35-52.2	120-25.9	6.8	1.0	6	316	8.3	0.3	1.5	0.8	0.01	C
14	10	49	20.2	35-56.5	120-29.0	5.0*	1.3	7	164	17.0	0.0	0.7		0.04	C
14	14	58	4.8	35-46.1	120-19.5	7.2	0.3	4	94	1.7				0.00	D
14	18	37	29.8	35-51.3	120-27.8?	0.2	1.8	5	201	10.2				0.11	D
15	10	12	20.5	35-44.9	120-18.0	9.8	0.2	7	84	1.4	0.0	0.2	0.6	0.02	A
15	12	27	36.1	35-57.5	120-29.1	5.0*	2.5	10	163	18.4	0.0	0.6		0.04	C
15	19	5	43.6	35-48.9	120-21.5	4.6	0.6	5	271	2.6				0.01	D
16	5	21	7.0	35-50.8	120-23.9	2.6	0.9	8	294	4.4	0.1	0.6	0.2	0.01	C
16	13	0	24.2	35-55.1	120-27.3	7.4*	1.0	7	321	13.4	0.2	1.0		0.01	D
16	15	48	11.8	35-48.2	120-20.9	2.2	1.0	6	156	3.2	0.0	0.3	0.4	0.02	B
16	23	11	30.8	35-58.3	120-29.6	5.0*	1.4	8	170	20.0	0.0	1.0		0.04	C
17	4	39	34.1	35-45.6	120-18.9	10.0	0.9	9	86	0.5	0.2	0.7	2.1	0.08	B
17	9	35	14.8	35-53.1	120-25.9	8.0	0.7	7	309	9.3	0.5	2.5	1.2	0.02	C
17	11	24	12.4	36- 2.6	120-35.2	5.0*	0.9	6	334	34.7	7.8	33.6		0.08	D
17	23	39	6.0	35-48.1	120-20.3	2.3	0.1	7	206	2.1	0.0	0.4	0.4	0.03	B
AUG 18	0	31	29.8	35-44.6	120-18.0	11.3	0.4	7	126	1.8	0.2	0.5	1.6	0.04	B
18	0	53	1.6	35-44.4	120-18.4	12.6	1.2	8	134	1.8	0.0	0.2	0.5	0.01	B
19	7	26	12.3	35-52.2	120-25.4	1.2	1.9	10	157	7.7	0.2	0.5	0.9	0.04	B
19	22	51	19.6	35-52.6	120-27.8?	0.1	3.3B	6	193	11.2	0.8	6.3	1.9	0.08	D
20	3	43	56.4	35-51.3	120-23.9	1.8	1.3	9	296	4.8	0.3	1.4	0.7	0.02	C
20	4	6	59.5	35-51.8	120-24.5	1.5	1.5	10	152	6.2	0.0	0.3	0.4	0.04	B
20	4	22	56.7	35-51.3	120-23.5?	5.0*	0.7	6	294	4.4	3.8	16.9		0.10	D
20	9	10	7.0	35-45.8	120-19.1	6.9	1.2	8	90	1.0	0.0	0.2	0.4	0.02	A
20	11	19	47.8	35-52.5	120-25.4	1.4	0.8	9	305	7.9	0.1	0.6	0.2	0.02	C
20	18	2	48.3	35-48.9	120-21.4	3.5	0.3	7	183	1.8	0.0	0.4	0.4	0.03	B
21	13	28	36.9	36- 0.7	120-32.2	12.9*	1.1	8	330	26.0	0.5	2.3		0.02	D
21	14	6	24.5	35-50.0	120-22.6	3.7	0.1	7	277	2.2	0.0	0.2	0.1	0.01	C
21	18	44	0.7	35-47.3	120-19.8	3.4	0.5	8	86	2.5	0.0	0.4	0.5	0.07	A
21	21	16	39.4	35-50.4	120-23.7	5.1	0.9	7	289	3.9	0.2	0.9	0.7	0.02	C
22	12	31	38.8	35-53.1	120-27.0?	0.0	2.1	10	164	10.5	0.3	1.1	0.8	0.05	C
22	13	7	10.4	35-47.1	120-20.4	8.6	1.7	9	91	1.8	0.1	0.4	0.9	0.04	A
22	22	15	1.0	35-50.4	120-23.5	3.4	0.8	8	289	3.6	0.6	3.0	0.9	0.08	D
23	10	24	16.5	35-53.9	120-26.5	8.0	1.2	9	312	11.0	0.3	1.7	0.9	0.02	C
23	17	5	57.6	35-56.3	120-29.0	5.0*	2.4	7	169	16.7	0.0	0.6		0.03	C
24	2	47	6.6	35-52.1	120-25.0	1.9	0.7	9	303	7.0	0.5	1.9	0.9	0.02	C
24	10	45	49.1	35-47.3	120-20.2	3.7	0.8	9	82	1.9	0.0	0.4	0.4	0.06	A
24	18	7	46.6	35-44.1	120-18.1	13.6	1.6	9	73	2.5	0.4	0.7	2.9	0.08	B
24	20	33	57.7	35-51.5	120-24.1	1.8	1.7	9	297	5.4	0.4	1.5	0.8	0.02	C
24	21	21	58.0	35-53.4	120-25.8?	5.0*	1.4	9	309	9.5	0.7	3.7		0.09	D
25	12	12	39.7	35-47.4	120-19.9	4.2	0.7	9	87	2.3	0.0	0.4	0.8	0.05	A
26	22	56	40.3	35-53.3	120-25.7?	2.7	1.0	8	316	9.3	1.4	6.6	1.7	0.06	D
26	23	36	15.2	35-45.8	120-19.6	8.4	1.2	9	99	1.5	0.1	0.6	1.5	0.07	A
27	5	14	24.3	35-52.8	120-25.6	1.7	1.5	10	157	8.6	0.0	0.3	0.3	0.02	B
27	8	33	48.0	35-55.3	120-28.0	5.0*	1.0	9	318	14.3	0.7	3.5		0.04	D
27	8	55	36.4	35-57.2	120-29.2	8.6*	1.7	9	323	18.1	0.5	2.4		0.02	D

TABLE 2 (CONTINUED)

1966	HR	MN	SEC	LAT N	LONG W	DEPTH	MAG	NO	GAP	DMIN	ERT	ERH	ERZ	MD	Q
AUG 27	12	14	41.0	35-55.4	120-28.4?	5.0*	1.3	7	323	14.9	1.2	5.7		0.07	D
27	13	13	46.0	35-48.3	120-20.3	2.1	0.4	8	108	2.3	0.0	0.3	0.5	0.04	A
27	16	9	57.3	35-48.3	120-20.2	2.4	0.4	8	107	2.4	0.0	0.5	0.6	0.06	A
28	3	19	3.5	35-51.9	120-24.8	1.8	1.1	9	301	6.6	0.4	1.5	0.8	0.02	C
28	14	10	31.2	35-45.1	120-18.9	11.6	1.2	8	137	0.5	0.1	0.5	1.3	0.04	B
28	17	56	34.3	35-56.4	120-27.9	5.0*	1.8	8	163	15.7	0.0	0.3		0.01	C
28	21	20	31.7	35-44.0	120-17.9	9.8	0.5	7	128	2.2	0.1	0.5	1.4	0.04	B
29	8	14	56.4	35-55.5	120-28.6	6.4*	0.9	8	324	15.3	1.4	6.4		0.04	D
30	14	18	57.5	35-46.9	120-20.9	8.9	1.6	7	150	1.3	0.0	0.2	0.4	0.01	B
31	5	52	30.8	35-48.3	120-20.8	3.3	0.6	7	230	1.9	0.0	0.6	0.4	0.03	C
31	14	13	56.5	35-47.9	120-21.1	8.1	1.0	7	232	1.0	0.0	0.3	0.5	0.01	C
SEP 1	0	37	22.9	35-55.5	120-28.3	5.0*	1.9	10	163	14.9	0.0	0.5		0.04	C
1	3	15	0.2	35-56.7	120-28.5	5.0*	1.8	10	161	16.8	0.0	0.4		0.03	C
1	7	59	58.0	35-47.6	120-19.8?	0.7	0.7	8	95	2.5	0.1	1.1	2.3	0.17	B
1	9	47	5.7	35-53.2	120-26.9	0.0	0.8	9	312	10.5	0.3	1.1	0.5	0.03	C
1	14	1	32.5	35-52.4	120-25.3	1.4	0.7	9	305	7.8	0.2	1.0	0.3	0.04	C
1	21	39	21.8	35-52.0	120-25.4	6.0	0.8	9	304	7.5	0.7	3.3	2.0	0.06	D
1	22	30	32.3	35-53.5	120-26.8	7.1	0.5	9	312	10.8	0.9	4.3	2.4	0.05	D
2	4	21	35.6	35-54.3	120-28.9	5.0*	0.3	9	318	14.1	1.5	6.8		0.08	D
2	13	0	40.5	35-50.9	120-24.1	2.6	0.6	9	171	3.7	0.0	0.4	0.4	0.04	B
2	23	25	10.1	35-51.1	120-23.7	4.1	0.8	10	134	3.5	0.0	0.3	0.5	0.03	B
3	2	2	28.4	35-52.6	120-28.6?	0.0	0.3	9	291	5.8	0.8	2.4	1.3	0.09	C
3	3	20	36.6	35-54.6	120-28.3	12.3	0.7	10	315	6.3	0.8	3.0	3.2	0.05	D
3	7	0	55.1	35-47.2	120-20.3	8.4	0.6	10	84	1.7	0.0	0.2	0.6	0.03	A
3	7	39	56.9	35-56.5	120-29.8	5.0*	0.7	10	322	10.2	2.1	9.3		0.08	D
3	9	59	40.2	35-56.9	120-29.7	1.0*	0.7	10	321	10.6	0.3	1.4		0.06	D
3	11	25	57.7	35-51.4	120-24.2	2.1	0.6	10	128	2.6	0.0	0.2	0.3	0.03	B
3	15	18	27.1	35-48.8	120-21.3	3.7	0.8	10	89	2.1	0.0	0.2	0.2	0.03	A
3	18	14	0.8	35-58.2	120-31.4	5.0*	1.6	11	170	14.2	0.0	1.0		0.08	C
4	2	44	3.9	35-48.4	120-20.8	3.5	0.5	11	94	1.9	0.0	0.1	0.1	0.02	A
SEP 4	16	44	26.1	35-54.5	120-30.1?	0.0	1.3	12	177	8.7	0.7	2.3	1.5	0.11	C
4	19	50	26.0	35-51.3	120-24.1?	2.7	0.4	11	126	3.0	0.0	0.2	0.2	0.03	B
4	19	54	47.3	35-50.3	120-23.7	9.3	0.7	11	118	3.9	0.1	0.5	0.9	0.04	A
5	1	8	28.1	35-56.1	120-29.4	5.0*	0.7	10	321	9.4	1.8	7.9		0.09	D
5	4	11	32.9	35-45.6	120-18.9	5.9	0.7	11	77	0.6	0.0	0.3	0.7	0.05	A
5	10	8	42.6	35-52.8	120-26.1?	3.0	0.9	10	269	2.1	0.2	1.5	0.7	0.04	C
5	10	39	7.1	35-57.5	120-30.4?	5.0*	0.6	11	325	12.2	0.8	3.7		0.12	D
5	10	52	23.8	35-50.4	120-23.0	2.7	-0.3	11	136	2.8	0.0	0.3	0.4	0.05	B
5	11	55	60.0	35-45.3	120-19.2	5.8	1.2	11	79	0.7	0.0	0.3	0.6	0.05	A
5	12	42	56.3	35-50.6	120-23.1	2.5	0.9	11	138	3.2	0.0	0.2	0.2	0.03	B
5	21	2	55.0	35-51.3	120-23.5?	1.8	-0.2	9	95	3.3	0.0	0.6	0.9	0.07	B
5	22	36	1.4	35-52.2	120-25.1	3.1	0.3	12	185	1.2	0.0	0.3	0.3	0.03	B
6	1	57	17.9	36- 1.2	120-38.2?	2.3	1.6	12	203	13.8	0.9	3.0	3.0	0.11	C
6	5	15	41.0	35-48.5	120-21.5	5.4	0.1	12	94	2.0	0.0	0.1	0.2	0.01	A
6	13	29	14.6	35-56.0	120-29.4	1.3*	0.8	11	312	9.2	0.2	1.1		0.05	D
6	21	18	53.1	35-55.1	120-28.3	2.2	1.3	13	161	6.9	0.0	0.4	0.6	0.04	B
6	21	40	11.4	35-55.1	120-28.3	2.4	1.8	13	161	6.9	0.0	0.3	0.4	0.04	B
6	22	27	41.0	35-50.8	120-24.1	7.2	0.4	11	111	3.8	0.0	0.2	0.5	0.03	A
6	22	39	5.2	35-48.2	120-20.6	3.9	0.3	12	79	1.8	0.0	0.2	0.3	0.03	A
7	0	20	52.8	36- 1.1	120- 1.9	5.0*	3.4	12	283	28.5	0.5	2.3		0.08	D
7	0	58	39.9	35-50.0	120-22.7	4.1	0.1	10	80	2.3	0.0	0.2	0.4	0.03	A
7	8	57	26.2	35-47.5	120-20.3	8.5	0.6	13	71	1.7	0.0	0.1	0.3	0.03	A
7	9	58	41.5	35-48.8	120-22.1	7.6	2.58	13	96	2.4	0.0	0.2	0.4	0.04	A
7	13	37	21.6	35-50.1	120-22.6	4.3	-0.4	12	77	2.2	0.0	0.3	0.5	0.05	A
7	14	0	25.5	35-47.6	120-20.8	7.9	1.0	13	70	1.0	0.0	0.1	0.3	0.02	A
7	22	56	4.2	35-55.5	120-28.1	3.5	1.7	13	145	1.1	0.0	0.4	0.3	0.05	B
8	2	43	2.7	35-54.9	120-27.9	9.8	1.0	12	177	1.3	0.2	1.0	1.5	0.05	B
8	12	7	39.8	35-48.7	120-21.1	3.6	0.7	12	89	2.3	0.0	0.2	0.2	0.04	A
9	3	2	35.5	35-47.4	120-20.6	8.2	0.5	12	79	1.3	0.0	0.3	0.6	0.05	A
9	5	15	5.6	35-54.6	120-28.0	1.9	0.6	11	151	1.3	0.0	0.4	0.4	0.05	B

TABLE 2 (CONTINUED)

1966	HR	MN	SEC	LAT N	LONG W	DEPTH	MAG	NO	GAP	DMIN	ERT	ERH	ERZ	MD	Q
SEP 9	6	43	28.3	35-55.8	120-28.6	4.9	1.1	12	287	1.3	0.1	0.8	0.9	0.05	C
9	10	26	48.4	35-47.9	120-21.4	9.7	0.8	13	99	0.8	0.0	0.2	0.5	0.04	A
9	18	2	40.8	35-52.6	120-26.1	9.6	2.0	14	137	2.1	0.0	0.3	0.5	0.04	B
9	20	16	17.3	35-53.4	120-26.5	9.9	1.4	13	137	2.9	0.0	0.3	0.5	0.02	B
10	8	34	36.8	35-44.4	120-17.7	12.4	1.1	10	118	2.3	0.0	0.3	0.7	0.03	A
10	8	58	0.6	35-54.9	120-28.0	3.0	0.8	12	171	1.1	0.0	0.6	0.5	0.04	B
10	10	32	26.3	35-47.3	120-20.6	8.6	1.6	12	82	1.3	0.0	0.3	0.6	0.04	A
10	12	15	18.4	35-53.8	120-27.1	9.5	0.8	12	143	3.4	0.2	0.9	1.5	0.05	B
10	13	12	0.9	35-52.6	120-26.2	3.2	1.1	12	138	2.2	0.0	0.3	0.3	0.04	B
10	15	6	51.1	35-54.6	120-28.2	1.9	0.7	11	162	1.2	0.0	0.8	0.7	0.07	B
11	3	50	30.7	36- 0.8	120-38.4	5.0*	1.2	11	207	14.4	0.1	1.0		0.07	C
12	4	20	24.2	35-47.2	120-19.9	2.3	1.3	12	105	2.4	0.0	0.2	0.3	0.06	A
12	4	22	50.2	35-46.9	120-19.9	7.2	0.8	11	117	2.5	0.0	0.3	0.5	0.04	A
12	7	55	3.1	35-45.6	120-19.3	5.8	1.4	12	125	1.0	0.0	0.2	0.3	0.03	B
12	14	15	46.9	35-54.1	120-27.2	3.2	1.1	13	149	2.8	0.0	0.5	0.5	0.05	B
12	23	37	31.6	35-53.3	120-26.8	11.0	1.1	12	145	3.3	0.1	0.4	0.8	0.03	B
13	1	44	36.6	35-51.5	120-24.3	3.7	0.9	13	95	2.5	0.0	0.2	0.3	0.05	A
13	1	50	26.6	35-48.8	120-21.9	5.3	0.8	13	94	2.2	0.0	0.1	0.3	0.03	A
13	5	18	16.9	35-53.5	120-26.6	3.0	0.7	14	139	3.2	0.0	0.6	0.6	0.08	B
13	6	0	36.3	35-51.4	120-23.9	2.3	0.2	13	88	2.9	0.0	0.3	0.4	0.06	A
14	0	6	14.0	35-48.1	120-20.6	3.8	0.5	11	79	1.8	0.0	0.1	0.2	0.03	A
14	2	59	8.8	35-43.9	120-16.9	5.5	1.2	12	145	3.9	0.1	0.5	1.5	0.09	B
14	12	30	30.5	35-58.0	120-32.0	6.9	1.0	13	175	7.4	0.0	0.5	1.1	0.04	B
14	13	37	54.7	35-46.3	120-19.5	7.2	0.8	11	84	2.0	0.0	0.1	0.3	0.02	A
14	18	58	44.2	36- 1.4	120-37.2	5.0*	1.5	13	195	13.7	0.0	1.0		0.06	C
15	3	27	7.8	35-53.4	120-26.6	10.9	0.8	12	138	3.0	0.0	0.3	0.5	0.02	B
15	4	32	40.0	35-47.8	120-20.2	3.4	0.1	12	76	1.9	0.0	0.2	0.2	0.03	A
15	4	37	1.0	35-53.3	120-26.4	10.3	0.7	12	136	2.7	0.0	0.3	0.5	0.02	B
15	9	29	46.1	35-56.7	120-31.5	8.3	1.0	13	177	5.2	0.0	0.6	0.8	0.04	B
15	13	36	1.7	35-51.2	120-23.8	3.2	0.4	10	85	3.2	0.0	0.2	0.3	0.04	A

Forty-nine aftershocks with magnitudes in the range 2.0 to 2.5 were assigned magnitudes from the special network records as well as from records of the Berkeley network (McEvilly *et al.*, 1967). The Berkeley magnitudes averaged 0.1 unit larger than those assigned by the methods used in this study. A number of aftershocks produced unrecordably large amplitudes at all stations of the special network, and the Berkeley magnitudes were adopted for these events. Magnitudes so assigned are flagged by the letter "B" in Table 2.

Spatial Distribution of the Aftershock Hypocenters

In the analysis of the spatial distribution of the aftershock hypocenters special emphasis was placed on well-located events. Such events were defined as those for which the focal depth was not constrained and for which $NO \geq 5$, $MD < 0.1$ sec, $ERX < 2.5$ km and $ERY < 2.5$ km. The 474 earthquakes that meet these conditions are plotted by *large letter symbols* (representing) focal depths: 0 to 1 km = *A*, 1 to 2 km = *B*, etc.) in Figure 7. Events that satisfy slightly relaxed conditions (limit on *MD* removed) are plotted by *small letter symbols*, and other events are indicated by +. The well-located events show much less scatter than the others, and all are heavily concentrated in a narrow zone bounded on the northeast by the zone of surface fracturing. A very small, but notable, group of earthquakes suggests a north-trending line of activity between 10 and 20 km approximately north of the zone where the surface fractures jump from the northeast side to the southwest side of Cholame Valley.

To establish the orientation of the zone of aftershock sources and to provide a meas-

ure of the concentration of hypocenters along it, a reference plane was fitted by least squares to the three-dimensional pattern of well-located aftershock hypocenters. The coordinates of the hypocenters in a cartesian system with origin on the active strand

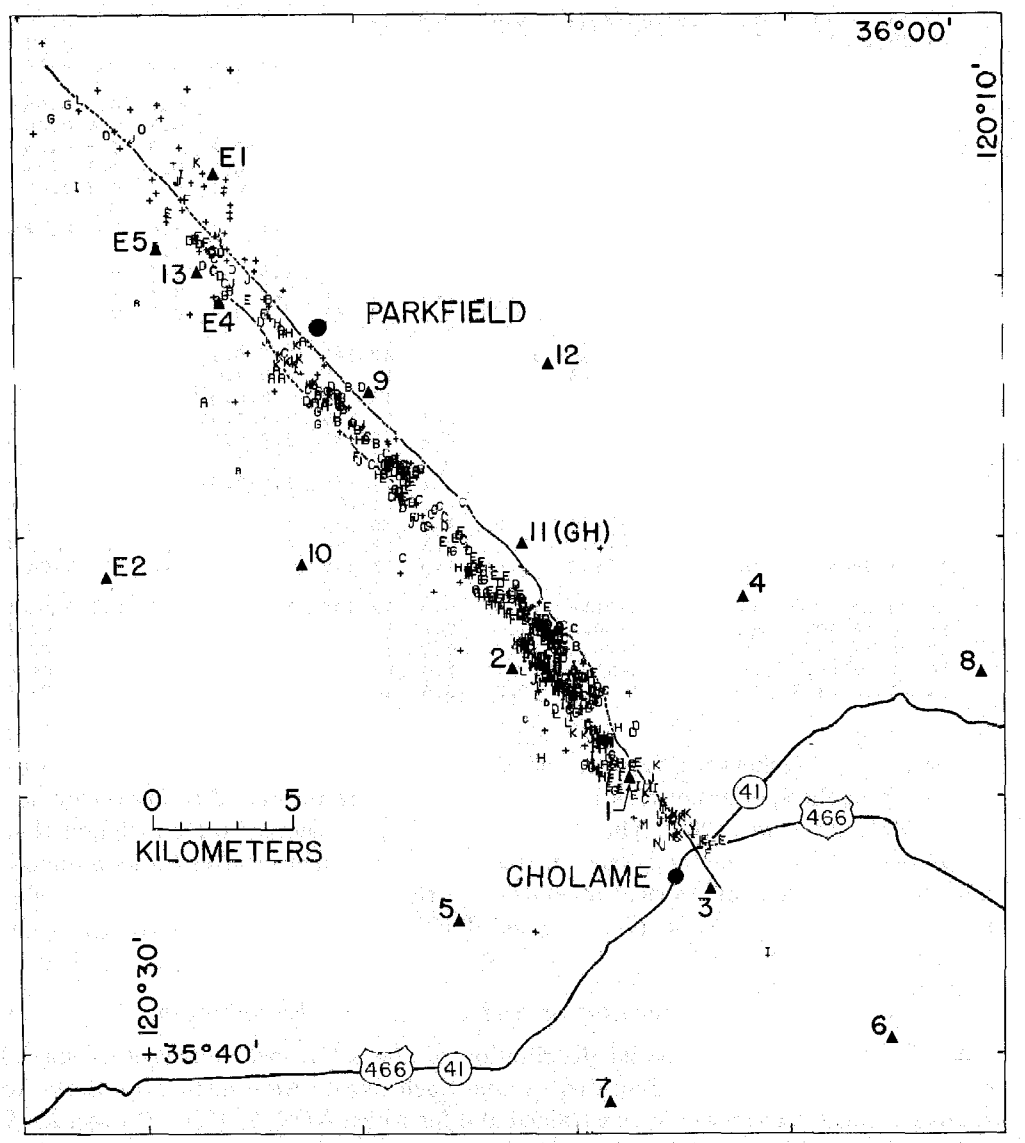

FIG. 7. Epicenters of Parkfield-Cholame earthquake aftershocks, July 1 through September 15 1966. Seismograph stations are indicated by *triangles*. Aftershock epicenters are indicated by *letters* and *crosses* according to their focal depths and the reliability of their hypocenters. Focal depths are indicated by *letter*: $A = 0$ to 1 km, $B = 1$ to 2 km, etc. *Large letters* designate well-located hypocenters, *small letters*, less well-located hypocenters, and *crosses* designate poorly located events of uncertain focal depth. *Solid* and *broken lines* trending NW-SE show trace of surface fractures associated with the main shocks.

of the San Andreas fault near station 6 and with axes directed toward the northwest along the fault, toward the southwest and downward were first computed. A plane was fitted by linear regression of the transverse coordinate (NE-SW) on the radial (NW-SE) and depth coordinates for all well-located events with epicenters within 10 km of the longitudinal axis (i.e., the surface trace of the fault). Of the 630 events to which

hypocenters were assigned, 618 fell within this zone, and these included all but one of the 484 well-located events. The standard deviation in the transverse coordinates with respect to the fitted plane was 0.71 km. To refine the fit, the nine well-located events that lay more than 2 standard deviations from the plane were rejected and the plane was refitted to the remaining 474 hypocenters. The standard deviation in the transverse coordinates of the hypocenters fitted to the final plane was 0.45 km.

The distribution of aftershocks along the fault is shown in Figure 8 where all events within 10 km of the surface trace of the reference plane are projected onto a vertical plane through that trace. Magnitude of the aftershocks is indicated by the size of the plotted symbols. An apparent concentration of aftershocks at a depth of 5 km in the *right half* of the plot results from the assignment of a 5-km depth to events for which focal depth cannot be determined. Most such aftershocks occurred between July 23

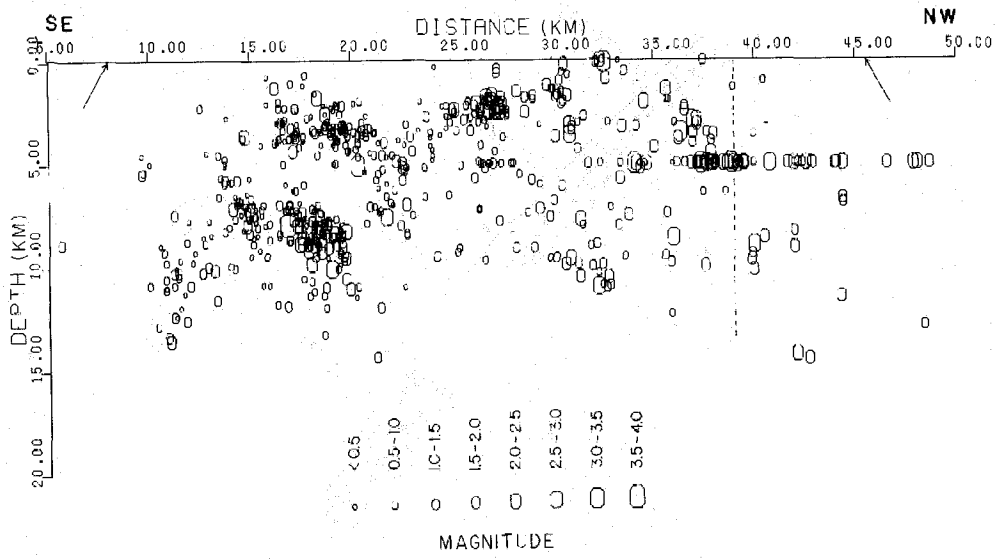

FIG. 8. Projection of hypocenters within 10 km of the fault onto a vertical plane through the surface outcrop of the reference plane. Distance along the fault is in terms of the longitudinal coordinate axis in Figure 9. The ends of the zone of the surface fracturing are indicated by *arrows*, and the approximate position of the main shock epicenter is shown by the *vertical dotted line*. The concentration of hypocenters at a depth of 5 km at ranges of 35 to 50 km should be disregarded: inadequately recorded aftershocks were constrained to that depth to permit their epicenters to be calculated.

and September 1, when the network was inadequate in the northwestern half of the aftershock region. The precision of their epicenters is also substandard.

The close correspondence between the surface trace of the fitted plane and the mapped zone of surface fracturing is illustrated in Figure 9, which also shows the epicenters of the well-located aftershocks used to establish the plane. In Figure 10, the hypocenters of the well-located aftershocks are projected onto a vertical plane perpendicular to the strike of the fitted plane. The strike of the plane fitted to the well-located hypocenters is N 39°W, and it dips 86° toward the southwest.

In Figure 11, hypocenters of well-located aftershocks with magnitudes larger than 0.5 are projected onto a vertical plane parallel to the surface trace of the fitted plane. Deviation of hypocenters from the fitted plane is indicated by the letter symbol and magnitudes are indicated by letter size. The aftershocks are virtually restricted to the depth range 1 to 12 km. They are also concentrated in patches on the slip surface, with

other patches entirely devoid of aftershocks. Moreover, they are not scattered uniformly about the reference plane but instead show systematic local deviations from it. In this figure, these deviations are contoured in 0.5-km intervals to show how the slip

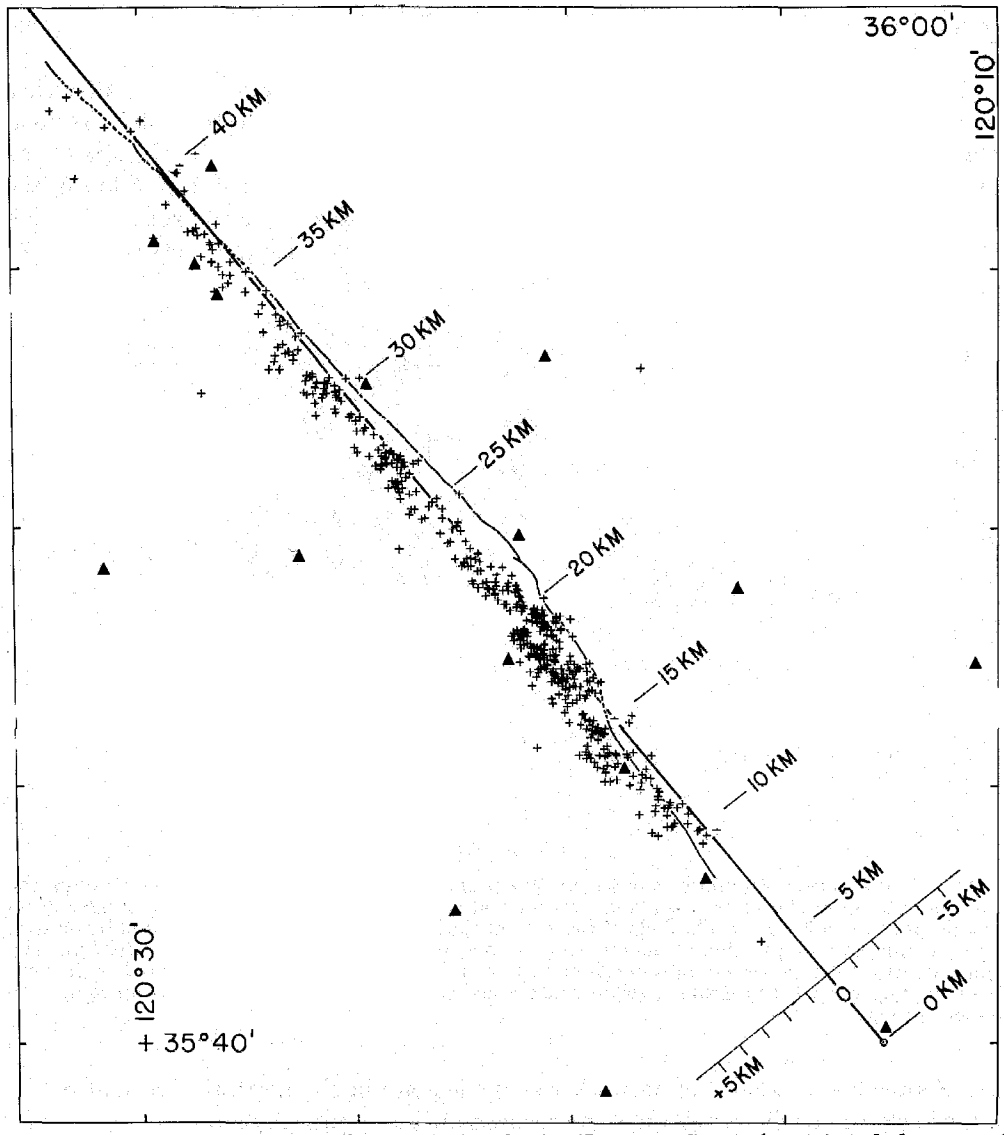

FIG. 9. Epicenters of the well-located aftershocks (July 1 to September 15) and the zone of surface fracturing of the Parkfield-Cholame earthquake. Epicenters are indicated by *crosses*, seismograph stations by *triangles*, and the zone of surface fracturing by the *heavy solid* and *dashed curves*. The surface outcrop of the reference plane (*heavy straight line*) is the longitudinal axis of a coordinate system, with origin near station 6, used in the analysis of the distribution of the hypocenters.

surface departs from the reference plane. Positive deviations are southwest of the plane and negative deviations are northeast of it.

The events plotted here (as in Figure 8) do not represent a uniform sample of all the aftershocks. None during the first 70 hr is shown, and relatively fewer small events were sampled and located from the region northwest of Gold Hill than from the south-

east of it. Accordingly, generalizations based on this figure should be accepted only with appropriate reservations.

It appears that the slip surface is relatively smooth northwest of Gold Hill (22 km on the profile) and that its dip increases northwestward along the fault from about 86°SW near Gold Hill to about vertical beyond 35 km. Southeast of Gold Hill, the slip surface is more complex. The shallow group of quakes southeast of Gold Hill (16 to 21 km along the profile) lies northeast of the reference plane, whereas the deeper group of quakes along the same part of the fault lies very near the reference plane. At about 15 km along the profile, where the zone of surface fractures swings across Cholame Valley from the northeast side to the southwest side (Figure 9), the center portion of the slip

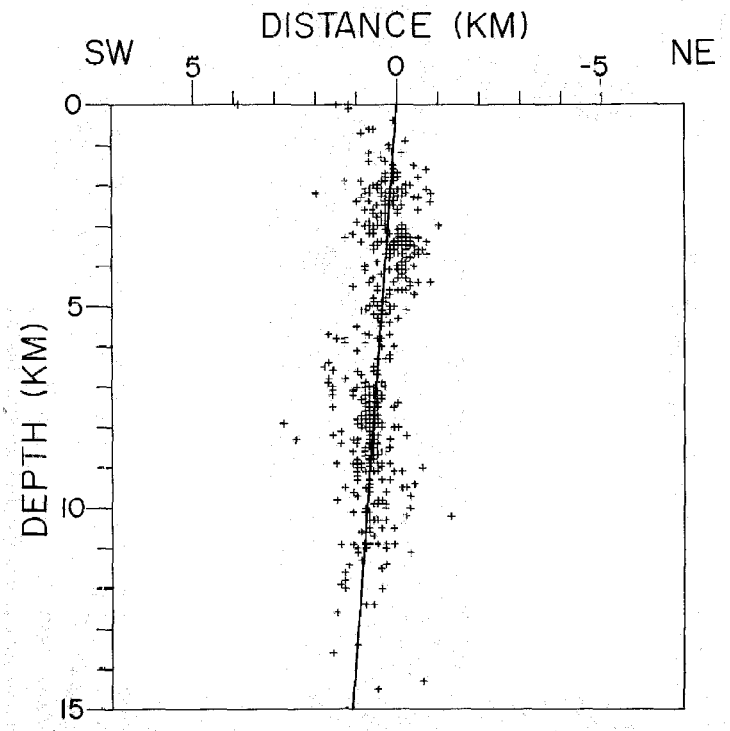

FIG. 10. Projection of well-located hypocenters onto a vertical plane perpendicular to the surface trace of the reference plane. The *solid line* is the trace of the fitted reference plane on the projection plane.

surface (depths of 5 to 10 km) curves abruptly southwestward through the reference plane. Still farther southeast, the prominent group of aftershocks below 8-km depth indicates that the slip surface in that region swings back to the northeast side of the reference plane again.

We may speculate that the increasing complexity of the slip surface at its southeast end was one of the factors responsible for arresting the southeastward extension of slippage along the fault during the main earthquake.

If we consider only well-located events, the region of concentrated hypocenters stops about 1 km short of the ends of the zone of surface fracturing. A few poorly located aftershocks of undetermined focal depth appear to have originated northwest of the end of the zone of surface fracturing.

A series of projections of hypocenters, section by section along the fault, onto vertical

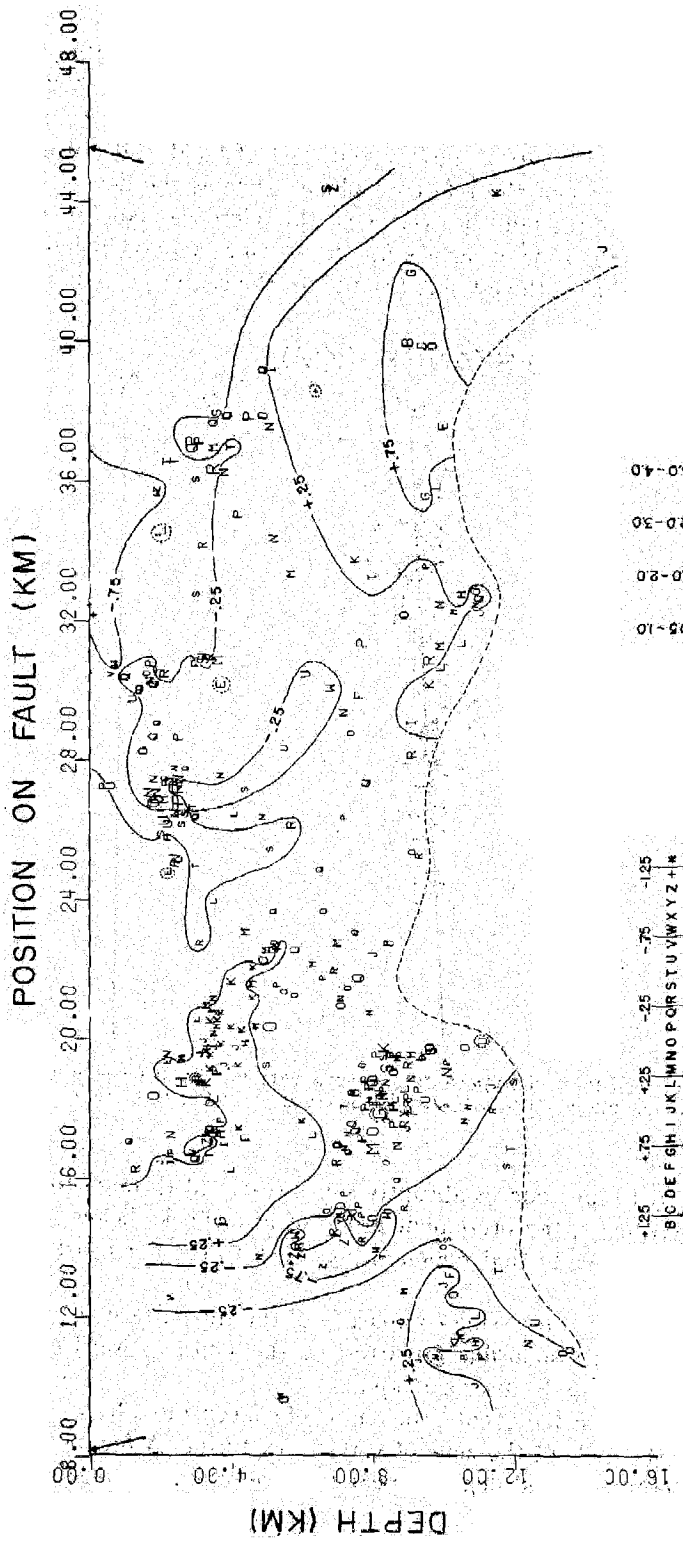

FIG. 11. Deviation of well-located aftershocks of magnitude 0.5 and greater from the fitted reference plane. Deviation is contoured in 0.5 km intervals from −0.75 km to +0.75 km. Hypocenters represented by *P-Z* (negative deviation) are southwest of the plane, those indicated by *N-B*, northeast of it. Events that are more than one contour interval out of place are encircled by *dotted lines*. The approximate lower limit of aftershocks is shown by the *dashed curve*, and the ends of the zone of surface fracturing are indicated by *arrows*.

planes perpendicular to the strike of the fitted plane is shown in Figure 12. The sections were chosen to permit the separation of different patches of hypocenters on the slip surface. It appears that the dips of individual active patches on the slip surface are nearly vertical and that the dip of the fitted plane reflects the relative lateral offset, perpendicular to the strike of the fault, of the shallow active zones from the deeper ones. Such an offset is particularly apparent on the section of the fault just southeast of Gold Hill (16 to 21 km).

First Motion Patterns and Focal Mechanisms of the Aftershocks

A sufficient number of stations recorded clear first motions for more than 200 events to warrant an attempt to establish the focal mechanisms of the individual aftershocks.

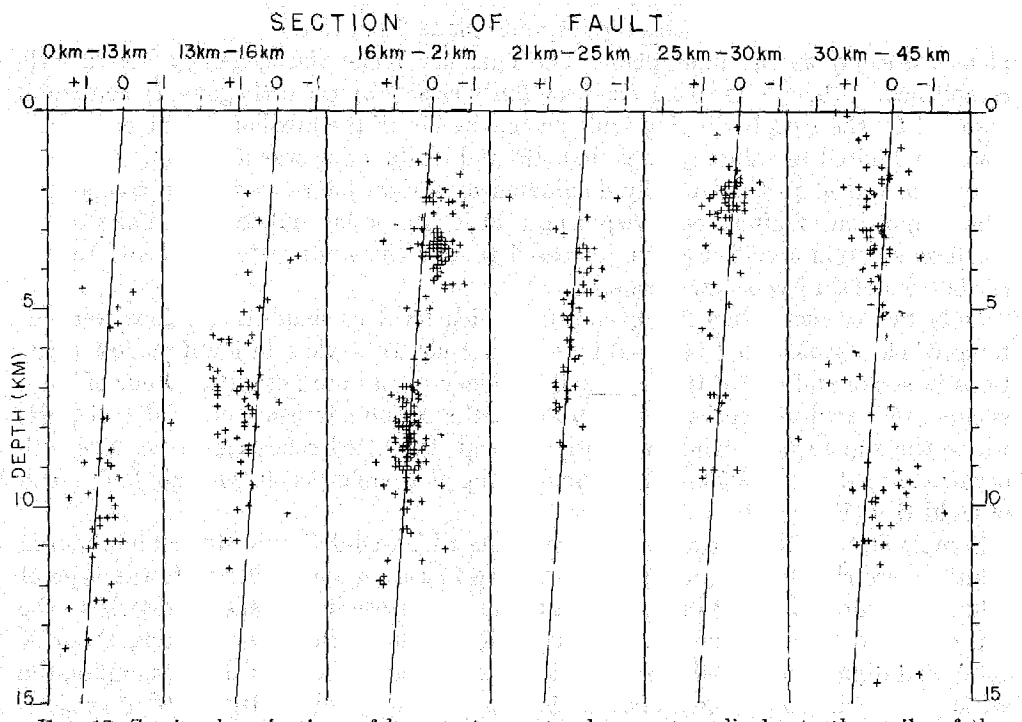

Fig. 12. Sectional projections of hypocenters onto planes perpendicular to the strike of the reference plane. The trace of the reference plane is shown as a *solid line*. Projected hypocenters are shown as *crosses*.

Epicenter-to-station azimuths, angles of incidence at the focus and direction of first motion are available in the HYPOLAYR station list punch-card output for each event. Equal-area stereographic projections of first motions on the lower half of the focal sphere, prepared from the foregoing data, were produced as printer plots; and orthogonal planes separating the first motions into quadrants of compression and dilatation were hand-fitted to the data with the aid of a Wulff net.

The distribution of data points over the focal spheres was more favorable for aftershocks southeast of Gold Hill than for those farther northwest and for deep aftershocks than for shallow ones. For shallow foci, most stations recorded boundary waves refracted along horizons deeper than the focus, and their projected first motions are concentrated near the outside of the projection circle. For deeper foci, many of the recorded first arrivals were direct waves, and their projected first motions are scattered

fairly uniformly over the projection circle. The latter case is much more favorable for establishing the dips of the fault and auxiliary planes than the former.

Except for the arrival at PRI, which is at the northeast edge of the San Andreas fault zone 44 km northwest of Gold Hill, almost all aftershocks were susceptible of a solution with no discordant arrivals, although many such solutions were not unique. The projected point for PRI usually lies very near the fault-plane nodal line, but its first motion corresponds to that expected southwest, rather than northeast, of the fault (which is very close to the nodal line) in the region northwest of the epicenter. Thus, first motions at PRI commonly appear to have been refracted horizontally across the rift zone from the faster crustal block southwest of the fault.

For most aftershocks, one steeply-dipping plane striking nearly parallel to the zone of surface fracturing was well established: strike N 40° ± 5°W, dip 80° ± 10°SW. Because this plane closely parallels the reference plane fitted to the hypocenters, it can be identified safely as the fault plane. The auxiliary plane was generally not so well-established. Although its strike was fixed fairly closely by the orthogonality constraint imposed by the steeply dipping fault plane, the dip of the auxiliary plane commonly was only limited to values greater than 45° and its direction was uncertain. The sense of motion was almost universally dominated by a right-lateral strike-slip component. The proportion of aftershocks requiring solutions that lay outside the limits of the common solution specified above increased toward the southeastern end and toward the bottom of the hypocentral zone.

Only five of more than 200 events for which focal mechanism solutions were attempted clearly could not be fitted by a "San Andreas" style solution if modest variations in strike and dip of the fault and auxiliary planes are permitted. Four of these events originated at depths of 6 to 9 km in the region southeast of Gold Hill (GH) where the slip surface swings abruptly through the fitted reference plane. The fifth occurred at a depth of 9.5 km in the small group of aftershocks off the main fault north of Gold Hill (Figure 7).

Sample first-motion diagrams for four events with well-determined focal mechanism solutions are shown in Figure 13. The first two cases, *a* and *b*, illustrate the type of solution required by most of the events studied. Because it corresponds closely to the slip surface defined by the distribution by hypocenters, the plane striking about N 40°W and dipping about 80°SW is identified as the fault plane. In these examples, the strike of the auxiliary plane is about N 50°E and its dip is within 10° to 20° of vertical. For both cases, the axis of compression is nearly horizontal and lies along an azimuth of about N 5°E.

The third case, *c*, is typical of most of the solutions that differ from that shown in *a* and *b*. The strike of the fault plane is about N 40°W, but its dip (toward the SW) is less than 70°. In some cases, the dip of the auxiliary plane also departs markedly from 90°, indicating a significant dip-slip displacement component. In this example, the axis of compression plunges about 35° in a direction N 5°W.

The fourth case, *d*, is representative of only five events studied. The axis of compression plunges slightly, nearly due east. The first-motion pattern is similar to that for cases *a* and *b* but with compressions and dilatations interchanged. Thus, if the plane striking about N 40°W is the fault plane, the motion is left lateral. If the motion is right lateral, the plane striking about N 50°E is the fault plane. Available data are insufficient to choose between these two possibilities.

To permit a more compact display of the first-motion data, composite first-motion diagrams were prepared for aftershocks from separate sections of the hypocentral zone.

The divisions employed in Figure 12 were again used, but two sections (16 to 21 km and 30 to 45 km) were further subdivided into shallow (<6 km) and deep (≥6 km) portions. Events with individual solutions that differed widely from the common solutions were not included in the composite plots. The percentages of events included in the composite plots are measures of the uniformity of the focal mechanism operating in individual sectors. The composite plot for region 4 (21 to 25 km) illustrates the char-

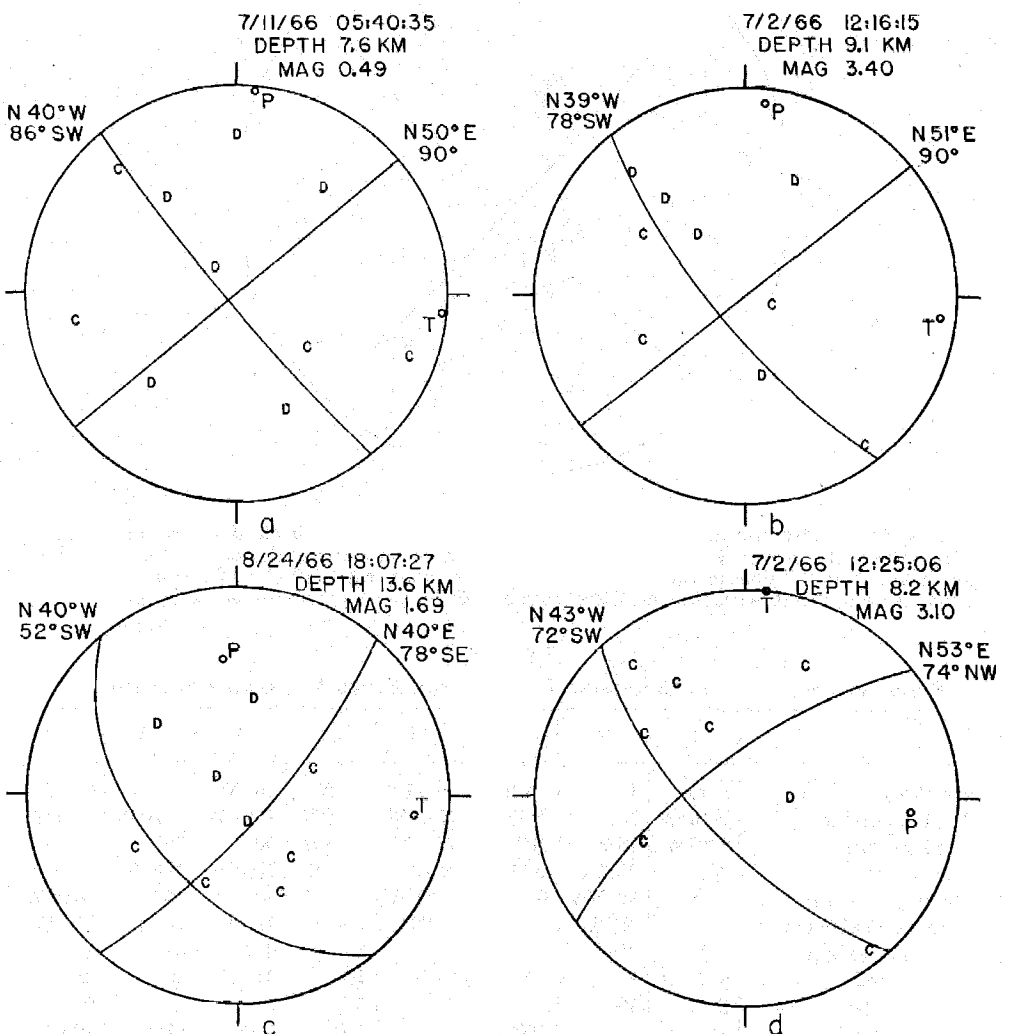

FIG. 13. *P*-wave fault plane solutions for 4 Parkfield-Cholame aftershocks. *C*'s and *D*'s indicate compressional and dilatational first motion respectively. *T* denotes the tension axis and *P*, the pressure axis.

acter of the sectional plots (Figure 14); summaries of the solutions obtained from the composite plots in the separate regions are given in Table 3.

The "first-motion" fault-plane solutions for the individual sectors agree quite well with the "reference" plane obtained in the least squares fitting of a plane to the distribution of hypocenter locations. The first-motion solutions strike somewhat more westerly (N 39°W to N 45°W) than the reference plane (N 39°W) and their average dip (80°SW) is somewhat smaller than that of the reference plane (86°SW). These

differences do not appear to be simply correlated with the irregularities in the slip surface suggested by Figure 11. They may result from variations in network coverage

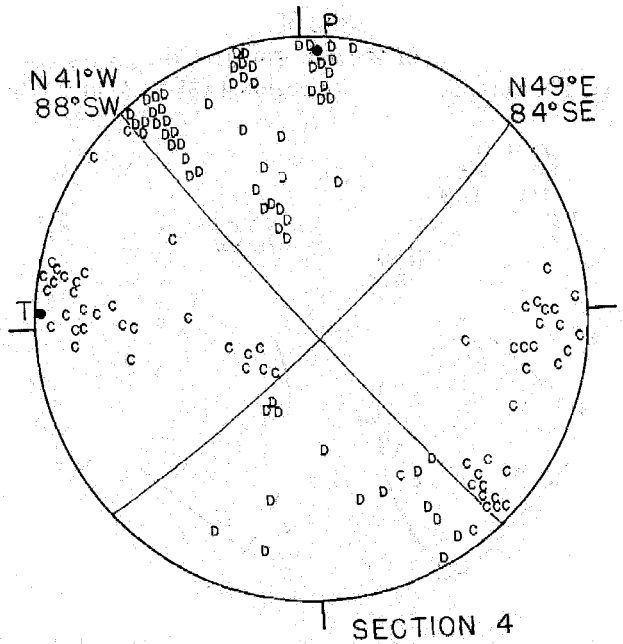

FIG. 14. Composite first motion plot of *P*-waves from aftershocks in the distance range 21 to 25 km along the fault (*section 4*). *C's* and *D's* indicate compressional and dilatational first motions, respectively. *T* and *P* denote the tension and pressure axes, respectively, of a fault-plane solution that is compatible with first motions from all of the earthquakes in this section.

TABLE 3

SUMMARY OF SECTIONAL COMPOSITE FIRST-MOTION FOCAL MECHANISM SOLUTIONS

Section	1	2	3s	3d	4	5	6s	6d
Limits (km)	8–13	13–16	16–21	16–21	21–25	25–30	30–45	30–45
Fault plane strike	N45°W	N41°W	N39°W	N39°W	N41°W	N40°W	N41°W	N41°W
Fault plane dip	80°SW	75°SW	90°	74°SW	88°SW	90°	90°	84°SW
Auxiliary plane strike	N45°E	N52°E	N51°E	N50°E	N49°E	N50°E	N49°E	N49°E
Auxiliary plane dip	70°SE	82°NW	90°	85°NW	84°SE	90°	90°	86°NW
Compression axis azimuth	N	N5°E	N6°E	N6°E	N4°E	N5°E	N4°E	N4°E
Compression axis plunge	17°	7°	0°	6°	3°	0°	0°	1°
Events plotted	6	8	23	39	15	31	39	25
Events omitted	8	10	0	4	0	0	1	0
Per cent plotted	43%	44%	100%	91%	100%	100%	97%	100%
Concordant points	43	72	208	337	148	292	220	228
Discordant points	8	5	19	32	2	31	23	42
Per cent concordant points	84%	94%	92%	91%	99%	90%	91%	84%
Sense of motion	—*	—*	—*	—*	—*	—*	—*	—*

* In all cases, the sense of motion is predominantly right-lateral strike slip.

from region to region and from errors in the velocity-depth model used to evaluate the seismic observations.

The strikes of the auxiliary planes deduced from the composite first-motion plots also vary little from region to region (N 45°E to N 51°E), but their dips vary somewhat

more (70°SE to 82°NW). Similarly, the direction of maximum pressure shows little variation (N to N 6°E) and its plunge ranges from 0° to 17° northward.

Distribution of Aftershocks along the Fault as a Function of Time and Magnitude

The spatial distribution of the hypocenters suggests that the aftershocks were caused by repeated movement along a narrow zone or slip surface of low complexity that was activated at the time of the principal shock. In such a simple system, it does not seem unreasonable to expect that we might be able to trace episodes of slipping along the fault by means of the associated aftershocks. To display the aftershock sequence in order to evaluate this possibility, the positions of aftershocks along the fault were plotted against their times of occurrence.

All located events within 5 km of the reference plane were plotted (Figure 15, *top*) to obtain an overview of the aftershock sequence. Network coverage between 0 and 25 km was reasonably uniform throughout the recording period. Between 25 and 50 km, coverage was fair during the first 4 weeks (but the detection threshold was higher than farther southeast) and the last 2 weeks. The data should be complete for aftershocks larger than magnitude 1.5, but hypocentral determinations (particularly focal depths) were poorer from 25 to 50 km than from 0 to 25 km, especially between 25 and 70 days after the main shock.

To eliminate regional differences in coverage resulting from variation of the detection threshold and to remove the overlay of small aftershocks that might obscure relationships among the larger ones, the data were replotted with rejection of events smaller than specified magnitude thresholds.

Plots for aftershocks with $M \geq 1.0$ (Figure 15, *middle*) and $M \geq 2.0$ (Figure 15, *bottom*) are presented for comparison with the plot for all events. The tendency for aftershocks to be grouped in clusters is apparent on all three plots, but it is clearest in Figure 15, *middle*, especially along the southeastern half of the fault and during the second half of the recording period. In a few instances, the occurrence of the largest event of the cluster near its beginning suggests that the cluster represents a moderate aftershock of the main quake that is followed by its own train of aftershocks. Other clusters of aftershocks are not marked by a dominant event and appear to represent only a series of associated earthquakes of subequal size occurring along a restricted section of the fault. The existence of the clusters indicates that continued movement along the fault was unsteady and the structure of the groups of aftershocks suggests the manner in which episodes of slipping were extended in space and time. The frequency of aftershocks recorded at Gold Hill versus time after the main shock during the first 100 days of the sequence can be represented quite closely by the relationship $R(t) = R_0/t$ (Eaton, in Brown *et al.*, 1967). The density of events on the plots in Figure 15 can therefore be expected to diminish with time approximately at $1/t$. The number of events in an interval of time dt can be written:

$$R(t)\,dt = R_0 \frac{dt}{t} = 2.30 \times R_0 \times d(\log_{10} t),$$

where t is time measured in days after the main shock. Thus, if we shift to a logarithmic time scale for the position versus time graphs, the density of events should be independent of the temporal variable, $\log_{10} t$. On such a plot, patterns of events occurring during the attenuated later stages of an aftershock sequence are restored to visual similarity with patterns of events during the initial stages of the sequence.

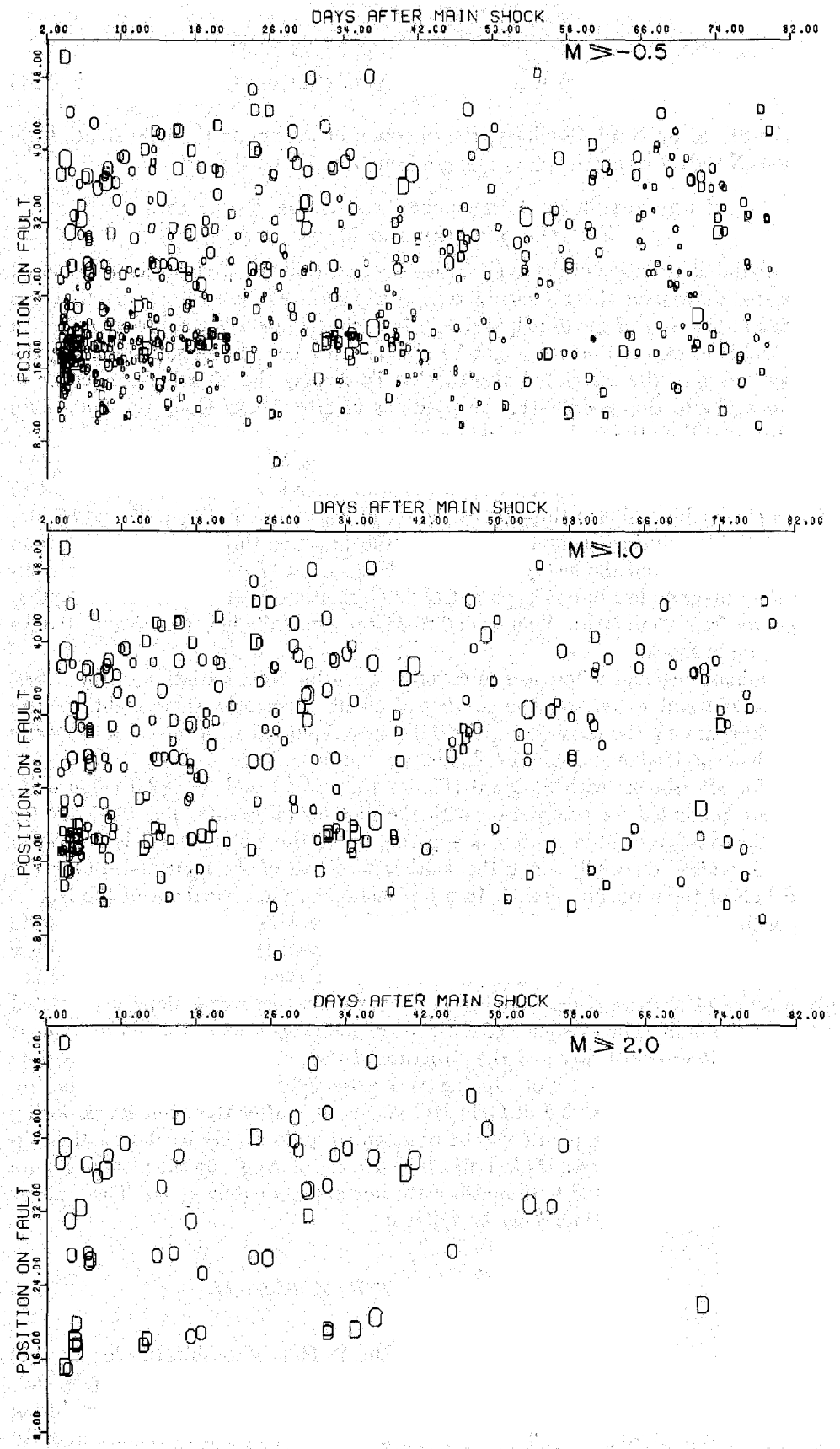

FIG. 15. Plots of position on fault versus time of occurrence of Parkfield-Cholame aftershocks. Events with focal depths of 6 km and greater are marked by *D's*, shallower events by *O's*. The size of the plotting symbol is proportional to the magnitude of the event. Position on the fault (in kilometers) is given in terms of the longitudinal coordinate axis of Figure 9.

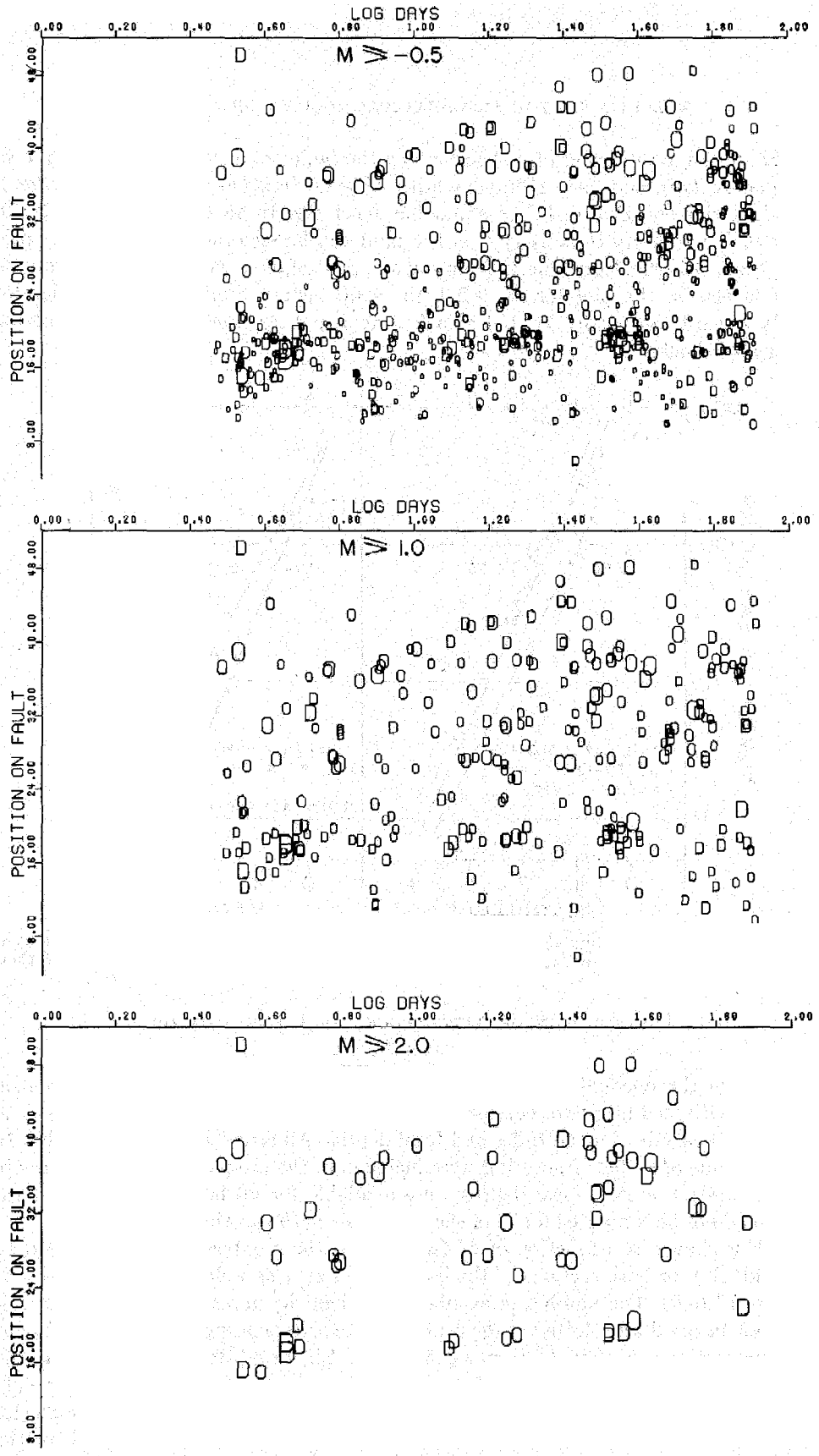

FIG. 16. Plots of position on fault versus the logarithm of time of occurrence of Parkfield-Cholame aftershocks. Events with focal depths of 6 km and greater are marked by *D's*, shallower events by *O's*. The size of the plotting symbol is proportional to the magnitude of the event. Time is measured from the main shock, and position on the fault (in kilometers) is given in terms of the longitudinal coordinate axis of Figure 9.

In Figure 16, positions of aftershocks along the fault are plotted versus log t for all earthquakes (*top*), and for earthquakes with $M \geq 1.0$ (*middle*) and $M \geq 2.0$ (*bottom*). Individual clusters of aftershocks stand out most clearly on the plot for $M \geq 1.0$. Larger scale variations in activity over the fault can be seen most clearly on the plot for $M \geq 2.0$. Other features emerge from a comparison of plots with different magnitude cut-off levels: on the plot for $M \geq 2.0$, the southeastern limit of activity migrates steadily toward the northwest, but this feature is not apparent on plots containing smaller aftershocks.

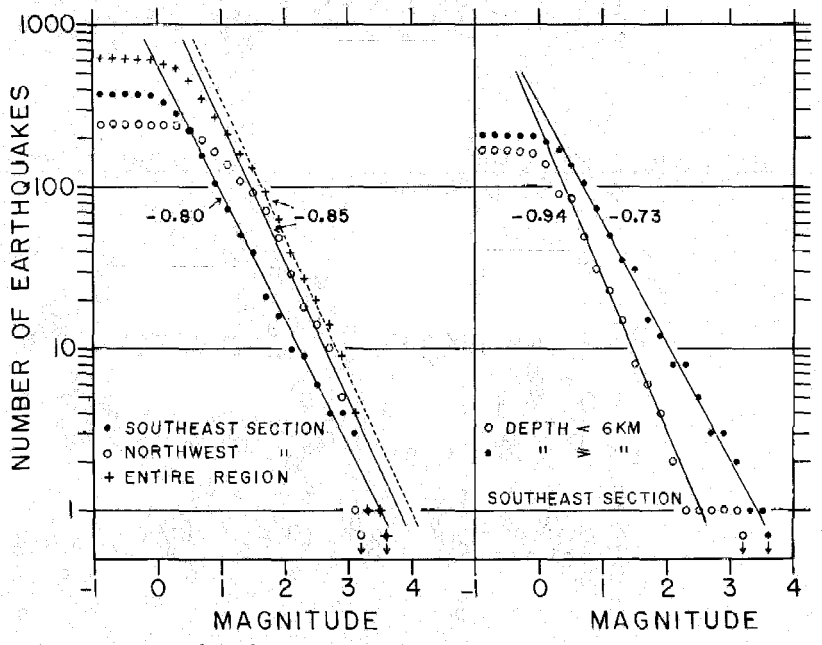

FIG. 17. Number of earthquakes larger than a given magnitude versus magnitude. The *symbols* above the *downward-pointing arrows* indicate the magnitudes of the largest events of their respective groups.

DISTRIBUTION OF AFTERSHOCKS AS A FUNCTION OF MAGNITUDE AND FOCAL DEPTH

Because of the unequal instrumental coverage of the two ends of the hypocentral zone, it was divided into two sections (southeast, 0 to 25 km, and northwest, 25 to 50 km) for the analysis of magnitudes and focal depths. All aftershocks located within 10 km of the zone of surface fracturing were included in the sample. Of the 376 events in the southwestern sector, focal depths were available for all but four, whereas focal depth could not be computed for 74 of the 243 events in the northwestern sector.

Log N is shown as a function of M (where N is the number of events larger than magnitude M) for both sections of the hypocentral zone as well as for the entire zone in Figure 17 (*left*). The number of events larger than the upper limit of each 0.2-unit magnitude interval was plotted at the center of the corresponding interval, and straight lines representing curves of the form $\log N = a + bM$ were fitted by inspection to the three sets of points over the range of magnitudes that appeared not to be too strongly affected by the detection threshold at small magnitudes or by inadequate sample size at the largest magnitudes recorded. The curves for both the entire zone and for the northwestern section have slopes (b values) of -0.85, and they fit the data points quite

closely from $M = 3.0$ to $M = 1.5$. The sharp departure of the data points from the line for $M < 1.5$ indicates that an increasing number of earthquakes escaped detection as M decreased from 1.5. The curve for the southeastern section has a slope of -0.8, and the data points that establish it remain on the line down to $M = 0.5$. Thus, asuming that the straight-line relationship holds to even smaller magnitudes, it appears that the threshold of reliable detection in the southeastern section was about $M = 0.5$.

To test for any gross dependence of the b value on focal depth, aftershocks in the southeastern section were divided into two groups, those shallower than 6 km and those 6 km or deeper, and log N versus M curves were drawn for both groups (Figure 17 (*right*). The b values differ significantly: -0.94 for the shallow group and -0.73 for the deep group. Results of further subdivision of the depth range are shown in Figure 18,

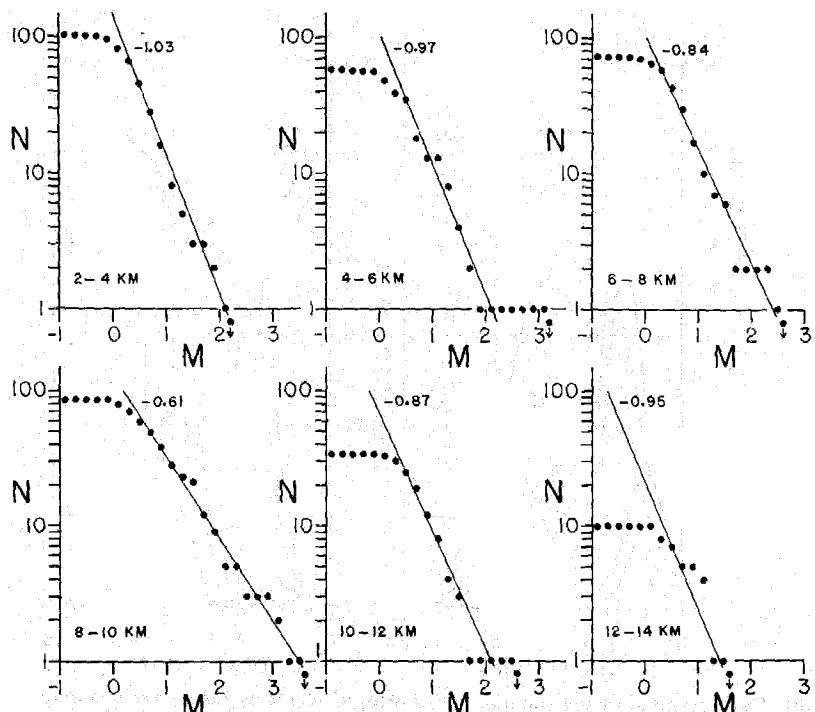

FIG. 18. Number of earthquakes larger than magnitude M versus M, for aftershocks in the southeastern section of the hypocentral zone, for various ranges of focal depth. The symbols below $N = 1$ indicate the magnitudes of the largest events of their respective groups.

where data for each 2-km depth interval from 2 to 14 km are plotted separately. The value of $-b$ decreases regularly from a maximum of 1.03 for the 2- to 4-km interval to a minimum of 0.61 for the 8- to 10-km interval and then increases to 0.95 for the 12- to 14-km interval. It is difficult to judge whether this variation in b stems from some accidental irregularity in the slip-surface geometry, from some local peculiarity in the rock types in contact across the slip surface or from depth-controlled variations in the behavior of rocks composing the Earth's crust.

Histograms of the number of aftershocks larger than specified magnitude thresholds in each 1-km interval of depth from 0 to 15 km are shown for the entire hypocentral region and separately for its northwestern and southeastern sections in Figure 19. The most pronounced feature of all three sets of curves is a strong minimum centered at 6 to 7 km that separates peaks at 2 to 4 km and at 8 to 10 km. From the evidence on

detection thresholds offered by the log N versus M graphs (Figures 17 and 18), the data are incomplete for magnitude thresholds below 0.5 in the southeastern section and for magnitude thresholds below 1.5 in the northwestern section and in the region as a whole. In the southeastern section, the ratio of larger aftershocks to the smaller ones is much larger in the deep zone than in the shallow one. This feature is reflected in the small slope (-0.6) of the log N versus M *curve* for the 8 to 10 km depth interval in Figure 18.

It is tempting to conclude that the strong minimum centered near the 6- to 7-km depth interval results from some depth-controlled characteristic of rocks composing the upper crust. The strong concentration of aftershocks in a few patches on the slip surface (Figures 8 and 11) raises the suspicion, however, that the two peaks on the frequency-versus-depth histograms may result from geometrical features of the slip

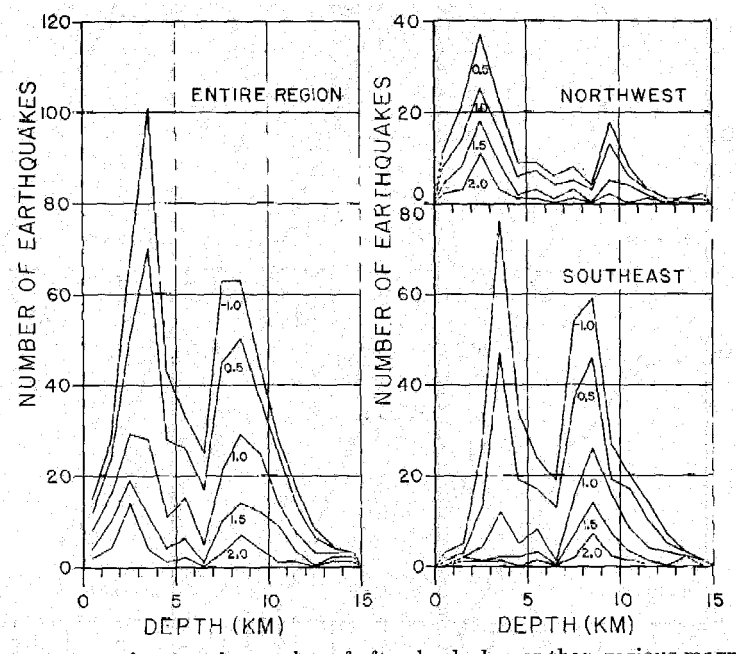

FIG. 19. Histograms showing the number of aftershocks larger than various magnitude thresholds as a function of focal depth for the entire hypocentral region and for its northwestern and southeastern sections.

surface or from non-depth-dependent variations in properties of rocks in contact across the slip surface.

FAULT CREEP AND AFTERSHOCKS AS A FUNCTION OF TIME

Progressive surface displacements continuing long after the main Parkfield-Cholame earthquake along the section of the San Andreas fault that slipped at the time of the main shock have been described by Wallace and Roth (in Brown *et al.*, 1967), Smith and Wyss (1968) and Scholz, Wyss and Smith (1969). Such displacements measured at a number of sites along the zone of surface fracturing initially were quite rapid, but their rates diminished logarithmically with time after the main shock in a manner similar to the decrease in frequency of aftershocks emanating from the same section of the fault (Eaton, in Brown *et al.*, 1967). The possibility that continuing surface displacement resulted simply from the cumulative slip on the fault associated with the

aftershocks has been convincingly refuted by the studies of Smith and Wyss (1968) and Scholz, Wyss, and Smith (1969). These authors estimated the cumulative average displacement over the entire slip surface (and over various parts of it) from the seismic moments of the earthquakes occurring along it in accordance with the relation

$$\sum \bar{u} = \frac{\sum M_0}{A_0 \mu}$$

where $\bar{u}$ is the average slip over the area A_0 (over which all of the "summed" events occur) due to an earthquake of seismic moment M_0, and μ is the rigidity of the material cut by the fault. They obtained the moments of the larger earthquakes from earlier direct estimates by Wyss and Brune (1968) and calculated the moments of smaller earthquakes for which magnitudes were available from the moment-magnitude relation for Parkfield earthquakes reported in the same study. The additional moment due to many small earthquakes for which magnitudes were not available was estimated by Scholz, Wyss and Smith from the number of such earthquakes, the frequency-versus-magnitude relationship given by McEvilly *et al.* (1967) and the moment-magnitude relationship of Wyss and Brune. Scholz, Wyss and Smith concluded that the total slip inferred from aftershocks is an order of magnitude smaller than the displacement measured at the surface for the period June 28 1966 to July 1968. Furthermore, when the total slip inferred from aftershocks during that period is compared section by section along the fault with the corresponding displacement measurements, the central part of the zone shows a minimum in inferred seismic slip and a maximum in measured displacement.

The relationship of creep measured at the Earth's surface to the aftershocks and the cumulative displacement inferred from them are displayed as a function of time in Figure 20. *Curves CQ, CC* and *CP* indicate cumulative strike-slip displacement along the fault at 13 km (quadilateral QAB, from Wallace and Roth, in Brown *et al.* 1967) and at 23 km and 31 km (Carr Ranch and Taylor Ranch, from Smith and Wyss, 1968). *Curves SE* and *NW* represent the cumulative number of earthquakes of magnitude 1.5 and larger along the southeastern (0 to 25 km) and northwestern (25 to 50 km) sections of the hypocentral zone, respectively; and *curves* $\sum \bar{u}$ *SE* and $\sum \bar{u}$ *NW*, respectively, show the cumulative average displacement over the corresponding sections of the fault surface inferred from those earthquakes. Moments of individual earthquakes were computed by the relationship $\log M_0 = 1.5\,M + 17.0$, where M is the magnitude of the earthquake reported in Table 2. In this equation the coefficient of M and the constant have been somewhat arbitrarily selected from the magnitude-moment relationships for Parkfield-Cholame earthquakes of magnitude 3.0 and greater obtained independently by Aki (1969) and by Wyss and Brune (1968).

For calculating average displacements corresponding to the moments so obtained we let $\mu = 3.0 \times 10^{11}$ dynes/cm^2 and assumed the same area, $A_0 = 200$ km^2, for both the southeastern and northwestern parts of the slip surface. The average displacement over the entire slip surface (with a total area of 400 km^2) expected from the main shock of magnitude 5.5, according to these relationships, is 140 mm. The average displacements inferred from aftershocks between the 3rd and 82nd day after the main shock are 6.0 mm and 2.5 mm for the southeastern and northwestern sections of the hypocentral zone, respectively. Displacements measured at the surface during the same period of time were about 60 mm (*CQ* and *CC*) along the southeastern section and about 140 mm (*CP*) along the northwestern section. The most striking features shown

by Figure 20 are the anticorrelation of measured surface displacement and inferred average displacement due to aftershocks over the two halves of the hypocentral zone and the order of magnitude deficiency of the inferred average seismic displacement as a source for the measured surface displacement. The main shock itself is the only adequate seismic source for the large displacements that were observed, after considerable delay, along the fault trace at the surface. However, the average seismic displacement over the slip surface at the time of the main shock is extremely

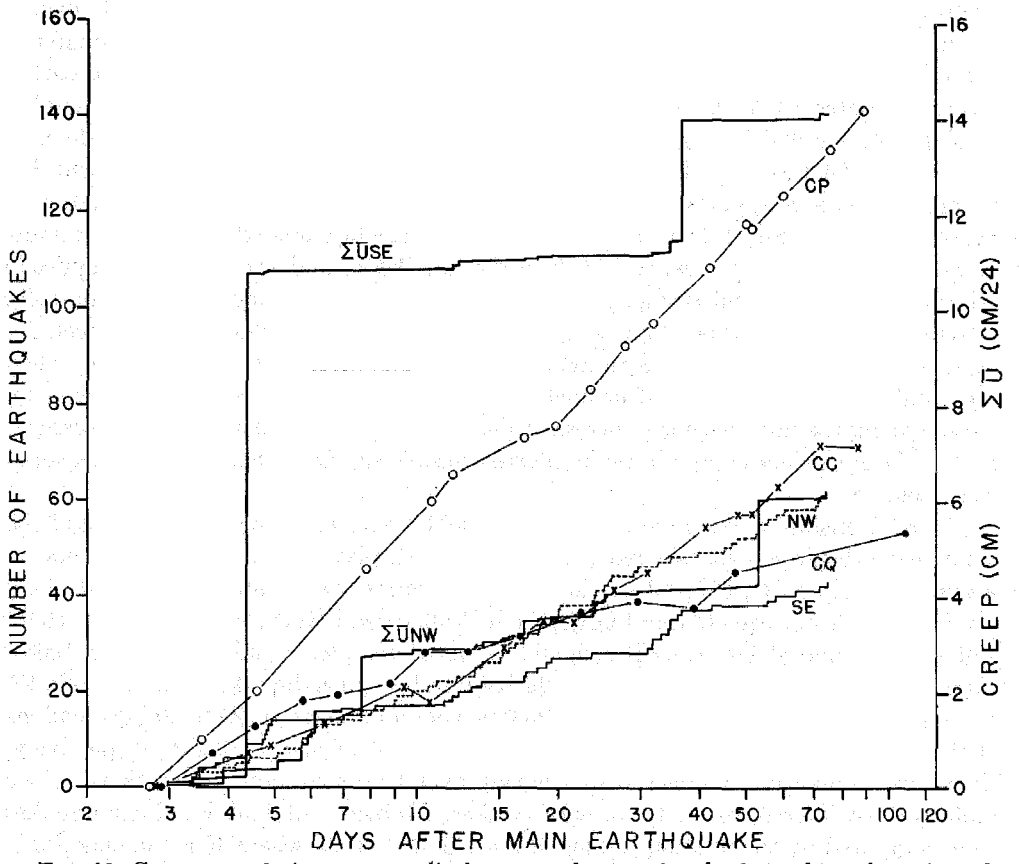

FIG. 20. Creep, cumulative average displacement due to aftershocks and number of earthquakes of magnitude 1.5 and greater as a function of time after the main shock. *Curves CQ, CC* and *CP* show cumulative offsets, across the 1966 fault break, due to creep near station 1, near station 11 and near station 9 (see Figure 7), respectively. *Curves SE* and *NW* show the number of earthquakes of magnitude 1.5 and greater along the southeastern section (0 to 25 km) and along the northwestern section (25 to 50 km) of the hypocentral zone, respectively. The cumulative calculated average displacements over those sections of the fault due to the aftershocks are shown by *curves* $\sum \bar{u}$ *SE* and $\sum \bar{u}$ *NW*.

difficult to calculate precisely, and detailed comparisons of that displacement with those obtained from direct geodetic measurements should be evaluated with due regard for the uncertainty in the calculated seismic displacement.

From the two seismic displacement curves in Figure 20, it is evident that most of the displacements due to aftershocks along the southeastern portion of the slip surface occurred in two short episodes, whereas that along the northwestern section of the slip surface was more uniformly distributed with time. The two largest steps in the curve for the northwest followed the sudden jumps in the curve for the southeast, perhaps

indicating a migration of episodes of slippage along the fault from the southeast toward the northwest during the first 2 months following the main earthquake.

Dependence of Ground Motion Amplitudes and Delays on Geological Conditions

Magnitudes based on the maximum amplitude of P, $PPMG(J)$, as well as on the maximum recorded amplitude, $XXMG(J)$, were computed for each earthquake at all of the stations for which adequate recordings of the earthquake and adequate calibration data were available. Deviations of values computed for individual stations from the average of all of the stations ($EPMG(J) = PPMG(J) - PMAG$, and $EXMG(J) = XXMG(J) - XMAG$) were also determined. For the calculation of P-magnitudes the constant in the magnitude equation was set at 1.45 rather than at 1.60 as for the X-magnitudes. The values of $PMAG$ obtained in this manner generally agree with the corresponding values for $XMAG$ within about 0.1 unit. The magnitude deviations at a given station are logarithmic measures of the deviations in the maximum recorded amplitude at that station from the values expected at an "average" site.

In the HYPOLAYR batch statistical summary, means, standard deviations and standard errors of the mean are computed for the arrival time residuals, $F(J)$, as well as for $EPMG(J)$ and $EXMG(J)$ at each station. For inclusion in the statistical summary, it was required that an earthquake be recorded at five or more stations and that the mean deviation of arrival-time residuals in its hypocentral solution, MD, not be larger than 0.15 sec. Individual station values were deleted for particular earthquakes if they exceeded 0.3 sec or had overall "weights" smaller than 0.5 for the $F(J)$, or if they exceeded 1.0 unit for $EPMG(J)$ and $EXMG(J)$. The earthquakes were separated into four calendar interval batches, based on the number and distribution of stations in the network, for processing in HYPOLAYR. Final values of $F(J)$, $EPMG(J)$, and $EXMG(J)$ were obtained by averaging the results from the four separate batches.

As indicated in the discussion of the dual crustal model used in the hypocenter calculations, the gross average differences in the crust beneath stations on opposite sides of the fault are incorporated into the model. A P-wave traveling vertically from a depth of 15 km to the surface on the SW side of the fault (model 1) takes 0.15 sec longer than one on the NE side of the fault (model 2), and most of the delay on the SW side is in the uppermost 2 km of the path. The station delays $DLY(J)$ that were incorporated as corrections to computed travel times in HYPOLAYR result from local departures of the crust beneath particular stations from the corresponding crustal models used in the hypocenter determinations. The average $F(J)$ described above are additional corrections that must be added to the corresponding station delays better to describe local departures of the real crust from the model. To account for the differences between the two models we must also add 0.15 sec to the corrected station delays for stations SW of the fault. Then $TD(J) = DLY(J) + \bar{F}(J) + 0.15$ sec (model 1) and $TD(J) = DLY(J) + \bar{F}(J)$ (model 2) are the total station delays that we shall use in comparing the various recording sites.

In Figure 21 the average magnitude residuals, $EPMG(J)$ and $EXMG(J)$, are plotted against the total station delays, $TD(J)$. A single line was fitted by inspection to both the $EPMG$ and $EXMG$ points for all stations SW of the fault (● and ■, for model 1). The equation of the line is $MR = -0.26 + 2.0 \times TD$, where MR is the magnitude residual and TD is the total arrival time delay with respect to the model 2 crust. The mean deviation of the model 1 station magnitude residuals from this line is 0.05 unit, and the extreme values are +0.12 and −0.11. Because of the logarithmic relationship

between recorded ground amplitude and magnitude, an increase of 0.15 in delay (and a 0.3-unit increase in magnitude residual) corresponds to a twofold increase in ground motion amplitude. Although the line through the model 1 station magnitude residuals also fits the model 2 station magnitude residuals (○ and □) quite well, the model 2 points are scattered rather widely about the line, with extreme variations from the line of 0.29 and −0.27.

Because the delay at a particular station depends primarily on the thickness of the unconsolidated (chiefly Tertiary) sedimentrary rocks beneath the station, the relationship between total delay and magnitude residual illustrated by Figure 21 also implies a relationship between the thickness and degree of consolidation (as it affects wave velocity) of such sediments and the ground-motion amplification of the site. An explanation of the difference in scatter of magnitude residuals of stations on opposite sides of the fault must be sought in the greater complexity of near-surface geology on

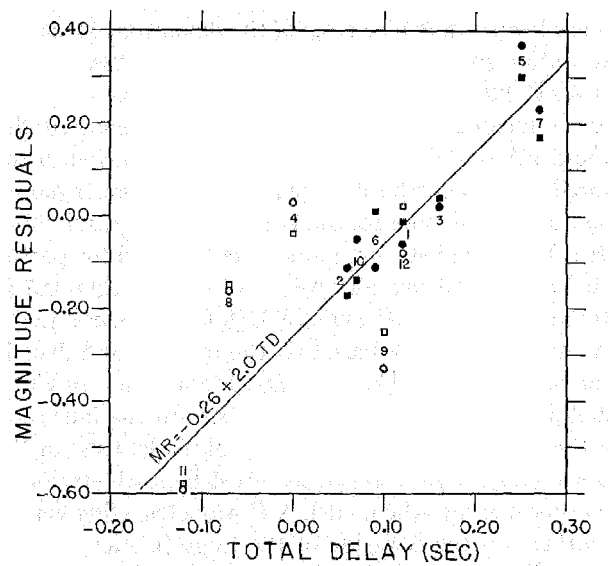

FIG. 21. Average magnitude residuals versus average P-wave arrival-time delays for stations of the portable network. *Circles* denote P-wave magnitude residuals and *squares* denote residuals of magnitudes computed from the largest recorded amplitudes. Stations southwest of the fault zone are plotted by *closed symbols;* stations northeast of the fault zone, by *open symbols.*

the northeast side of the fault than on the southwest side in the region covered by the network. As noted by Aki (1969), the smallest ground-motion amplification occurs at sites with little or no Tertiary sedimentary cover, which have the smallest delays, and the largest amplification occurs at sites with a thick sequence of such rocks, which have the largest delays.

More detailed analyses of the relationships between magnitude anomalies and travel-time delays and the near-surface geological features of the recording sites can be expected to yield methods for the quantitative prediction of ground-motion amplification at specific sites from geological data.

Ground-motion amplification factors based on P-magnitude and X-magnitude residuals are presented in Table 4, together with the corresponding magnitude residuals, corrected station delays and total delays with respect to the model 2 crustal structure. Standard deviations and standard errors of the means of individual station values of travel-time residuals, X-magnitude residuals and P-magnitude residuals,

respectively, averaged 0.06 sec and 0.01 sec, 0.23 unit and 0.04 unit, and 0.21 unit and 0.04 unit. The number of observations used in calculating individual station values relating to arrival-time residuals and magnitude residuals averaged about 500 and 300, respectively, for stations 1 through 7 and about 50 and 40, respectively, for stations 8 through 12. Because the separate stations were not equally represented in the determination of hypocenters and magnitudes (i.e., records were available much more frequently from some than from others) the residuals in Table 4 do not sum to 0.

TABLE 4

GROUND-MOTION AMPLIFICATION FACTORS BASED ON P-MAGNITUDE AND X-MAGNITUDE RESIDUALS

Station	Model	Corrected Delay	Total Delay	$\overline{EPMG}$	$\overline{EXMG}$	Amplification Factor	
						P	Max
GH	2	−0.01	−0.01	—*	—*	—*	—*
1	1	−0.03	+0.12	−0.06	−0.01	0.87	0.98
2	1	−0.09	+0.06	−0.11	−0.17	0.78	0.68
3	1	+0.01	+0.16	+0.02	+0.04	1.05	1.10
4	2	0.00	0.0	+0.03	−0.04	1.07	0.91
5	1	+0.10	+0.25	+0.37	+0.30	2.34	2.00
6	1	−0.06	+0.09	−0.11	+0.01	0.78	1.02
7	1	+0.12	+0.27	+0.23	+0.17	1.70	1.48
8	2	−0.07	−0.07	−0.15	−0.15	0.71	0.71
9	2	+0.10	+0.10	−0.33	−0.25	0.47	0.56
10	1	−0.08	+0.07	−0.05	−0.14	0.89	0.72
11	2	−0.12	−0.12	−0.59	−0.58	0.26	0.26
12	2	+0.12	+0.12	−0.08	+0.02	0.83	1.05
13	1	−0.13	+0.02	—*	—*	—*	—*
E1	2	+0.26	+0.26	—*	—*	—*	—*
E2	1	+0.04	+0.19	—*	—*	—*	—*
E3	1	+0.12	+0.27	—*	—*	—*	—*
E4	1	−0.19	−0.04	—*	—*	—*	—*
E5	1	−0.27	−0.12	—*	—*	—*	—*
PRI	2	+0.33	+0.33	—*	—*	—*	—*

* Not used in magnitude calculations.

CONCLUSIONS

The portable cluster of high-sensitivity, short-period seismographs employed in the study of aftershocks of the Parkfield-Cholame earthquake provided hypocenter determinations of sufficient precision to permit the mapping in three dimensions of the slip surface on which the aftershocks (and presumably the main shock, too) occurred. Calculated standard errors in epicentral position did not exceed 1.0 km for 80 per cent, nor 0.5 km for 59 per cent of the 537 aftershocks for which calculation could be made. The calculated standard error in focal depth rarely exceeded twice that in the epicentral position. A reference plane fitted to all but 10 of the 484 well-located aftershock hypocenters, which have a standard deviation from the plane of 0.45 km, strikes N 39°W and dips 86°SW. Its surface trace is a good straight-line approximation to the gently curved zone of surface fracturing that accompanied the main earthquake. Systematic variations in the deviation of hypocenters from the reference plane suggest even finer details of the geometry of the slip surface.

About 95 per cent of the aftershocks studied had focal depths between 1 km and 12 km, and none were deeper than 15 km. Strong concentrations of foci at depths of 2 to

4 km and 8 to 10 km were separated by a pronounced minimum at 5 to 7 km. The lower limit of aftershocks (and the sudden release of stored elastic strain energy that generates them) at about 15 km coincides approximately with the top of the probable intermediate-velocity layer of the lower crust and is about 10 km shallower than the top of the mantle.

Aftershocks were concentrated in patches on the slip surface, especially near its southeastern end; other patches were entirely quiet, and with only a few exceptions (most of them poorly located events northwest of the portable network) aftershocks were restricted to the section of the San Andreas fault marked by surface fracturing at the time of the main shock.

Focal mechanism solutions based on the direction of first motion in the P-waves for individual events and for composite plots of data from various sections of the slip surface indicate that a very large majority of the aftershocks originated by right-lateral strike-slip displacement on surfaces that very nearly parallel the reference plane fitted to the aftershock hypocenters. Departures from this usual solution, mostly involving smaller dip of the fault plane and larger plunge in slip direction, were most prevalent among deep aftershocks at the southeastern end of the hypocentral zone.

Separate plots of log N versus M, where N is the number of aftershocks larger than magnitude M, for the well-instrumented southeastern section and the sparsely instrumented northwestern section of the hypocentral zone suggest that recording of aftershocks was essentially complete down to magnitude 0.5 in the southeastern section but only to magnitude 1.5 in the northwestern section. In the southeastern section of the hypocentral zone, the slope b of the log N versus M curve is a function of focal depth: it is about -0.6 for events between 8- and 10-km depth but averages about -0.95 for events at other depths.

An analysis of arrival-time and magnitude residuals suggests a relationship of the form $MR = -0.26 + 2.0 \times TD$, where MR is the magnitude residual and TD is the corresponding arrival-time residual with respect to crustal model 2 (northeast of the fault). Thus maximum recorded amplitudes increase systematically with increasing thickness of the low-velocity, near-surface sediments that are primarily responsible for the arrival-time delays.

References

Aki, K. (1969). Analysis of the seismic coda of local earthquakes as scattered waves, *J. Geophys. Res.* **74**, 615–631.

Bailey, E. H., W. P. Irwin and D. L. Jones (1964). Franciscan and related rocks and their significance on the geology of western California, *California Div. Mines Geol. Bull.* **183**, 177 p.

Bolt, B. A. and F. T. Turcotte (1964). Computer location of local earthquakes within the Berkeley Seismograph Network, in *Computers in the Mineral Industry, Part 2*, George Parks, Editor, *Stanford University Publications*, **9**, 561–576.

Brown, R. D., Jr., J. G. Vedder, Robert E. Wallace, Edward F. Roth, R. F. Yerkes, R. O. Castle, A. O. Waananen, R. W. Page and Jerry P. Eaton (1967). The Parkfield-Cholame earthquakes of June to August 1966, *Geological Survey Professional Paper 579*.

Eaton, J. P. (1966). Crustal structure in northern and central California, in *Geology of Northern California*, *California Div. Mines Geol. Bull.* **190**, pp 419–426.

Eaton, J. P. (1969). HYPOLAYR—a computer program for determining hypocenters of local earthquakes in an earth consisting of uniform flat layers over a half space, *U. S. Geological Survey Open File Report*.

Geiger, Ludwig (1910). Herdbestimmung bei Erdbeben aus den Ankunftszeiten, Nachrichten von der Königlichen Gesellaschaft der Wissenschaften zu Göttingen, *Mat.-Physikal. Klasse*, **4**, 331–349.

Gutenberg, B. and C. F. Ritcher (1942). Earthquake magnitude, intensity, energy, and acceleration, *Bull. Seism. Soc. Am.* **32**, 163–191.

Healy, J. H. (1963). Crustal structure along the coast of California from seismic refraction measurements, *J. Geophys. Res.* **68**, 5777–5787.

McEvilly, T. V., W. M. Bakun and K. B. Casaday (1967). The Parkfield, California, earthquakes of 1966, *Bull. Seism. Soc. Am.* **57**, 1221–1244.

Richter, C. F. (1935). An instrumental earthquake magnitude scale, *Bull. Seism. Soc. Am.* **25**, 1–32.

Scholz, C. H., M. Wyss and S. W. Smith (1969). Seismic and aseismic slip on the San Andreas Fault, *J. Geophys. Res.* **74**, 2049–2069.

Smith, S. W. and M. Wyss (1968). Displacement on the San Andreas Fault subsequent to the 1966 Parkfield earthquake, *Bull. Seism. Soc. Am.* **58**, 1955–1973.

Wyss, M. and J. Brune (1968). Seismic moment, stress, and source dimensions for earthquakes in the California-Nevada region, *J. Geophys. Res.* **73**, 4681–4694.

NATIONAL CENTER FOR EARTHQUAKE RESEARCH
USGS
MENLO PARK, CALIFORNIA (J.P.E., M.E.O.)

EARTHQUAKE MECHANISM LABORATORY
ESSA
390 MAIN STREET
SAN FRANCISCO, CALIFORNIA (J.N.M.)

Manuscript received August 24 1969